KfK 4891
September 1991

Experiments on Thermal Interactions: Tests with Al_2O_3 Droplets and Water

W. Peppler, W. Till, A. Kaiser
Institut für Reaktorentwicklung
Projekt Nukleare Sicherheitsforschung

Kernforschungszentrum Karlsruhe

KERNFORSCHUNGSZENTRUM KARLSRUHE

Institut für Reaktorentwicklung

Projekt Nukleare Sicherheitsforschung

KfK 4891

Experiments on Thermal Interactions: Tests with Al_2O_3 Droplets and Water

W. Peppler, W. Till, A. Kaiser

Kernforschungszentrum Karlsruhe GmbH, Karlsruhe

Kernforschungszentrum Karlsruhe GmbH
Postfach 3640, 7500 Karlsruhe 1

ISSN 0303-4003

Experiments on Thermal Interactions: Tests with Al_2O_3-Droplets and Water

Within the analysis of severe highly hypothetical fast breeder accidents the consequences of a fuel-coolant interaction have to be considered, i.e. the thermal interaction between hot molten fuel and sodium. To improve principal knowledge on the fragmentation process during the interaction of a hot droplet with a cold fluid, a series of experiments was performed with single droplets of molten Al_2O_3 as the hot liquid and water as the cold and easily volatile fluid. To initiate fragmentation of the droplet pressure pulses of up to 1 MPa were generated in the water by a magnetic hammer. The events were filmed by a high speed camera with up to 10^5 pictures per second. Details of the interactions can be deduced from the films and from the pressure histories. The existence of a vapour trail in all experiments indicates complex heat and mass transfer processes occurring in the vapour film spontaneously formed between droplet and cold fluid. Fragmentation was initiated by local events in the vapour trail area.

Experimentelle Arbeiten zur thermischen Wechselwirkung: Versuche mit Al_2O_3-Tropfen und Wasser

Bei der Analyse von schweren, hypothetischen Schnellbrüterstörfällen sind die Auswirkungen einer thermischen Wechselwirkung des heißen Brennstoffes mit Natrium zu berücksichtigen. Um das allgemeine Verständnis des entscheidenden Reaktionsvorgangs bei der Wechselwirkung eines heißen Tropfens mit einer kalten Flüssigkeit zu verbessern, wurde eine Versuchsreihe mit Einzeltropfen aus schmelzflüssigem Al_2O_3 als heiße Flüssigkeit und Wasser als kalte, leichtflüchtige Flüssigkeit durchgeführt. Die Fragmentation des Tropfens wurde über einen Magnethammer eingeleitet, der Druckpulse im Wasser bis zu 1 MPa erzeugte. Das Versuchsgeschehen wurde von einer Hochgeschwindigkeitskamera mit bis zu 10^5 Bildern pro Sekunde aufgenommen. Aus den Filmen und aus dem Druckverlauf lassen sich Einzelheiten der Wechselwirkungen ableiten. Die Existenz einer Dampfschleppe in allen Versuchen weist auf komplexe Wärme- und Stofftransportvorgänge in dem zwischen Tropfen und kalter Flüssigkeit spontan sich bildenden Dampffilm hin. Die Fragmentation wurde durch lokale Vorgänge im Bereich der Dampfschleppe ausgelöst.

Table of Contents

List of Figures and Tables

1. Introduction

Studies on fast breeder safety comprise investigations of highly hypothetical accidents in which fuel elements melt down and the melt contacts the sodium coolant. The temperature of the melt is far higher than the coolant temperature, so that a more or less violent thermal interaction, a so-called fuel/sodium interaction, may take place. In certain conditions, this will lead to a vapour explosion, i.e. a sudden evaporation of cold liquid at the interface as a result of rapid heat transfer from the hot liquid. A vapour explosion can take place only if heat is transferred much faster than the mixture of the two liquids and the vapour produced is capable of expanding. This is the only way in which a substantial part of the thermal energy can be converted into mechanical energy. Several conditions must be met for initiating a violent interaction:

1. The cold and hot liquids mix without significant heat transfer. This is the case, e.g., if the molten fuel is dispersed into droplets and separated from the coolant by a coherent vapour film around each droplet.

2. A spontaneous or externally applied shock wave, i.e. a trigger, makes the vapour film around the droplet collapse, causing direct contact between the coolant and the melt.

3. All droplets in a mixing region are finely fragmented within a short time so that a large contact surface is created required for fast heat transfer.

The experiments described in this report* were intended to investigate the processes involved in the triggered fragmentation of single droplets, i.e. the processes in conditions (1) and (2). This would have been highly difficult with the fast breeder materials UO_2 and sodium, as the UO_2 would have to be heated beyond its melting temperature of 3113 K and made to contact sodium of, say, 1073 K. Apart from the extremely high apparative requirements, there is the further problem that reaction processes cannot be filmed in sodium. For this reason, fundamental studies are carried out world-wide on systems of materials that are easier to handle and in which reaction processes can be filmed. For example, single

---

* This KfK report is regarded as a documentation. First results have previously been reported in Ref. 1.

droplets are made to react in a transparent liquid, and the most varied systems of materials are investigated.

After Ando /2/ had carried out experiments on hot Cu droplets in water at IRE, the present study was to determine the influence of the physical parameters of a ceramic material on the fragmentation process. Al_2O_3 was chosen for this purpose; its melting temperature is about 2300 K, so that fragmentation events can still be expected in experiments with sodium at a later stage. The experimental findings in the Al_2O_3 / water tests were expected to help in the interpretation of the Al_2O_3 / sodium tests that have been carried out in the meantime; c.f. Ref. 3. In these tests no X-ray cinematography was used.

With regard to the physical characteristics of this system, the following considerations are important: A hot droplet is separated from the surrounding cold liquid by a boiling film if the temperature difference between the two interfaces is higher than the minimum film boiling temperature difference ΔT_{min}. The latter, also called minimum film boiling superheat, is defined as (cf. Ref. 4)

$$\Delta T_{min} = T_{min} - T_{sat}, \qquad (1)$$

where T_{min} is the minimum wall temperature of the hot material prior to contact and T_{sat} is the saturation temperature of the cold liquid. Based on analytical and experimental results published in the literature, covering a wide range of thermal properties and fluid subcooling, Henry /5/ established a correlation for T_{min} as a function of the thermodynamic properties of both materials participating in the interaction.

Ladisch /6/, who tested Al_2O_3-coated metallic cylinders under quasi steady conditions, determined the surface temperature at which film boiling changed to bulk boiling. In water of 303 K under standard atmospheric conditions, this temperature was T_{min} = 983 K; using eq. (1) one obtains ΔT_{min} = 983 K - 373 K = 610 K. It should be mentioned that in Ladisch's tests T_{min} decreased with increasing water temperature. All experimental data were well above the values predicted by the Henry correlation mentioned above. It is therefore concluded that in the tests with Al_2O_3 droplets ($T_H \gg T_{min}$) and water the conditions for film boiling will certainly be reached at the first contact.

Fauske's model /7/ predicts particularly energetic interactions at contact temperatures above the spontaneous nucleation temperature. For water under standard atmospheric conditions the latter was found by Pavlov and Nikitin /8/ to be T_{SN} = 586 $\pm$5 K (for comparison, the critical temperature of water is 647 K). The contact

temperature between an Al_2O_3 droplet at a temperature just above solidification and water is much higher (2105 K; cf. Table 1), i.e. liquid-to-liquid contact between molten Al_2O_3 and water will result in immediate evaporation. Experiments involving a contact temperature below the spontaneous nucleation temperature cannot be carried out with this system, as the droplet temperature is always higher than or equal to the melting temperature of Al_2O_3.

2. Experimental Goals and Parameters

The experiments were intended to determine the processes involved in triggered fragmentation of single Al_2O_3 droplets in water and to develop experimental methods for similar tests with Al_2O_3 droplets and sodium. The main preconditions for this were the melting and superheating of Al_2O_3.

The experimental parameters were:

- Three different trigger pressure levels (0.95, 0.66, and 0.25 MPa)
- Droplet temperature (maximum possible superheating above the melting temperature, in this case 260 K, was aimed at)
- Droplet diameter 4.9 ...5.9 mm
- Droplet mass 0.2 ...0.3 g
- Water of room temperature

3. Experimental Set-Up

Fig. 1 is a schematic representation of the experimental set-up, while Fig. 2 shows the photographic picture. The main features are the melting device, the experimental vessel, the trigger pulse generating device, the measuring system, and the film camera system.

3.1 Melting Device

The main problem of these experiments was the development of a method by which single, hot droplets with a temperature as far above melting temperature as possible could be melted off Al_2O_3. Direct inductive heating was impossible as Al_2O_3 is an electrically non-conductive, ceramic material. A plasma torch appeared to be a promising solution: it can be applied to non-conductive materials,

and the arc reaches temperatures of several 1000 K. Various types of plasma torches were tested for the envisaged purpose. Overheating up to 400 K above the melting temperature was possible with the system chosen of a total power of 22 kW, combined with a plasma torch generating a laminar arc. The torch is operated with an Ar/He mixture. It works with an enclosed plasma, i.e. both the anode and the cathode are arranged inside the torch, with laminar blow-out of the arc through the gas mixture. Turbulent plasma flow would blow the molten droplet off and fragment it.

A horizontal graphite rod of 20 mm diameter, with a vertically drilled hole of 7 mm diameter and with partial thermal insulation, prevents the droplet from flying away. The graphite rod is preheated in order to reduce the heat loss during melting. A pyrometer whose measuring beam is directed at the lower edge of the hole measures the temperature of the droplet during its crossing the beam.

3.2 Experimental Vessel

The geometry of the experimental vessel is similar to the one used by Ando/1/ in his experiments on Cu droplets in water in order to facilitate a comparison of the findings. Instead of screwed walls of polymethylacrylic acid ester (plexiglass, PMMA) with a thickness of 25 mm, a welded construction of austenitic material with two screwed-on PMMA windows facing each other is used. The experimental vessel has a height of 300 mm, internal dimensions of 40 x 40 mm, and a wall thickness of 5 mm. It is bolted onto a 25 mm Al slab. At 110 mm below the upper edge of the vessel, there is a photocell whose slot aperture has a large horizontal and only a narrow vertical field of vision. The falling droplet initiates a signal in the photocell which releases the camera shutter, fires the flash, and starts, after a preset delay, the trigger. A pressure transducer P1 is arranged in the center of the envisaged viewing section of the camera, i.e. at 122 mm from the upper edge of the vessel, and a second pressure transducer, P2, at 80 mm below the first one.

The fragments produced in the experiments are collected in a pyramidal stainless steel screen with a mesh of 0.1 mm and a wire diameter of 0.063 mm.

3.3 Generation of the Trigger Pulse

Fragmentation experiments in water usually rely on an exploding wire for generating the trigger pulse, but this method cannot be used in the experiments

planned with sodium. For this reason, a magnetic hammer was developed which is triggered by an electronic pulse and hits the floor of the experimental vessel.

The magnetic hammer works as follows:

- A 100 μF condenser battery is charged with a voltage of up to 2000 V.
- The energy is transferred to a coil by an ignitron (electronic device).
- The 90-turn coil pushes off a short-circuiting ring which, via a tappet, impacts on the bottom of a bellows.
- The bellows is flanged onto the bottom side of the experimental vessel; it has a rigid bottom from which the impact shock is transferred to the liquid.

This way, pressure pulses with a maximum pressure of 2 MPa and a duration of 0.4... 0.55 ms can be generated. Due to the characteristics of the system, rise times cannot be shorter than 0.12 ms. The charging voltage U is 700, 1000, or 1350 V depending on the experiment.

3.4 Measuring System and Data Acquisition

The temperature of the falling droplet is measured by a spectral pyrometer with a response time of 0.1 ms and a measuring spot about 1mm in diameter.

The pressure curves are recorded by piezoelectric pressure transducers with a resonance frequency > 400 kHz. In order to prevent oscillations of the measuring signal near this frequency, a low-pass filter of 100 kHz is installed in the charge amplifier.

The photocell directly above the reaction site is placed there, in the first instance, to release the camera shutter. In order to obtain a steep signal of the falling hot droplet, the photocell is connected to the window of the experimental vessel only via a narrow horizontal slot. Further steep signals are generated by the flashing light and by the fragments dispersed after the reaction.

The data are recorded by a transient recorder capable of sliding recording of 4096 data per channel. The sliding recording process is stopped by a defined signal (trigger), and the data stored can then be transferred to a floppy disk. The onset of recording can be set in eight steps before or after the triggering event. The measuring signals are recorded in parallel in two ways:

Survey:

(Frequency f_R = 10 kHz, duration 410 ms, start at 358 ms before trigger onset)

Pyrometer

Photocell

Camera pulse

Pressure transducer P1

Detail:

(Frequence f_R = 500 kHz, duration 8.2 ms, start at 1 ms before trigger onset)

Pressure transducer P1

Pressure transducer P2

Photocell

The triggering event for the transient recorder in both cases was the signal rise of the pressure transducer P1 resulting from the trigger pulse.

3.5 Film Camera

The tests were recorded by a drum camera with a maximum framing rate of 10^5 pictures/s, and with a film 70 mm wide and 1000 mm long producing 512 pictures. The camera drum rotates at 12,000 rpm. The drum is connected to mirrors with a higher rotational speed, which project the images onto the film in four parallel tracks. The self-luminosity of a molten Al_2O_3 droplet is high enough to expose the single frame even at the short exposure time of 0.005 ms chosen which is half the time between two succeeding frames. The opening time of the shutter includes the duration of the flash which is set to 4 ms (Fig. 3).

4. Experimental Procedure

Preliminary experiments were carried out in order to find out whether spontaneous fragmentation occurs after immersion in hot Al_2O_3 droplets heated to up to 400 K above the melting temperature. No spontaneous fragmentation was found to take place, neither during impact on the water nor during the fall through the water down to the bottom of the vessel. An external trigger (produced by the magnetic hammer) was required in all cases for initiating fragmentation.

Prior to each experiment, distilled water at room temperature was filled into the vessel through a flexible siphon tube up to 5 mm below its upper edge, and air bubbles were removed by applying several trigger pulses of the magnetic hammer.

The graphite rod was preheated to 2300 K by the plasma torch, after which the plasma jet was directed tangentially above the bore hole in the graphite rod, so that part of the plasma was deflected downwards. An Al_2O_3 rod with a diameter of 3 mm was held into the plasma jet, so that a droplet with a diameter of 5-6 mm was melted off and fell through the bore hole. Enveloped in plasma, the droplet then fell through the air for about 20 mm until immersing in the water.

After a falling period of 240 - 260 ms ($v \approx 0.44$ m/s) the droplet passed the photo diode whose signal released the camera shutter. Fig. 3 shows the synchronisation of the different events of the experiment. The "M" contact of the shutter is released 13 ms prior to the preset opening time of the shutter. Two electronic delay elements connected to the "M" contact triggered the ignitron for the trigger and the flash, one after the other.

The collected fragments were scanned by an image processing system and sized in the range of 0.2 to 2.5 mm. Some fragments were also reproduced on different (imaging) scales by an electron-beam scanning microscope.

5. Evaluation

5.1 Synchronisation of Pressure History and Film Records

The flashing light generates a signal in the photocell which is used for synchronizing the film records with the pressure curves. The onset of the signal is assigned to the first film frame and the end of the signal to the last one.

In synchronizing the film frames with the pressure history, it is important to note that a pressure event starting from the vessel floor arrives simultaneously at the droplet and at the pressure transducer P1. If a pressure pulse is generated by a reaction at the droplet, the distance between the pressure transducer and the droplet must be taken into account. At a minimum pressure wave velocity evaluated of 530 m/s, and a distance of 10 to 12 mm between reaction site and pressure

transducer, the transit time will be 0.02 ms, which corresponds to a shift of two film frames at a framing rate of 10^5 pictures/s.

5.2 Correction of Optical Distortion

The boiling film around the droplet acts as a lens, i.e. it magnifies the vapour film around the droplet in the camera images. To determine the real vapour film thickness, we used the film frames of experiment AOW 11 (AOW = Aluminium Oxide in Water) which were recorded prior to the impact of the trigger pulse. The self-luminosity of the droplet is clearly visible; further, the droplet is not fragmented at the end of the experiment and can be used for a comparison of size with the image on the film frames (Fig. 4). The diameter during film boiling can be calculated from the mass and density. Assuming that the outer diameter of the boiling film is represented correctly, the refractive index of the water vapour is 1.16, i.e. the vapour film is shown too thick by a factor of 1.4. This value is accounted for in the vapour film thickness data following in the next section.

5.3 Determination of the Vapour Film Thickness

The thickness of the vapour film is determined from the pictures of experiment AOW 4 (Fig. 5), filmed at 45,000 pictures/s. The resulting longer exposure time clearly shows the self-luminosity of the droplet. Four horizontal orbital surface waves are visible which cause an optical distortion of the image of the droplet surface, giving it a torn look. In the short recording time (1.8 ms = 72 pictures) prior to the impact of the trigger, there is no long-wave motion of the surface waves. The corrected film thickness (see section 5.2) is 0.7 mm at the front side of the droplet, about 0.6 mm at the wave crests of the water projecting into the vapour film, and 0.9 m at the wave troughs.

*5.4 Determination of the Normalized Droplet Projection Area A**

For a simpler representation of the experimental dynamics, the droplet projection areas in the film pictures were determined by planimetrisation of the projected areas defined by the water/vapour boundary and then normalized by the area prior to the impact of the trigger:

$$A^*(t) = A(t) / A(0) \qquad (2)$$

However, this method is applicable only as long as the whole contour is still visible on the film frame. An attempt to establish two different relationships, i.e. one

for the top section of the droplet and one for the bottom section, failed as there is no clearly defined boundary between them. In most cases, vapour bubbles were scarcely present in the bottom section, so that A* will mostly show the dynamics of the reaction events in the top section.

5.5 Description of the Three Trigger Pressure Levels Applied

Apart from initiating the reaction between the hot droplet and the water, the trigger also influences the pressure level throughout the reaction. The following sequence of events is typical of vessels with a free liquid surface:

Fig. 6 shows a trigger initiated with 700 V. There is a pressure pulse with an amplitude of 0.25 MPa at the pressure transducer P1 and with a rise of 1300 MPa/s, followed by decreasing pressure oscillations of about 750 Hz resulting from the vibration of the water column.

Things are different at and above a voltage of 1000 V (Fig. 7): After a pressure pulse with an amplitude of 0.66 MPa at P1, a rise of 2300 MPa/s and a duration of 0.5 ms, the pressure drops below the initial system pressure because of a slowing-down effect on the water column accelerated in the upward direction. A tensile stress in the water is observed for a certain period of time, during which the pressure level is at absolute zero or even slightly below. Cavitation bubbles start to form in the water which are visible on the film records. The duration of this phase is the longer the heigher the preceding pressure pulse is. With the experimental geometry and with the experimental pressure pulse, it lasted for about 3.5 ms. After this, the cavitation bubbles will condense and recompression occurs resulting in a second pressure pulse. The amplitude of recompression is half as high as the amplitude of the first pressure pulse. This is followed by new events of negative pressure and recompression, until the impulse has faded away. In Fig. 7, pressure peaks are visible in the signal of transducer P2 in the rise phase of the second and third pulse, which may be due to condensation shocks of cavitation bubbles directly in front of the transducer membrane.

The courses of the pressures P1 and P2 are compared. The pressure signal at P2 consists of two successive pulses, while P1 (located 80 mm higher) registers only a single pulse which is shorter by 0.1 ms. The time difference of the onsets of the pressure rise at P2 (time t1) and P1 (time t2), respectively, yields a sound velocity of 680 m/s. The shock wave hits the water surface 0.16 ms later (time t3), from which it is reflected as an expansion wave and is back at P1 after another 0.16 ms (time t4). There, the negative reflection wave superposes on the second pulse

coming from below, making the pressure curve at P2 half-sinusoidal. As soon as the reflection wave reaches P2 (time t5), the pressure drop will become steeper.

The sound velocity of 680 m/s in the water of the test vessel is far below the theoretical sound velocity in water, i.e. 1440 m/s. However, this can be explained by the fact that the sound velocity is determined not only by the compressibility of the water but also, and very strongly, by the elasticity of the vessel walls. The two opposite PMMA plates at the level of the pressure transducers appear to have their effect here.

If a hot droplet enveloped by a vapour film is inside the vessel, the velocity is still lower. Fig. 8 shows a trigger pulse of the third trigger pressure level generated with U = 1350 V (maximum pressure 0.95 MPa at P1, pressure rise 5500 MPa/s). The picture is of a preliminary experiment, in which a solifidied Al_2O_3 droplet of about 1900 K was in the reaction site. A sound velocity of 595 m/s was determined. In experiment AOW 6, with the highest droplet temperature, it was only 530 m/s.

At voltages higher than 1000 V, the condenser discharge used to disturb the pressure records 0.8 ms prior to the onset of the pressure pulse at P1. The amplitude of this disturbance is less than 0.1 MPa. In consequence, in most tests the zero point of the pressure record seems to be located in the negative range.

6. Experimental Findings

6.1 Experimental Data; General Remarks

Table 1 lists the experiments from which evaluable film records were obtained.

The droplet temperatures could not be chosen exactly at will but were determined by the melting process. The interface temperatures at the first contact were calculated as described in Annex A. The temperature at the time of the reaction was calculated from the measured initial temperature and the time of fall in the water, assuming a mean total heat transfer coefficient of 800 W/cm^2 K during film boiling on ceramic surfaces as proposed by Ladisch /2/. In three experiments, the calculation yieldes droplets at solidification temperature (2313 K) with part of the mass solidified.

The images of the drum camera are identified by the number of the experiment and the consecutive number of the film frame, e.g. 6.48: Experiment AOW 6, frame No. 48. For each of the experiments described in the following, an equation will be presented by which a given film frame can be matched to the corresponding time of the experiment.

The time of the experiment was generally set at zero at the onset of the trigger pressure rise at pressure transducer P1.

6.2 Experiments with High Trigger-Induced Pressure

6.2.1 Experiment AOW 6

Experimental parameters:

Droplet diameter	5.3	mm
Starting temperature	2670	K
Reaction temperature	2565	K
Trigger pressure	0.95	MPa
Framing rate	$1 \cdot 10^5$	f/s

A frame n of the drum camera can be matched to the time t in this experiment as follows:

$t = 0.0101\ n - 0.36;$ t in ms

In Figs. 9, 10 and 11, the pressure recorded during the test is presented in different time scales.

Short Description of the Experiment:

The falling droplet is enveloped in a boiling film which is deformed by projections of horizontal, orbital surface waves of the water. A vapour trail has formed in the wake region on top of the droplet. Both the boiling film and the vapour trail are compressed by the trigger pressure. Initial reactions start to occur on the horizontal orbital surface waves of the water and in the stagnation point of the falling droplet. This is followed by a short-term pressure rise to 1.2 MPa above the trigger pressure, during which the vapour trail disappears almost completely. The boiling film then re-expands, and vapour clouds start to form on top of the droplet. While the pressure drops back to the initial system pressure, the vapour

clouds are observed to shrink. For a period of 6.5 ms, the pressure remains below the initial system pressure. At the onset of this period, cavitation bubbles are observed in the water (Fig. 11). The droplet is enveloped in vapour bubbles mainly in its top section and is also widened and fragmented from above. After this, there are three further pressure pulses with decreasing amplitudes.

In order to enable a comparison between experiments, the reaction process is divided tentatively into six stages:

I Film boiling

II Compression

III Thermal reaction

IV Transition

V Deformation and coarse fragmentation

VI Recompression and fragmentation

These observations will be discussed in more detail in the following sections.

Phase I: Film boiling

Time: -0.34 - 0.0 ms

Frames: 6.1 - 6.36

Fig. 13, frame 6.28 shows the outline and the surface of the vapour film surrounding the Al_2O_3 droplet in the film boiling state. Indentations observed at the left and right edge are caused by horizontal orbital surface waves of the water projecting into the boiling film. The droplet itself is not observable; neither is the thickness of the vapour film. Section 5.3 showed that at a droplet temperature around 2313 K the vapour film will have a thickness of 0.6 to 0.9 mm (wave crest and wave trough of the water). The droplet temperature in this experiment was higher by 270 K, i.e. 2570 K, so that the vapour film should be somewhat thicker than that evaluated in Section 5.3.

An unsymmetrical vapour trail has formed in the upper section which is also fed by the vapour generated in the bottom section. The vapour is transported to the upper section due to the pressure difference (which also includes buoyancy effects) arising between the lower and upper stagnation points. The presence of entrained air can be excluded as the vapour trail condenses almost completely shortly after the pressure peak (frame 6.49).

Phase II: Compression

Time: 0.0 - 0.145 ms

Frames: 6.36 - 6.50

In order to determine inhowfar a thermal reaction will cause a deviation from the trigger-induced pressure history alone, the pressure at P1 of experiment AOW 6 and a reference trigger pressure ($P1^{Trigger}$) are shown in Fig. 11. The latter was recorded during a preliminary test with a solidified droplet whose temperature was just below the melting temperature. The droplet did not fragmentate, so the pressure history was not changed in any significant degree; instead of a sinusoidal trigger pressure peak as in Fig. 7, we find a pressure peak superposed by four oscillations as in Fig. 8.

The vapour film enveloping the droplet is compressed parallel to the rise of the trigger-induced pressure. This is clearly seen in the size of the normalized area A*, which decreases continuously from 1 to 0.7 (Fig.11).

Detailed observations show that shortly after the onset of the trigger-induced pressure rise, a short pressure pulse occurs which is not observed in the reference trigger. The corresponding frames (39, 40) show no noticeable changes. In the matching of the frames, the shifting of the pressure signals by two frames as explained in Section 5.1 has already been taken into account. Immediately after this, there is another pressure rise which later continues up to 1.2 MPa above the reference trigger. In frame 6.42 the first visible change is a thin white line below the droplet equator. Level with this line, the picture of Phase I (frame 6.28) shows a wave crest of the water projecting into the vapour film at the right edge of the contour. This first line has disappeared in the next frame (6.43). Instead, there is a new, clearer line at the droplet equator with a wave crest on its right end directly at the droplet contour. As the further evaluation shows, the white lines have no influence on the fragmentation process. At the same time, an evaporation bubble forms in the stagnation point, which indicates initial interactions between droplet surface and water. The resulting pressure rise propagates in the water and superposes on the trigger pressure (Fig. 11). This first reaction pressure follows the arrival of the external trigger pressure wave with a delay of only about 100 µs. The process can thus be considered as a prompt reaction. This reaction which was not expected because of the large difference between contact temperature and critical temperature of the water was observed only in the tests with high trigger pressures. As the reaction pressure propagates as a spherical

wave it is evident that the local peak pressure was higher than the peak measured in P1 at the vessel wall. In P2, the superposed pressure increase due to the reaction cannot be quantified as it coincides with the second trigger pressure pulse (see Section 5.5).

Starting from the droplet equator, the vapour trail collapses within the next 0.04 ms, during which a circumferential bright zone is observable in frames 6.44 to 6.47. This suggests formation of a different structure of the water/vapour interface during shrinkage of the vapour volume resulting in a more diffuse reflection of the impinging light. Due to the higher pressure, the saturation temperature of the water increases, so that the vapour is not only compressed but also partly condensed. During the collapse the water is accelerated towards the droplet. The velocity of the interface in the droplet direction was determined from frames 6.44 and 6.48, whose contours are presented in Fig. 12. The velocity is about 4 m/s in the bottom section and 10 to 17 m/s in the vapour trail.

In frame 6.48, the minimum volume of the vapour film is determined: $A^* = 0.7$. The point of time at which the recorded pressure reaches its peak (1.9 MPa) is about 0.02 ms later (Fig. 11). The two events coincide if the transit time of the pressure wave from the droplet to the transducer is taken into account.

Phase III: Thermal Reaction

Time: 0.15 - 0.25 ms

Frames: 6.51 - 6.61

At the onset of this phase, the reaction pressure decreases to the level of the reference trigger pressure within a time of 0.03 ms. This causes the saturation temperature of the water to decrease by about 45 K, and additional evaporation will occur as a result of overheating of the water boundary layer. In addition, the vapour compressed during Phase II will reexpand. As the size of the normalized area A^* increases from 0.7 to far beyond 1, there must be still another cause for the enhanced evaporation.

In the stagnation point, the vapour bubble which was almost invisible in frame No.6.48 begins to grow again. Irregular vapour clouds form in the upper hemisphere of the droplet, whose outlines move away from the droplet at a speed of up to 55 m/s (Fig. 13, frames 6.52, 6.56, 6.60, Fig. 12). In the preceding Phase II, this was the region where the water/vapour interface reached its maximum velocity moving towards the droplet. It is therefore assumed that the enhanced evapora-

tion in the region of the original vapour trail is caused by intensive contact between droplet and water. The film frames give no indication of whether this contact is due to the water/vapour interface approaching the hot droplet, by impinging or penetrating water droplets, or by jets.

Phase IV: Transition

Time: 0.26 - 0.43 ms

Frames: 6.62 - 6.78

Although the pressure decreases by 0.6 MPa to the initial system pressure, there is no further expansion of the vapour clouds (Pictures 6.64 and 6.72); instead, the normalized area A* decreases from 1.7 to 1.6. One possible explanation is that enhanced vapour formation on top of the droplet during Phase III had a slowing-down effect on the water front moving towards the droplet, and that the water is separated again from the hot droplet by restoration of the boiling film. There is more vapour condensing on the cold water surface than is being produced.

The pressure integral over time, $\int p_1 dt$, up to the end of this phase (see Table 1) amounts to 240 Pa s, i.e. it is higher by 15% than the pressure integral of the trigger alone (208 Pa s).

Phase V: Deformation and Coarse Fragmentation

Time: 0.44 - 7 ms

Frames: 6.79 - 6.400 (End of film at 3.68 ms)

During this whole phase, the pressure is below the initial system pressure. The reference trigger pressure curve is similar, only its time to recompression is shorter by 3 ms. During the first 0.3 ms (Fig. 14, frame No.6.88), cavitation bubbles form in the water, due to tensile stresses induced in the water by the slowing-down of the water column in its upward movement (see Section 5.5).

The droplet widens from the top, accompanied by continuously growing vapour clouds in this region. At the end of the film record, the equatorial diameter of the droplet has increased to 3.5 times its initial size. Fig. 10 shows the growth of the diameter. In Fig. 14, frame 6.404, the flash of light has faded almost completely, and the self-luminosity of the fragments is visible through the vapour film. The top region of the droplet is distorted in a cup-like geometry, and a rim of coherent fragments has formed. In the bottom section, only isolated spherules are visible which were ejected from the droplet.

Phase VI: Recompression

During this phase the following recompression peaks are observed:

Time:	7.2	11.7	13.6 ms
Pressure peak:	0.5	0.4	0.23 MPa

As explained in the description of the trigger pressure curve, a pressure pulse generated at the bottom of a vessel with a free liquid surface will accelerate the liquid column in the upward direction. It will take some time for the liquid column to return to its original position in a so-called recompression process which is accompanied by another pressure pulse. The time interval between the pulses depends on the magnitude of the first pressure pulse. Between the two, the pressure drops below the initial system pressure. In the pressure curve of Fig. 9, three further pressure peaks with decreasing amplitudes are visible. As the recording frequency was only 1/50 of the detail record, the pressure peaks usually are not recorded; for example, the reaction pressure peak was registered at only half its amplitude.

The signal of the photocell (Fig. 9) suggests that the fragments are still luminous during the second and third pulse, possibly accompanied by further fragmentations.

Description of the Fragments

The histogram of Fig. 16 shows that more than half of the 500 fragments collected were smaller than 0.4 mm, and only 8 fragments were bigger than 2.5 mm. The applied scanning with a minimum fragment size of 0.2 mm is sufficient as no smaller fragments were found in this experiment. Most of the fragments are molten spheroids; some are agglomerates, and a small fraction is of oblong shape. Their surfaces are smooth and crossed by partly fused crystal boundaries (see Fig. 15).

6.2.2 Experiment AOW 4

Experimental parameters:

Droplet diameter	4.9	mm
Starting temperature	2350	K
Reaction temperature	2313	K

Trigger pressure	0.95	MPa
Framing rate	$4.5 \cdot 10^4$	f/s

A frame n of the drum camera can be matched to the time t in this experiment by:

$t = 0.22\ n - 1.6;$ t in ms

The transient recorder was not available for experiment AOW 4, so the pressure curve is presented only in a photographic image of a storage oscilloscope screen (Figs. 17,18), whose scanning frequency was only 1/10 of that of the transient recorder. The framing rate was only half as high as in the later experiments.

The pictures of Phase I have already been described in detail in Section 5.3. Details of the fragmentation process are not clearly visible on the film frames (Fig. 19). The reaction process differs somewhat from experiment AOW 6, in that evaporation clouds are formed not only on top of the droplet but on all sides. Fragmentation starts from the top as well, but not in a cup geometry but rather in the manner of an inflated balloon.

The droplet is completely fragmented although the calculated reaction temperature (Table 1) is just at melting temperature. Fig. 20 shows that all fragments are molten spheroids. The histogram of fragments in Fig. 16 shows that about 750 fragments have been produced, i.e. about 250 more than in experiment AOW 6.

6.3 Experiments with Medium Trigger-Induced Pressure

6.3.1 Experiment AOW 8

Experimental parameters:

Droplet diameter	5.7	mm
Starting temperature	2580	K
Reaction temperature	2470	K
Trigger pressure	0.66	MPa

A frame n of the drum camera can be matched to the time t in this experiment as follows:

$t = 0.01\ n - 0.51;$ t in ms

Figs. 21, 22, 23 present the pressure history of this experiment in different time scales.

Short Description of the Experiment

The boiling film around the droplet, as well as the vapour trail on top of the droplet, are compressed by the trigger pressure. Initial changes are observed only in the horizontal orbital waves of the water towards the boiling film (not in the stagnation point). The pressure does not rise above the given trigger pressure but oscillates around it. The vapour trail does not collapse completely and expands to its original size after the pressure peak. After this, the shape of the vapour trail changes as if by vapour expansion from the center of the upper droplet hemisphere. While the pressure drops to the initial system pressure, the area defined by the water/vapour interface remains constant. The pressure then drops below the initial system pressure, and cavitation bubbles start to form in the water (0.12 ms). Starting from the upper droplet section, a vapour bulging progagates whose diameter has doubled at the level of the droplet equator after 5.5 ms. The final pictures show the droplet deformed to a cup-like geometry. This is followed by a violent thermal reaction with a pressure far beyond 2 MPa. After this, six further pressure pulses of decreasing amplitudes are registered.

In the following, the experimental phases will be described as in Experiment AOW 6.

Phase I: Film boiling

Time: -0.49 - 0.0 ms

Frames: 8.1 - 8.50

The boiling film around the falling droplet (Fig. 25, frame No. 8.50) looks similar to experiment AOW 6, except that the vapour trail has a plane, symmetrical upper edge. This may be due to the fact that the droplet temperature in this experiment was lower by about 100 K.

Phase II: Compression

Time: 0.0 - 0.22 ms

Frames: 8.51 - 8.73

In Fig. 23, apart from the pressure P1 and the normalized area A*, the course of a reference trigger pressure is shown which was recorded shortly before the experiment (no hot droplet in the experimental vessel).

The first significant changes in the droplet are observed after 0.07 ms (frame 8.58): A thin, horizontal line appears in the bottom quarter of the droplet, at whose level there is a wave crest of the water at the vapour outline . During the next 0.03 ms, the white line moves upwards from frame to frame, i.e. while the trigger pressure rises, certain changes of the vapour state are induced in the region of the wave crests, due to their shorter distances from the droplet surface. From the framing sequence and the spacing of the lines, the white lines are found to move at a speed of 55 m/s, i.e. about 1/10 of the measured propagation velocity rate of the trigger-induced pressure pulse between the two pressure transducers.

In contrast to experiment AOW 6, there is no permanent pressure rise beyond the trigger pressure, i.e. no autocatalytic effect. Indeed, the pressure rise is slower than for the trigger alone; an overshoot of 0.19 MPa is observed only at the end of this phase. In this case, the vapour trail is not compressed completely, and the normalized area A* remains at a constant minimum value of 0.7 for a period of 0.04 ms. The velocity of the water front moving towards the droplet (Fig.24) is about 2 m/s in the lower section of the droplet and about 12 m/s in its upper section. At the starting point of the vapour trail, the condensation front moves tangentially to the droplet surface at a speed of 25 to 30 m/s. In this phase, there is no change in the stagnation point; the sickle-shaped reflection of the flashing light is undisturbed.

Phase III: Thermal reaction

Time: 0.22 - 0.31 ms

Frames: 8.73 - 8.82

In this phase, the pressure drops below the trigger pressure by the same amount as it was above the trigger pressure and then returns to the trigger pressure at the end of this phase. The saturation temperature of the water therefore drops only by 10 K, so that no high overheating energy is available for enhanced evaporation. Compared with experiment AOW 6, the vapour clouds on top of the droplet expand more slowly and to a smaller volume; the normalized area A* increases only to 1 and not to 1.7. The expansion velocity of the vapour/water inter-

face is about 2 m/s in the bottom section of the droplet and about 22 m/s in its top section (Fig. 24).

Directly above the droplet equator, there is a zone of small, slowly growing bubbles indicating reactions in this region which may be caused by the tangential movement of the water boundary layer in the preceding phase.

Phase IV: Transition

Time: 0.31 - 0.46 ms

Frames: 8.82 - 8.97

During this phase, the normalized area A* remains constant at 1 although the pressure drops by 0.5 MPa to nearly the initial system pressure. The evaporation at the droplet equals the condensation at the water/vapour interface. The shape of the vapour trail changes as if by vapour propagation from the "north pole" of the sphere.

In the lower stagnation point, a vapour bubble about 1 mm in diameter has formed which does not expand further. The rest of the bottom section of the droplet has a more or less smooth surface.

The pressure integrated over time from the onset of the trigger to the end of this phase (see Table 1) amounts to 164 Pa s, i.e. the same value as for the trigger alone. This indicates that no significant energetic reactions have occurred, so far.

Phase V: Fragmentation

Time: 0.46 - 6 ms

Frame: 8.97 - 8.406 (film ends after 3.56 ms)

Once the pressure has dropped below system pressure, it remains at this lower level during the whole of Phase V (see Fig. 22). Continuously growing vapour bubbles are formed in the bottom section of the droplet, and the vapour trail now starts to expand beyond its initial dimensions.

Compared with experiment AOW 6, frames 8.104 to 8.116 show only a few cavitation bubbles in the water; these remain stable for only 0.12 ms, as the pressure increases to system pressure for a short period of time.

The droplet with the surrounding vapour bubbles starts to widen. Isolated vapour eruptions occur but no fragments are visible (see Fig. 26). On the last frames, the

droplet diameter can be seen to have grown to 2.5 times its initial size. Due to its self-luminosity the droplet is visible through the vapour film; it is deformed to a cup geometry with a smooth surface.

Phase VI: Recompression

Time:	6.6	23.8	28.2	32.4	36.1	39.2	41.9	44.9	ms
Pressure peak:	$\gg 2$	0.61	0.26	0.19	0.1	0.11	0.10	0.07	MPa

Induced by the recompression of the water column, a reaction occurs after 6.6 ms which makes the pressure at P1 and P2 rise far above the measuring range of 2 MPa, owing to the fact that the droplet now deformed to a cup geometry offers a large coherent contact surface for the reaction. Possibly, the droplet has given off so much energy that it is already partly solidified. However, an estimate of the heat losses occurring during the time period of 6.6 ms between trigger incidence and recompression assuming both, a surface three times larger than in the pictures, and a heat transfer three times higher corresponding to film boiling conditions yields a temperature drop of only about 20 K.

Until the next pressure pulse after 17 ms, i.e. outside the film window (Fig. 21), the photocell signal indicates intensive self-luminosity of fragments in its recording field. The further pressure pulses again follow at certain intervals depending on the heights of the preceding pressure pulses.

Description of Fragments

Of the fragments collected in this experiment, the number of fine fragments was several times larger than in the other experiments as shown in the histogram of Fig. 28. The total number of 2500 fragments in Fig. 28 was determined by counting an estimated sub-fraction.

Many fragments were much smaller than 0.2 mm, so another method was applied for determining the per cent fragment size distribution for fragments with diameters between 0.001 and 0.2 mm. For this purpose, part of the fragments were dispersed in water and sized using a laser. The largest fraction, i.e. 31.4%, was in the range between 0.096 and 0.128 mm. The smallest fragments were 0.02 mm in diameter, with a fraction of 4.2%. The result was not entered in the histogram as this second technique yields only per cent fractions.

The picture of several fragments in Fig. 27 shows that only few fragments are spherical. Most of the fragments are of irregular shape, partly with a surface having a coarse crystalline structure.

6.3.2 Experiment AOW 7

Experimental parameters:

Droplet diameter	5.8	mm
Starting temperature	2570	K
Reaction temperature	2460	K
Trigger pressure	0.66	MPa

A frame n of the drum camera can be matched to the time t in this experiment by:

$t = 0.0098\,n - 0.50$; t in ms

Figs. 29, 30, 31 show the pressure curves of this experiment in different time scales.

Short Description of the Experiment

Both the boiling film around the droplet and the vapour trail in the wake region above the droplet are compressed by the trigger pressure. Initial changes are observable only in the horizontal orbital surface waves of the water at the boiling film (not in the stagnation point). The pressure does not rise above the given trigger pressure but oscillates around it. During pressure rise, the vapour trail condenses almost completely. During pressure drop, a three-part vapour cloud is formed on top of the droplet and then condenses partly. While the pressure drops back to system pressure, the normalized area A* first remains constant and then increases continuously in size. Cavitation bubbles are visible in the water almost during the whole time of 3 ms during which the pressure remains below the initial system pressure. The droplet is enveloped in vapour clouds on all sides. The final frames coincide with the recompression of the water column. During this pressure rise, the vapour clouds around the droplet condense. After this, the droplet is seen to have been broken up irregularly, among others into bigger or smaller spherical, molten droplets. The reaction pressure caused by recompression reaches the amplitude of the trigger pressure pulse. This is followed by 15 further pressure pulses of 0.15 to 0.1 MPa at intervals of about 3 ms.

Phase I: Film boiling

Time: -0.51 - 0.0 ms

Frames: 7.1 - 7.51

The boiling film around the falling droplet is deformed by four horizontal orbital surface waves of the water projecting into the boiling film (Fig. 33, frame 7.44). The vapour trail is of conical shape.

Phase II: Compression

Time: 0.0 - 0.19 ms

Frames: 7.51 - 7.71

Apart from the pressure P1 and the normalized area A*, Fig. 31 shows also the pressure history of a reference trigger recorded shortly before the experiment (no hot droplet in the experimental vessel). It takes 0.09 ms for the first visible changes in the droplet to occur in frame 7.61: A thin, horizontal white line is visible in the bottom quarter of the droplet at whose level there is a wave crest of the water at the vapour outline. During the next 0.03 ms, the white line moves upward from frame to frame. This again suggests changes of the vapour state in the region of the wave crests protruding into the boiling film. There is no marked pressure rise beyond the trigger pressure until 0.17 ms after the onset of the trigger ($\Delta p \approx 0.2$ MPa). Frame 7.71 shows how the vapour trail is condensed resp. compressed except for a small part. The normalized area A* has its lowest value here, i.e. 0.7. From frame No.7.65, there are irregularities in the boiling film in the lower stagnation point which, however, are found to have disappeared after 0.06 ms. The velocity of the water front moving towards the droplet (Fig. 32) is about 2.5 m/s in the bottom section of the droplet and about 15 m/s in its top section. At the starting point of the vapour trail, the condensation front has a velocity of 22 to 25 m/s.

Phase III: Thermal reaction

Time: 0.19 - 0.27 ms

Frames: 7.71 - 7.79

In this phase, the pressure (Fig. 31) drops below the trigger pressure by the same amount it had risen before and then rises again to meet the reference trigger pressure at the end of this phase. The saturation temperature of the water is reduced by only about 11 K, so that there is no high overheating energy available

for enhanced evaporation as in experiment AOW 6. The volume of the vapour trail expands only slightly, so that A* increases to only 0.85. The boiling film around the top half of the droplet is not as smooth as in Phase I, which possibly suggests a reaction in this region. The expansion rate of the vapour film is about 2.5 m/s in the bottom section of the droplet and up to 38 m/s in the center of the vapour trail (see Fig. 32).No widening of the droplet is observed in this phase.

Phase IV: Transition

Time: 0.27 - 0.46 ms

Frames: 7.79 - 7.98

The pressure (Fig. 31) continues to oscillate remaining on average below the reference trigger pressure; at the end of this phase, it drops to the initial system pressure. The pressure integrated over time from the onset of the trigger to zero crossing was found to be 162 Pa s, i.e. almost as much as for the trigger alone (see Table 1). This means that the reactions so far were not accompanied by any highly energetic reaction.

There is hardly any visible change of the droplet surface in the film frames. At the end of this phase, the vapour cloud on the droplet surface expands, so that A* returns to 1 in an irregular course.

Phase V: Deformation and Coarse Fragmentation

Time: 0.46 - 3.5 ms

Frames: 7.98 - 7.405 (end of film at 3.53 ms)

Almost during the whole of Phase V, the pressure remains below system pressure by about 0.1 MPa, i.e. at absolute zero (see Fig. 30). Cavitation bubbles are visible in the water more or less clearly from frame 7.104 to frame 7.360 in Fig. 34. The cavitation bubbles do not collapse after 0.35 ms at the latest as in the other experiments but remain stable for nearly 3 ms; this is interpreted as being due to the pressure remaining at absolute zero without any oscillations.

The whole droplet is enveloped in continuously growing vapour bubbles. After about 1 ms, the vapour clouds are partly broken up in the upper section of the droplet (frame 7.160). From frame 7.200, there is no further expansion of the vapour bubbles, and from frame 7.280 there are reddish, luminous film boiling bubbles around single fragments. The pressure increases again at the end of this phase. The vapour bubbles condense, and the fragments formed in the meantime

are enveloped in transparent boiling films, which can be seen in flashlight reflections at the bottom outline.

Phase VI: Recompression

Time:	3.7	6.6	9.0	12.0	14.5	17.1	20.1	23.5	ms
Pressure peak:	0.9	0.14	0.17	0.18	0.13	0.11	0.09	0.09	MPa

The recompression induces another reaction in the coarsely fragmented droplet. A pressure rise is initiated which is in the same order of magnitude as the first, trigger-induced pressure pulse. It is assumed that this is the point of fragmentation proper into more than 500 fragments. The signal of the photocell is rather weak in this phase, suggesting a small size or low luminosity of the fragments. The further pressure pulses follow at intervals determined by the heights of the preceding pressure pulses.

Description of the Fragments Collected

The histogram of the fragments collected in this experiment (Fig. 28) has a similar characteristic as the histogram of experiment AOW 6, but there are some incrustations which probably were not further fragmented during the second fragmentation event. A picture of some fragments (Fig. 35) shows partly spheroidal fragments and some smaller fragments, most of which have smooth-molten surfaces.

6.4 Experiments with Low Trigger-Induced Pressure

At low pressures, the course of the trigger pressure is not as well reproducible as at medium and higher pressures. Both the height and the shape of the pressure pulse may vary due to friction in the magnetic hammer.

6.4.1 Experiment AOW 9

Experimental parameters:

Droplet diameter	5.9	mm
Starting temperature	2380	K
Reaction temperature	2313	K
Trigger pressure	0.25	MPa

The approximated reaction temperature showed that the droplet had already cooled down to melting temperature. As it was fragmented during this experiment, it is to be assumed that it was still in the liquid phase at least in its interior.

In this experiment, a frame n of the drum camera can be matched to the time t by

$t = 0.01\,n - 0.96$; t in ms

Figs. 36, 37, 38 show the pressure history of this experiment on different time scales.

Short Description of the Experiment

The vapour trail of the droplet is particularly long in this experiment. The increasing trigger pressure causes only a single change in form of a line running around the droplet at the level of the droplet equator, from which the vapour trail is compressed. A reaction in the region of the upper hemisphere of the droplet is observable even before it becomes visible after collapse of the vapour trail. A cylindrical, opaque vapour space is formed which remains below the diminishing vapour trail. The pressure curve is irregular, with four pressure peaks. During the third peak, A* reaches its minimum value, and the remainder of the vapour trail is cut off from the droplet. Until the fourth pressure peak, both the boiling film and the vapour trail re-expand and remain constant until the initial system pressure is reached again. No cavitation bubbles are observed in the water during the subsequent phase of negative pressure. As in the other experiments, the droplet is enveloped in vapour clouds. After about 2 ms, the pressure rises again, and the vapour bubbles recondense. The final frames show that part of the droplet is cut off in the upper droplet hemisphere. After this, there is another 2 ms phase of negative pressure, and then the pressure returns to the initial system pressure. The droplet was broken up into two fragments of unequal size in this experiment.

Phase I: Film boiling

Time: -0.96 - 0.0 ms

Frames: 9.1 - 9.95

In the colour frames, the droplet is visible through the boiling film. In the wake region on its top, there is a rather long, nearly symmetrical vapour trail with two radial contractions.

Phase II: Compression

Time: 0.0 - 0.26 ms

Frames: 9.95 - 9.122

Fig. 38 shows the pressure P1 and the normalized area A*. At 0.08 ms after the trigger pressure rise, the first change is visible in an inclined annular zone at the level of the droplet equator (Fig. 40, frame 9.104). In contrast to the experiments with higher trigger pressures, there are no further reactions in other annular zones; instead, from the next picture the condensation of the vapour trail starts from this annular zone.

No velocity of the water/vapour interface towards the droplet is observed in the bottom section of the droplet (see Fig. 39). At the top of the vapour trail, the velocity was 14 m/s, and at the periphery of the vapour trail about 20 m/s.

Phase III: Thermal Reaction

Time: 0.16 - 0.34 ms

Frames: 9.112 - 9.130

In this experiment, Phases II and III interfere, i.e. initial thermal reactions are observed in the upper hemisphere of the droplet even while the boiling film is still in the compression resp. condensation stage. In frame 9.112, light spots are observed in the upper hemisphere from which a cylindrical vapour volume starts to form. As this vapour volume continues to expand in the axial direction also during the pressure rise, it is assumed to be caused by a thermal reaction. A similar phenomenon was observed in experiment AOW 8, while the upper droplet hemisphere remained completely smooth during experiment AOW 7. The vapour trail does not condense completely but is separated from the droplet. During the pressure drop from the third pressure peak until the rise to the fourth pressure peak, A* increases from 0.63 to 0.84. At the same time, the contour of the vapour trail expands at a rate of 9...23 m/s (see Fig. 39).

Phase IV: Transition

Time: 0.34 - 0.48 ms

Frames: 9.130 - 9.144

During this phase, the pressure drops to the initial system pressure. The film frames show only a slight growth of the vapour/water interface in the radial direction. The axial growth has reached the upper edge of the frame, so that A* is no longer clearly defined.

Phase V: Deformation

Time: 0.48 - 2.75 ms

Frames: 9.144 - 9.371

Once the pressure has fallen below system pressure, it remains at this level for 2.25 ms (Fig. 37). The vapour clouds enveloping the droplet (diameter 7.5 mm) do not expand at the droplet equator; instead, there is a radial expansion of the vapour contour from 5.2 mm to 13 mm on top of the droplet. The deformation of the droplet is not yet visible in these pictures on account of the vapour clouds.

Phase VI: Recompression

Time: 2.75 - 3.25 ms

Frames: 9.371 - 9.406 (film ends at 3.1 ms)

The pressure rise due to recompression causes recondensation of the the vapour clouds. Fig. 40, frame 9.406 shows the self-luminosity of the fragmented droplet through the remainder of the boiling film. The bottom part remains a compact hemisphere, and the upper part is cut off and flattened.

The last frame in Fig. 40 shows the two fragments; the bigger fragment has a half-cylindrical shape while the smaller one is an irregular, hollow fragment.

6.4.2 Experiment AOW 11

Experimental parameters:

Droplet diameter	5.6	mm
Starting temperature	2300	K
Reaction temperature	2313	K
Trigger pressure	0.25	MPa

The measurement of the droplet surface temperature prior to immersion in the water yielded a value below the melting temperature of Al_2O_3. The droplet was deformed during the experiment, so it must be assumed that it was still liquid inside.

A frame n of the drum camera can be matched to the time t as follows:

$t = 0.01\,n - 0.21$; t in ms

Figs. 41, 42, 43 present the pressure history of this experiment in different time scales.

Short Description of the Experiment

In the film frames of this test, the droplet is displayed close to the top edge of the frame (Fig. 45). It has a clearly visible, relatively small vapour trail. There are four indentations of the water into the boiling film. As in experiment AOW 9, the only change observed during the trigger-induced pressure rise is on an annular zone. The vapour trail is not completely compressed resp. condensed in this experiment and thus not separated completely from the droplet. Although there is a reaction on the upper hemisphere, it is not as marked as in experiment AOW 9. The minumum value of A* is reached 0.13 ms before the peak pressure. While the pressure drops to the initial system pressure, there are no changes in the droplet. In the following negative pressure phase of 1.5 ms, there are no cavitation bubbles in the water. The vapour clouds around the droplet widen by only 20%; an annular bulging is formed in the upper droplet hemisphere. After this, the pressure rises to 0.03 MPa, and the vapour clouds slightly decrease in size. After another period of negative pressure, the vapour zone re-expands. On the final frames, the self-luminosity of the droplet is visible as an irregular shape through the vapour film. The collected droplet proves that only deformation took place during this experiment: The droplet was widened and distorted into a cup geometry.

Phase I: Film boiling

Time: -0.21 - 0.0 ms

Frames: 11.1 - 11.21

The droplet is enveloped in a vapour film which is deformed by four indentations at the water/vapour interface. The vapour trail is rather small and non-symmetrical.

Phase II: Compression

Time: 0.0 - 0.28 ms

Frames: 11.21 - 11.49

Fig. 43 shows the pressure P1 and the normalized area A*. At 0.12 ms after the trigger pressure rise, the first change is observed along an annular zone just below the droplet equator. There, on the left and right edges of the contour, there are indentations of the water into the boiling film (Fig. 45, frame 11.33). The next frame shows a similar zone at the level of the droplet equator, which remains stable during the next frame; after this, the vapour trail is compressed from this region. The water front moves towards the droplet at a velocity of 10...22 m/s (see Fig. 44).

Phase III: Thermal Reaction

Time: 0.28 - 0.41 ms

Frames: 11.49 - 11.62

In this experiment, too, there is a thermal reaction while the trigger pressure is still rising. No change is observed in the droplet itself, as in contrast to experiment AOW 9. The only evidence of a reaction is the expansion of the vapour trail.

The expansion rate of the vapour trail is only 8 m/s (see Fig. 44).

Phase IV: Transition

Time: 0.41 - 0 ms

Frames: 11.62 - 11.81

The outline of the expanding vapour trail has reached the upper edge of the film frames. No further expansion is observed in the visible region while the pressure drops to the initial system pressure.

Phase V: Deformation

Time: 0.60 - 2.1 ms

Frames: 11.81 - 11.231

While the pressure remains below system pressure, there is a linear expansion (about 20%) of the vapour clouds around the droplet and an annular ring of vapour bubbles forms in the upper droplet hemisphere.

Phase VI: Recompression

Time: 2.1 - 2.9 ms

Frames: 11.231 - 11.311 (film ends at 3.87 ms)

The recompression amplitude is small (about 0.04 MPa). There is another linear expansion of the vapour clouds by 5% as referred to the onset of Phase V.

After recompression, the pressure oscillates below the system pressure more than ten times with decreasing amplitudes. Frame 11.408 in Fig. 45 shows the self-luminosity of the droplet. The irregularly formed vapour bubbles around the droplet cause a noncircular, striated distortion of the droplet image.

The last frame of Fig. 45 shows the solidified droplet. It has a cup geometry, its surface is smooth. Droplets falling through the water in preliminary experiments without external trigger as a rule also had a hole in their surface but were not as deformed as in this experiment.

7. Summary Description of the Observed Reaction Processes

Boundary Conditions

Coolant: Water of room temperature in an open vessel

Hot droplet: Al_2O_3 heated above melting temperature by up to 260 K; mass of 0.2 g to 0.3 g; diameter between 4.9 mm and 5.9 mm;

Trigger levels: Low pressure pulse of 0.25 MPa, medium pressure pulse of 0.66 MPa, high pressure pulse of 0.95 MPa.

Phase I: Film Boiling

The hot droplet falls through the water enveloped in a vapour film. The boiling film is about 0.7 mm thick in the lower droplet section and is deformed by horizontal orbital surface waves of the water with amplitudes of $\pm$ 0.1 mm. In the wake region on top of the droplet there is a normally irregularly shaped vapour trail whose thickness in the radial direction is up to 1.5 to 2.5 mm.

Phase II: Compression

A low or medium trigger pressure pulse induces compression and condensation of the boiling film and vapour trail but no direct reaction between droplet and water. The water front is accelerated towards the droplet to a velocity of about

3 m/s in the bottom section and about 8 m/s in the top section. There is no pressure increase; the pressure only oscillates around the given trigger pressure applied.

A higher trigger pressure pulse causes liquid-to-liquid contact in the rear stagnation point of the droplet which results in flash evaporation and a superposed pressure rise. This event occurring shortly after trigger pressure rise is referred to as a prompt reaction. The water front moving from the top towards the droplet reaches velocities of 10 to 17 m/s.

Phase III: Thermal Reaction

While the pressure drops, reactions take place in the regions where the water front was strongly accelerated towards the droplet. Vapour clouds form and expand at a rate of up to 50 m/s in the upper hemisphere. The enhanced local vapour formation slows down the velocity of the water front in the other regions moving towards the droplet and even reverses it. The expansion rates were up to 4 m/s in the lower hemisphere. Water/droplet contacts are cut off by the restored vapour film later.

Phase IV: Transition

In this phase, the pressure drops to the initial system pressure. The outline of boiling film and vapour clouds does not expand further. On the contrary, the vapour volume condensed at the cold vapour/water interface is larger than the new vapour volume generated.

Phase V: Deformation and Coarse Fragmentation

During this phase, the pressure is near absolute zero. After a medium or high trigger pressure pulse, cavitation bubbles form in the water which may remain stable for up to 3ms.

The droplet is enveloped in vapour clouds, first in its upper hemisphere and then throughout. At low trigger pressures the droplet is deformed into a cup geometry; at higher pressures, a rim of fragments is formed. If the initial droplet temperature was near the melting temperature, the droplet may also be fragmented into a small number of spherules.

Phase VI: Recompression

Recompression of the water causes another pressure rise. The vapour bubbles condense, and the boiling film around the droplet fragments is visible again. Big-

ger fragments may be fragmented again by another acceleration of the water front towards the fragment surface. Even after partial solidification, coherent large-surface fragments may react more violently than smaller molten fragments. This is followed by several further phases of negative pressure and recompression in the water depending on the violence of the reaction.

8. Concluding Remarks

The reaction process is determined not only by the trigger magnitude of the pressure peak and the integral of the trigger pulse but also by the subsequent pressure oscillations in the water. Because of the large difference between contact temperature and critical temperature of the water, prompt reactions were observed in the tests with high trigger pressure. Deleayed reactions occurred locally, preferably in the region of the vapour trail.

After the first reaction and the following transition period the pressure in the water becomes negative leading to a certain degree of separation of the water from the hot droplet. The subsequent recompression accelerates the water again in the direction of the droplet.

The existence of the vapour trail in all experiments shows that it would be inappropriate to assume spherically symmetrical conditions in the vapour film. The non-symmetrical conditions govern the break-down process of the film in the case of an external trigger pressure.

9. Nomenclature

Symbols and Abbreviations

A	area within the vapour film contour on the film pictures
A*	normalized area
c_p, c_v	heat capacity at constant pressure, resp. constant volume
f_R	recording frequency
h_f	heat of fusion
n	number
P1	upper pressure transducer
P2	lower pressure transducer
t	time
T	temperature
T_{min}	minimum wall temperature
T_{SN}	spontaneous nucleation temperature
ΔT_{min}	minimum film boiling temperature difference
T_l	contact temperature
T_{melt}	melting temperature
U	charging voltage of the condenser for the magnetic hammer
v	velocity
ß	ratio defined by eqs. (A-3) + (A-4)
λ	thermal conductivity
ρ	density
κ	ratio defined by eq. (A-5)

Subscripts

C	cold
H	hot
I	interface
Liq	liquid
S	solid
sat	saturation

10. References

[1] W. Peppler, W. Till, Mechanisms Observed during Triggered Fragmentation of a Droplet of Molten Alumina in Water, Int. Conf. on the Science and Techn. of Fast Reactor Safety, Guernsey, May 12-16, 1986, Vol. 2, pp. 497-502

[2] M. Ando, Experiment zur getriggerten Fragmentation an einem schmelzflüssigen Kupfertropfen in Wasser, KfK 3667, 1983

[3] H.-J. Zimmer, Investigation of Vapor Explosions with Alumina Droplets in Sodium, KfK 4574e, Febr. 1991

[4] P.J. Berenson, Film Boiling Heat Transfer from a Horizontal Surface, Trans. ASME, J. Heat Transfer **83**, pp. 351-358, 1961

[5] R.E. Henry, A Correlation for the Minimum Film Boiling Temperature, AICHE Symposium Series 70 (1974), No. 138, pp. 81-90

[6] R. Ladisch, Untersuchung der minimalen Filmsiedetemperatur auf keramischen und metallischen Heizern, KfK 2970, 1980

[7] H.K. Fauske, On the Mechanism of Uranium Dioxide-Sodium Explosive Interactions, Nucl. Science Eng. **51**, pp. 95-110, 1973

[8] P.A. Pavlov and E.D. Nikitin, Kinetics of Nuclei Formation in Superheated Water, High Temperature **18**, pp. 292-296, 1980

[9] H.S. Carslaw, J.C. Jaeger, Conduction of Heat in Solids, Clarendon Press, Oxford, 2nd ed., 1959

Annex

Calculation of the Contact Temperature

At sudden contact between a hot and a cold liquid assumed to take place in the form of two semi-infinite slabs (cf. Ref. 9) - the contact temperature T_I will be established instantaneously according to the equation

$$T_I = \frac{T_{melt} + \beta_{C,S}\, T_C\, erf\phi}{1 + \beta_{C,S}\, erf\phi} \qquad \text{(A-1)}$$

where ϕ is the root of

$$\Phi = \frac{c_{p,S}}{h_f \sqrt{\pi}} \left[\frac{(T_{melt} - T_C)\, e^{-\phi^2}}{1/\beta_{C,S} + erf\phi} - \frac{\beta_{H,S}\, (T_H - T_{melt})\, e^{-\phi^2 \kappa_{S,H}}}{1 - erf\,(\phi \sqrt{\kappa_{S,H}})} \right] \qquad \text{(A-2)}$$

with

$$\beta_{H,S} = \frac{\sqrt{(\rho c_p \lambda)_H}}{\sqrt{(\rho c_p \lambda)_S}} \qquad \text{(A-3)}$$

$$\beta_{C,S} = \frac{\sqrt{(\rho c_v \lambda)_C}}{\sqrt{(\rho c_p \lambda)_S}} \qquad \text{(A-4)}$$

$$\kappa_{S,H} = \frac{(\lambda/\rho c_p)_S}{(\lambda/\rho c_p)_H} \qquad \text{(A-5)}$$

The contact temperatures listed in Table 1 are calculated using eqs. (A-2) and (A-3) and the physical properties for water and Al_2O_3 compiled in Table 2.

Table 1: Experimental Data

Exp. AOW	Droplet temperatures, K		Interface temperature at first contact, K	Reference trigger			First reaction			Post examination of fragments, number / size
	Start (Pyrometer)	Estimated just before reaction		Max. pressure, MPa		∫P1·dt, Pa·s	Max. pressure, MPa		∫P1·dt, Pa·s	
				P1	P2		P1	P2		
4	2350	2313[1]	2125	0.95	1.14	260	1.25	1.23	280	some / 1-2 mm many / < 0.5 mm
6	2670	2565	2245	0.95	1.14	208	1.90	1.41	240	some / 1-2 mm many / < 0.5 mm
7	2570	2460	2205	0.66	0.90	164	0.86	0.90	162	crusts many / < 0.5 mm
8	2580	2470	2210	0.66	0.90	164	0.85	0.74	165	some / 1-2 mm many / < 0.5 mm
9	2380	2313[1]	2135	0.25	0.35	63	0.32	0.52	77	two fragments only
11	2313	2313[1]	2105	0.25	0.35	63	0.23	0.30	63	no fragmentation, only deformation

[1] about 4 %, 8 %, and 12 % of the mass solidified in tests 9, 4, and 11, respectively

Table 2: **Thermal-physical Properties of the Test Materials Used for the Determination of T_I**

	$(Al_2O_3)_S$	$(Al_2O_3)_{Liq}$	H_2O
Melting point (K)	2313		
Boiling point (K)		3260	373
Critical temperature (K)			647
Thermal conductivity (W/m K)	6	8	0.6
Specific heat (J/kg)	1300	1320	4184
Density (kg/m^3)	3600	3400	1000
Heat of fusion (J/kg)	$1.067 \cdot 10^6$		

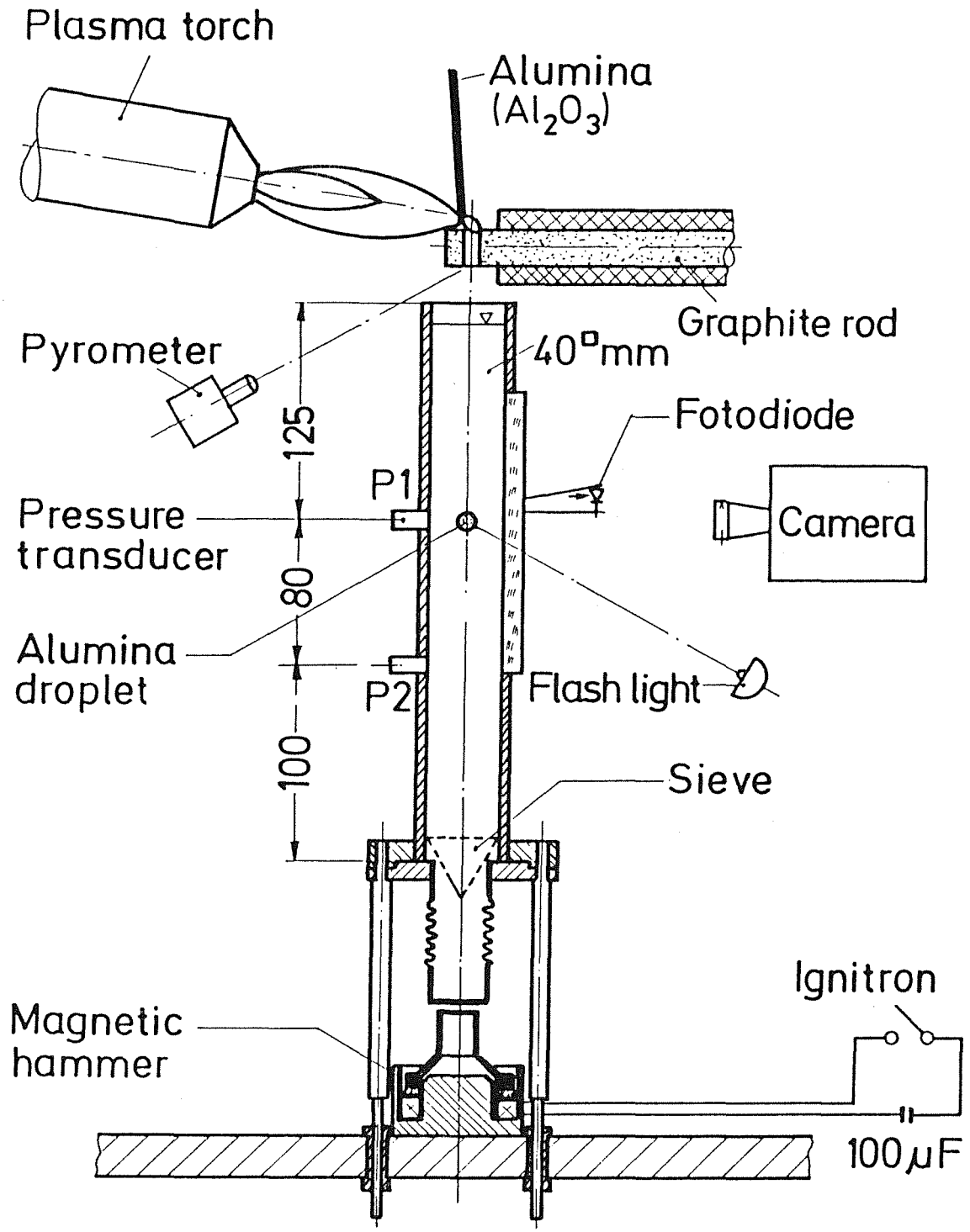

KfK IRE8712071

Fig. 1 Test Set-up

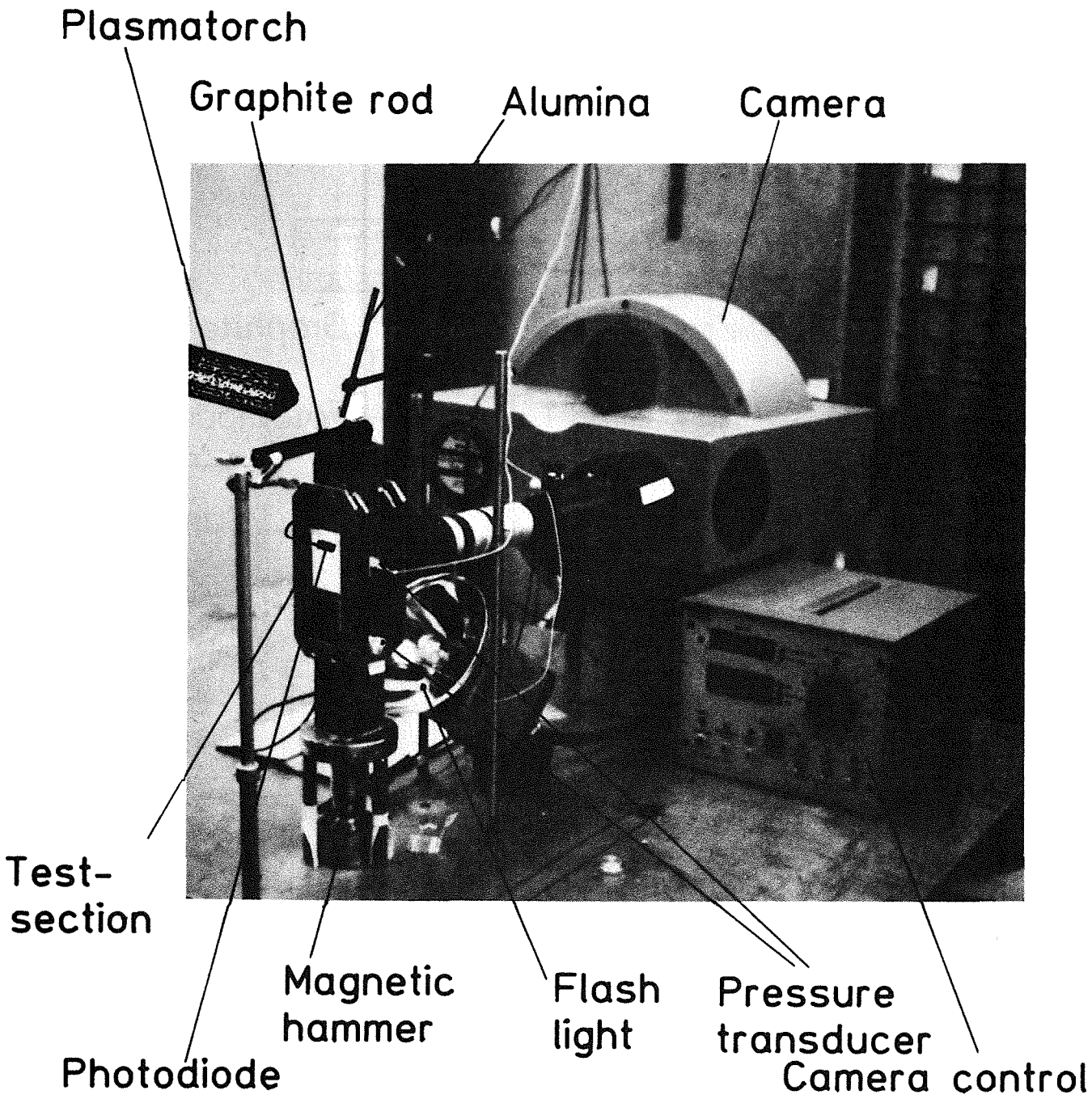

KfK IRE8712072

Fig. 2 Photo of Test Set-up

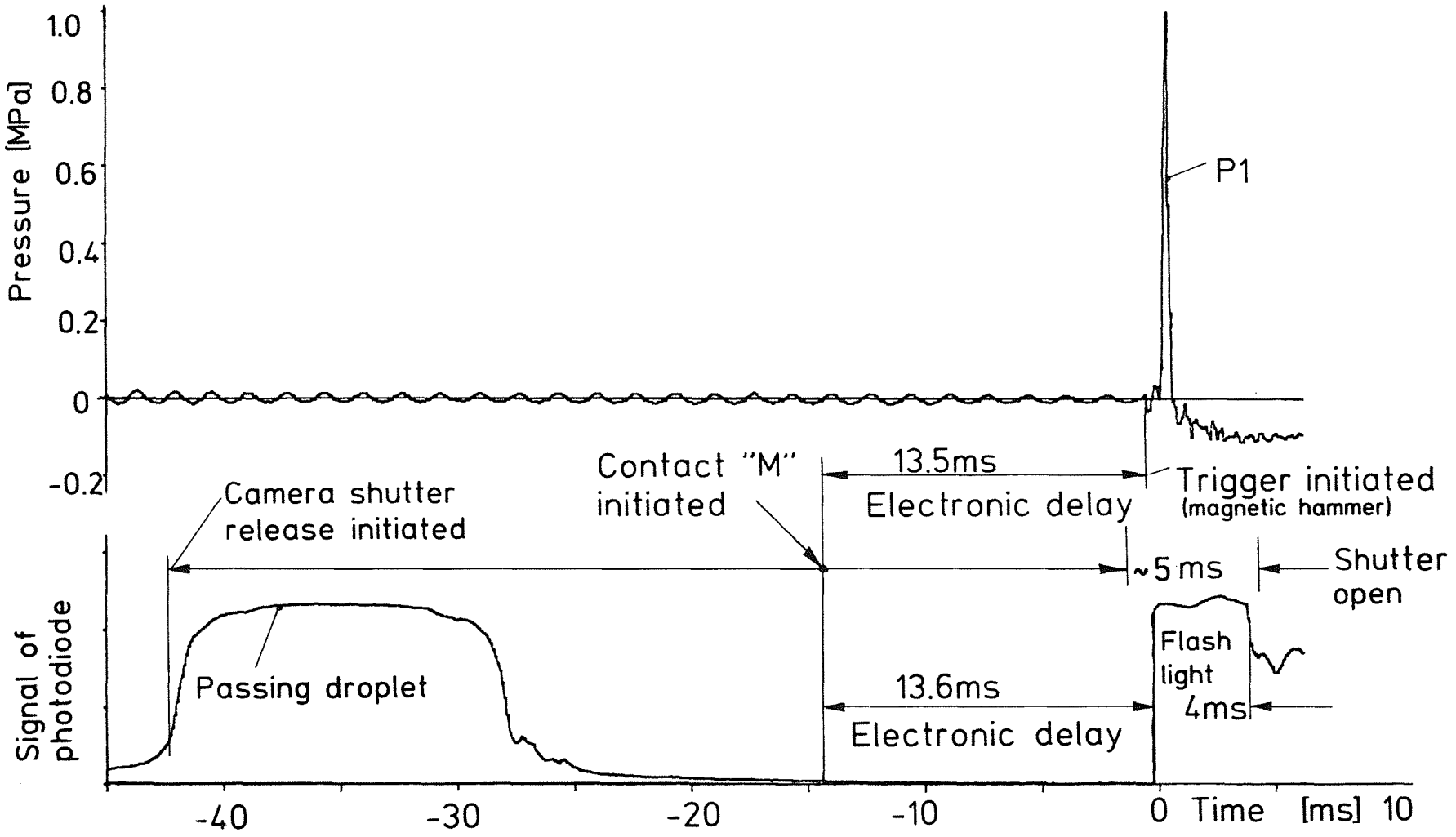

Fig. 3 Test AOW6, Synchronisation of Test Apparatus

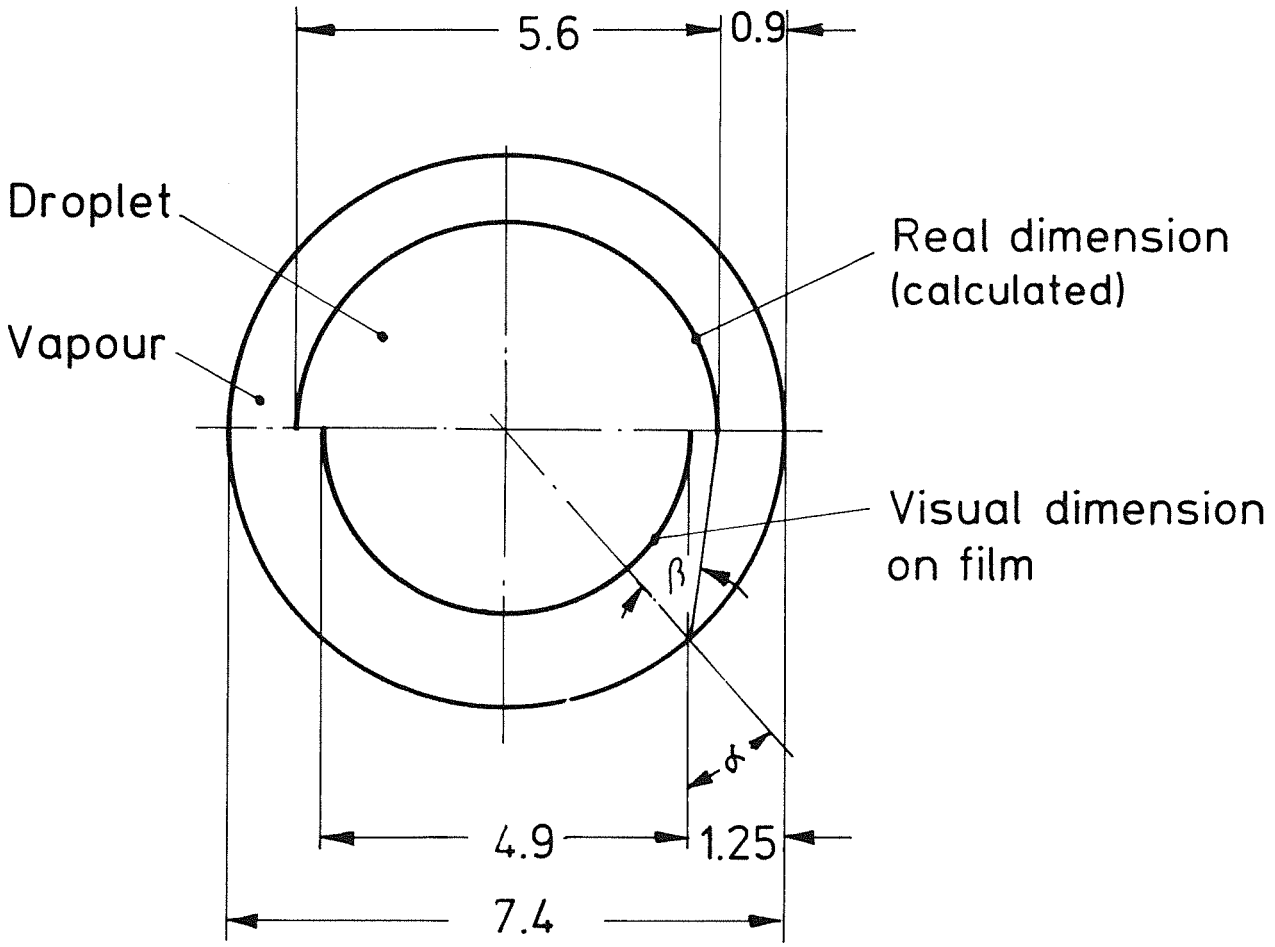

Actual refractive index of vapour:

$$n_2 = n_1 \frac{\sin\alpha}{\sin\beta} = 1.33 \frac{\sin 41^\circ}{\sin 49^\circ} = 1.16$$

$n_1 = 1.33$ for water

Fig. 4 Test AOW11, Correction of Visual Dimension of Droplet on the Film

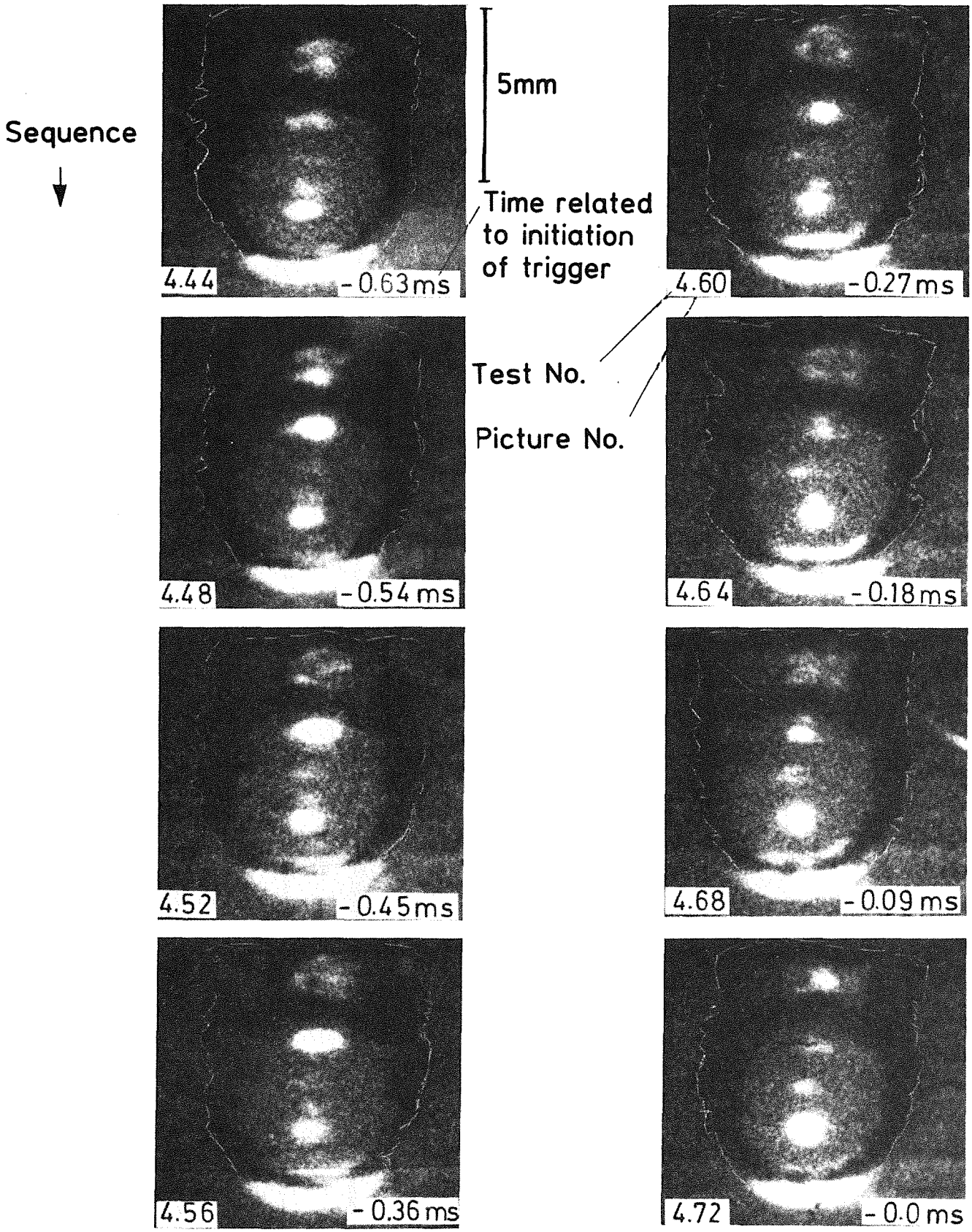

KfK IRE8712075

Fig. 5 Test AOW4, Droplet at Film Boiling

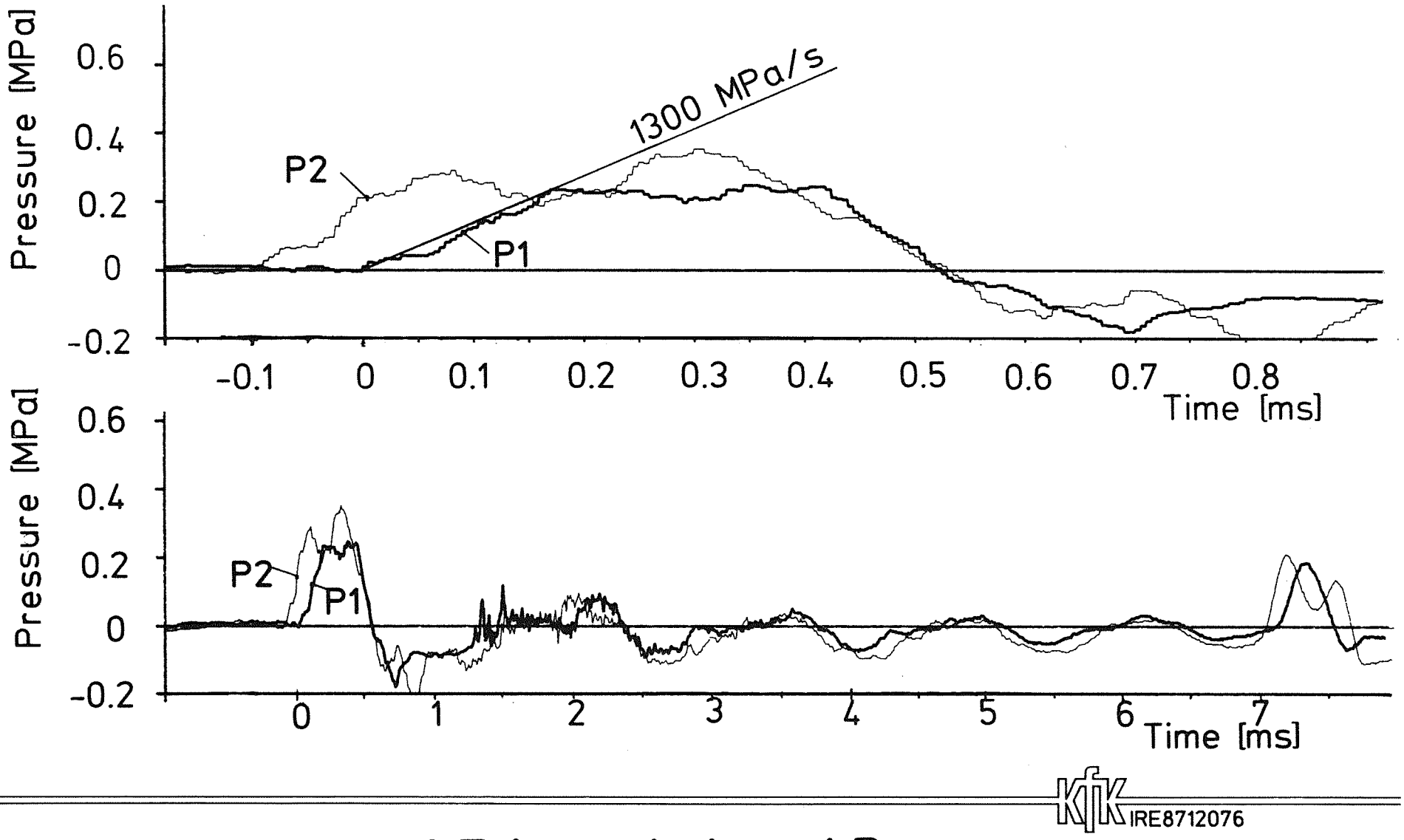

Fig. 6 Course of Trigger Induced Pressure
(U = 700 V ; f_R = 250 kHz)

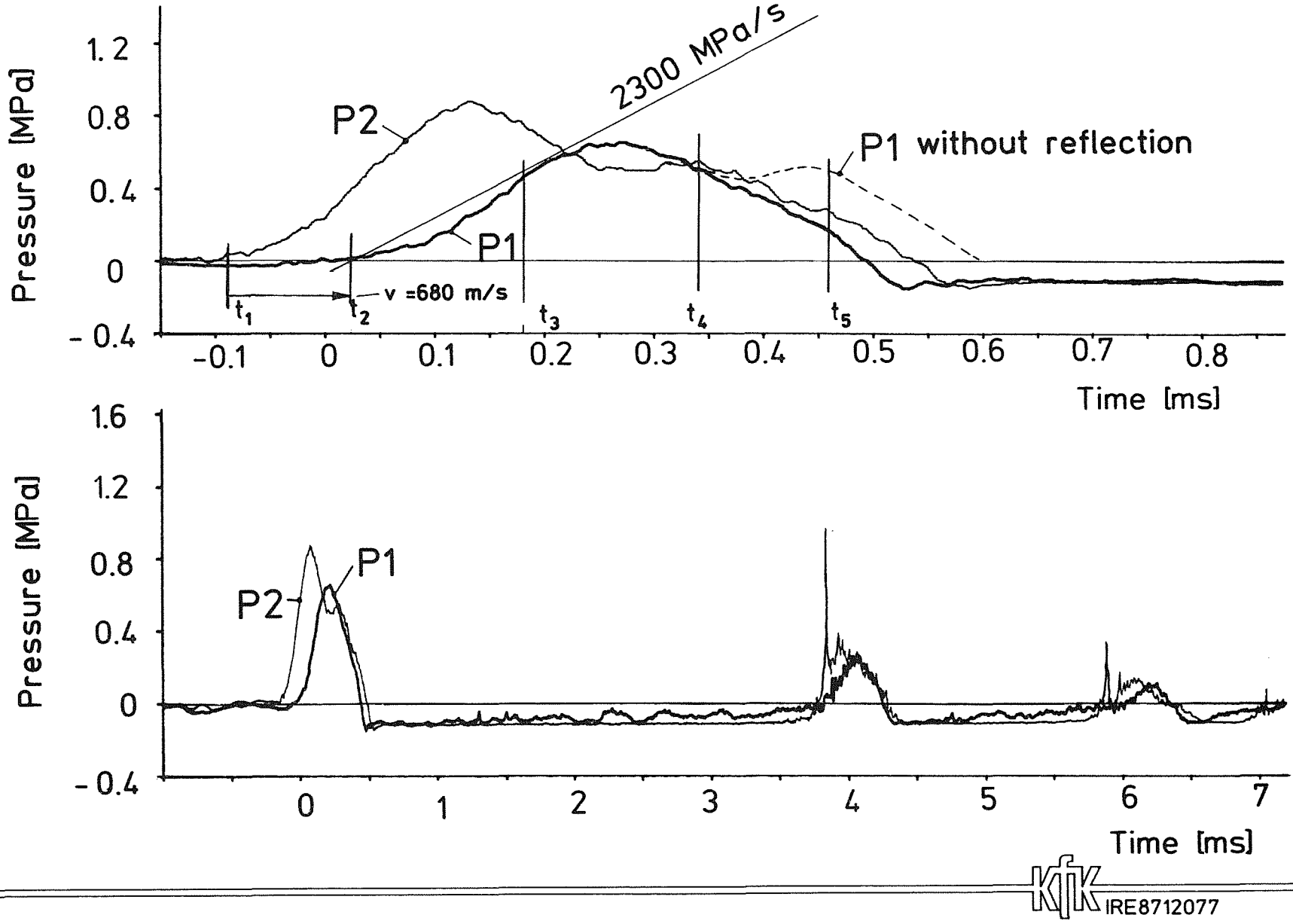

KfK IRE8712077

Fig.7 Course of Trigger Induced Pressure (U = 1000 V ; f_R = 500 kHz)

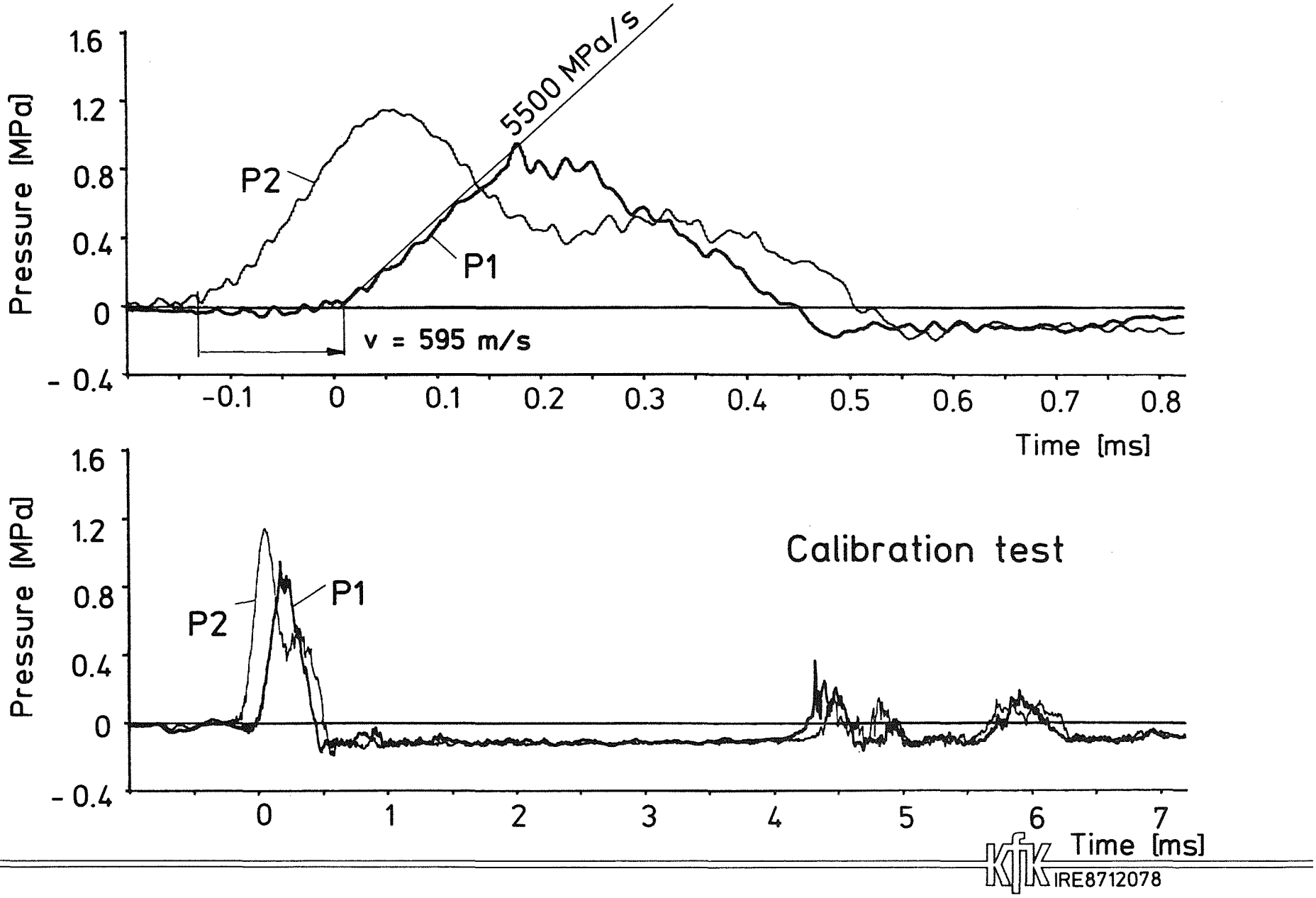

Fig. 8 Course of Trigger Induced Pressure for a Droplet below Melting Temperature (U = 1350 V; f_R = 500 kHz)

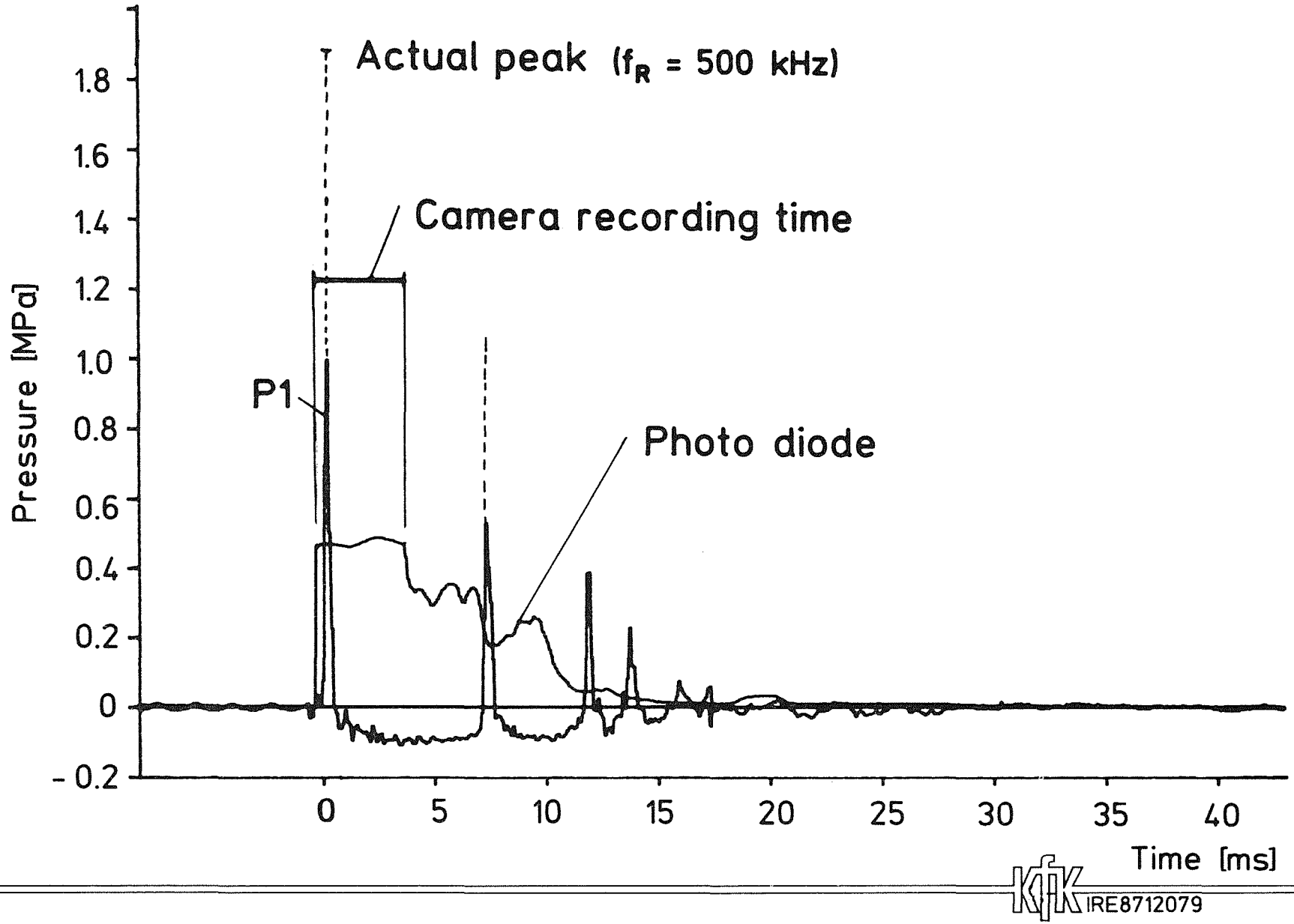

Fig. 9 Survey of Test AOW6, (f_R = 10 KHz)

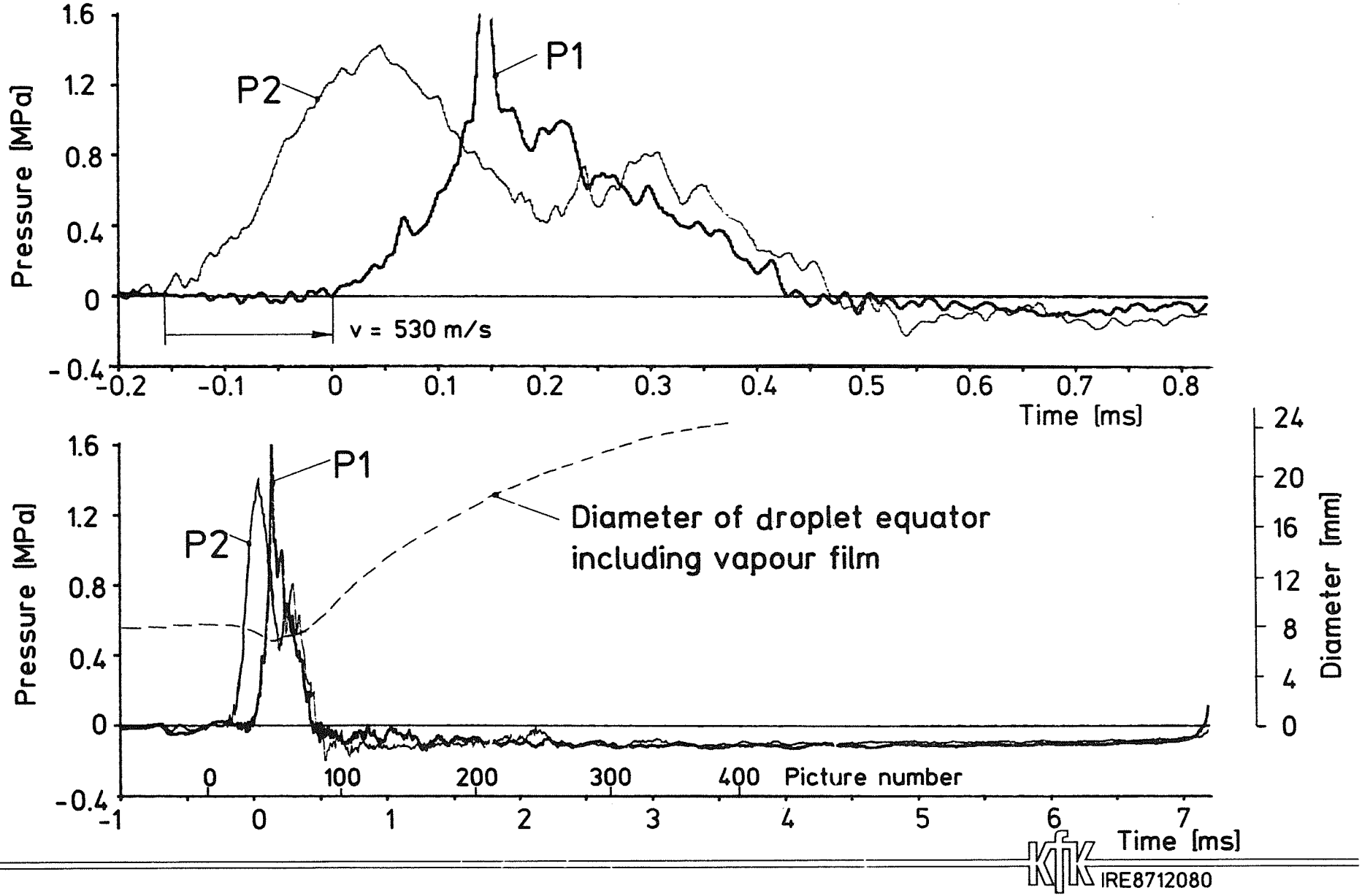

Fig. 10 Test AOW6, Course of Pressures
(U = 1350 V ; f_R = 500 kHz)

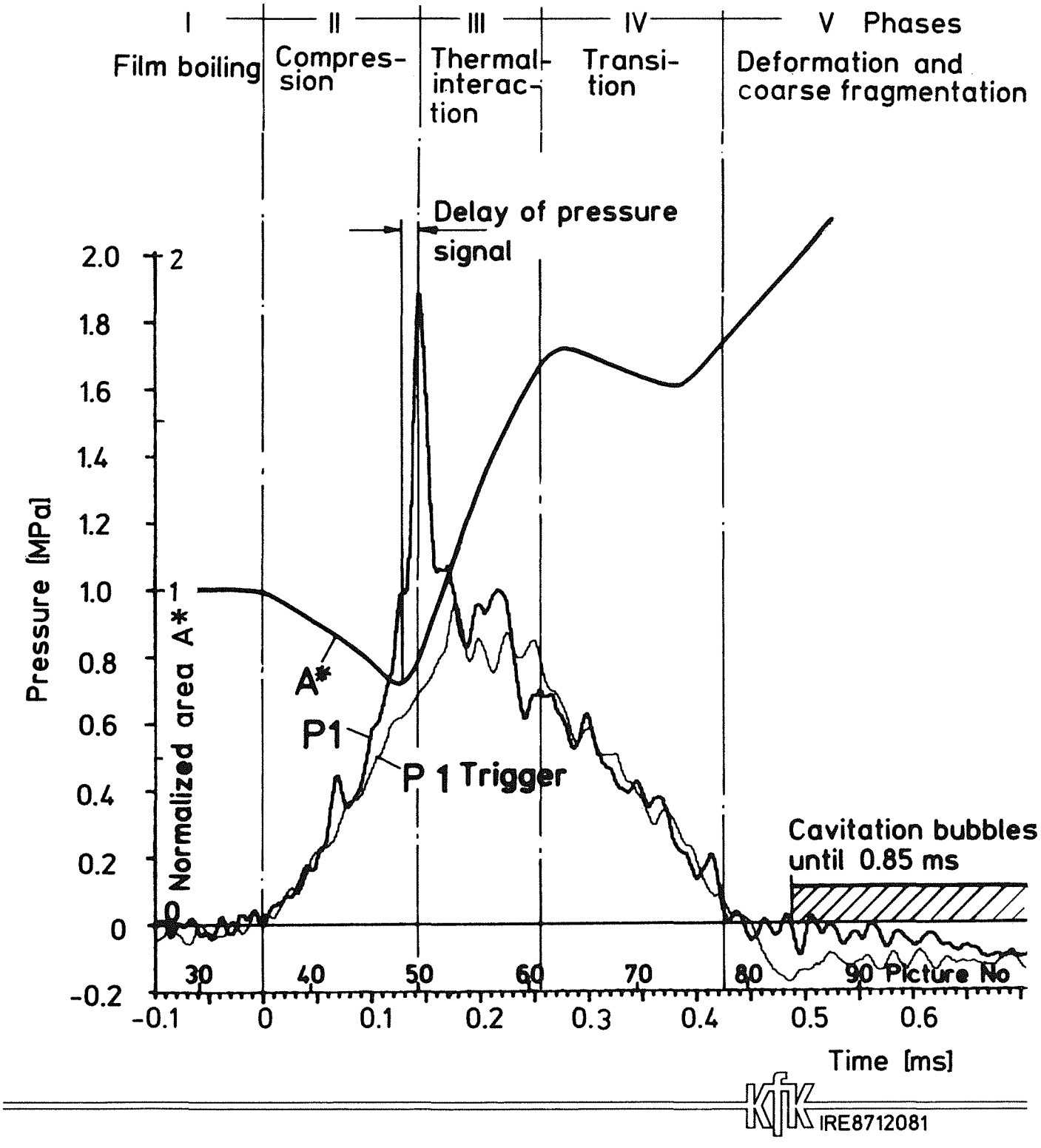

Fig. 11 Test A0W6, Sequence of Events

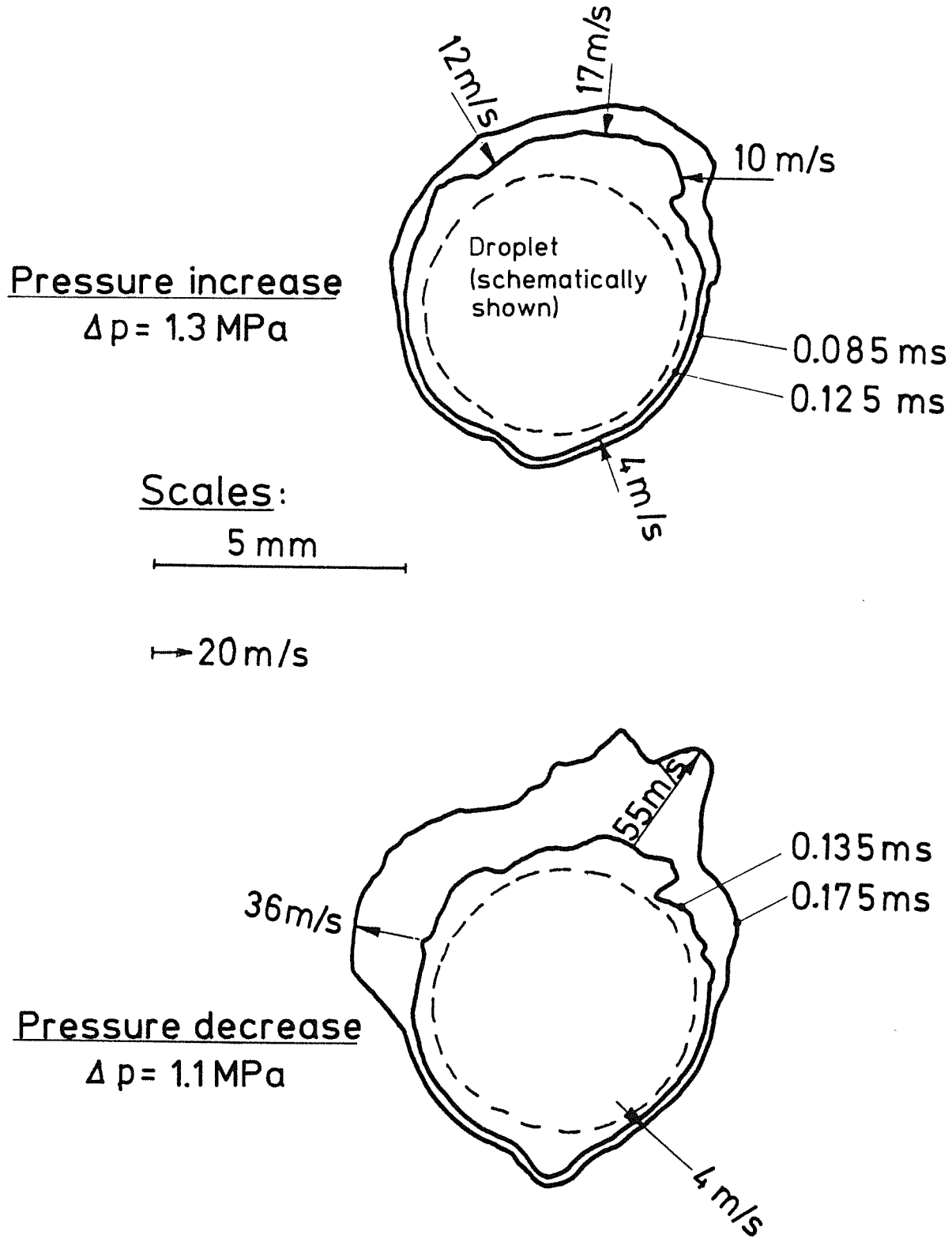

Fig. 12 Test AOW6, Velocity of Water-Vapour Interface

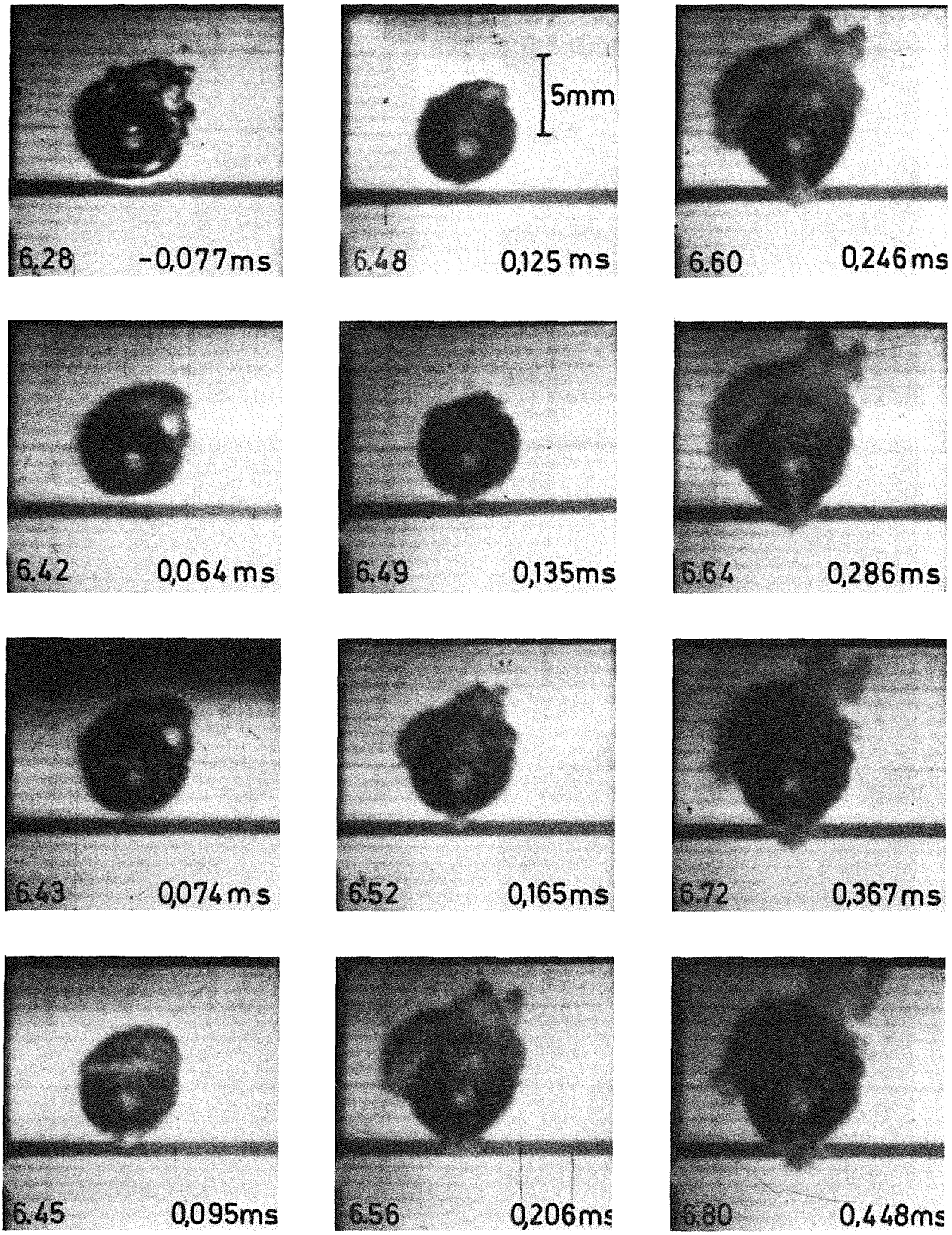

Fig. 13 Test AOW6, Sequence of Pictures (Phases I ... IV)

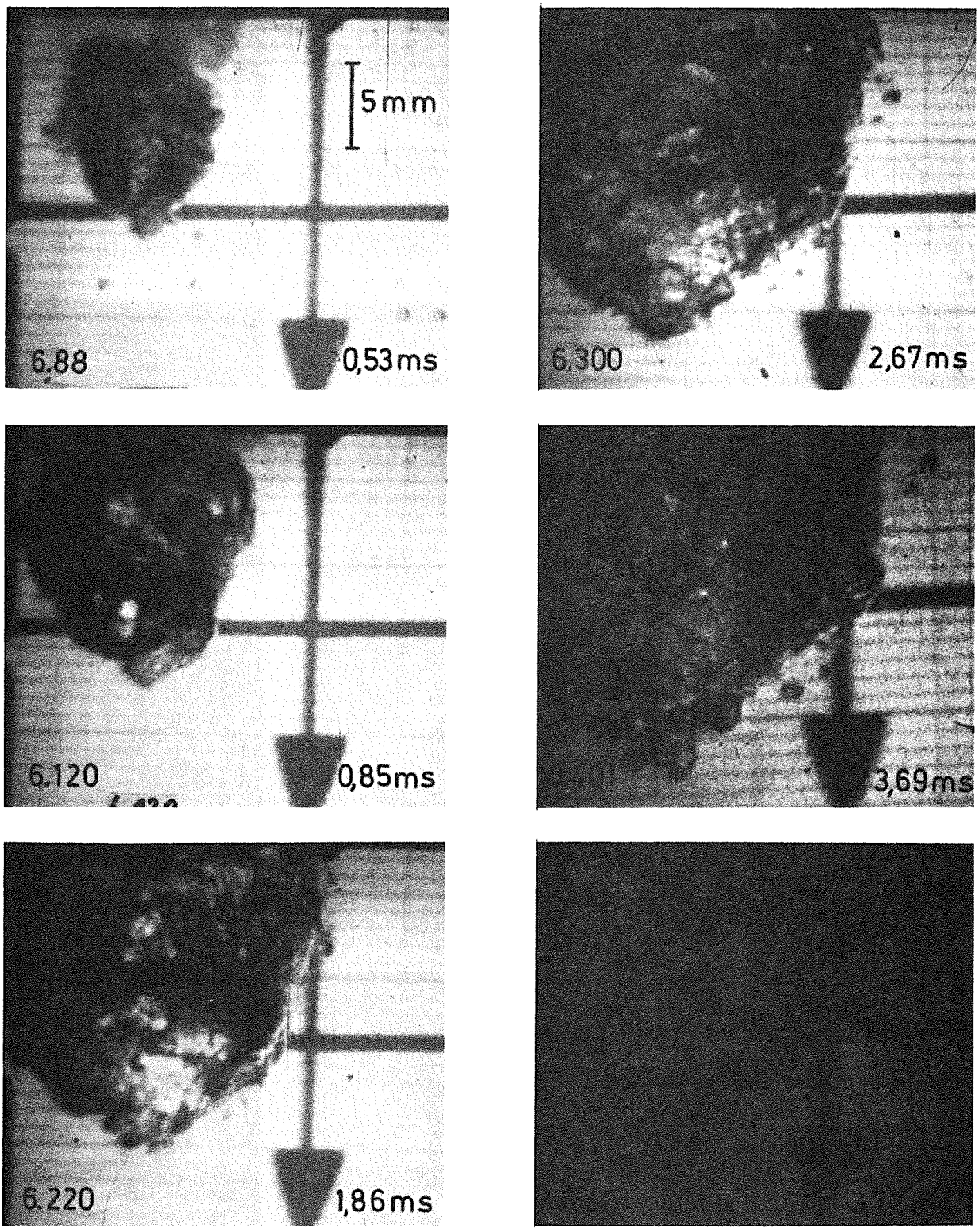

Fig. 14 Test AOW6, Sequence of Pictures (Phase V)

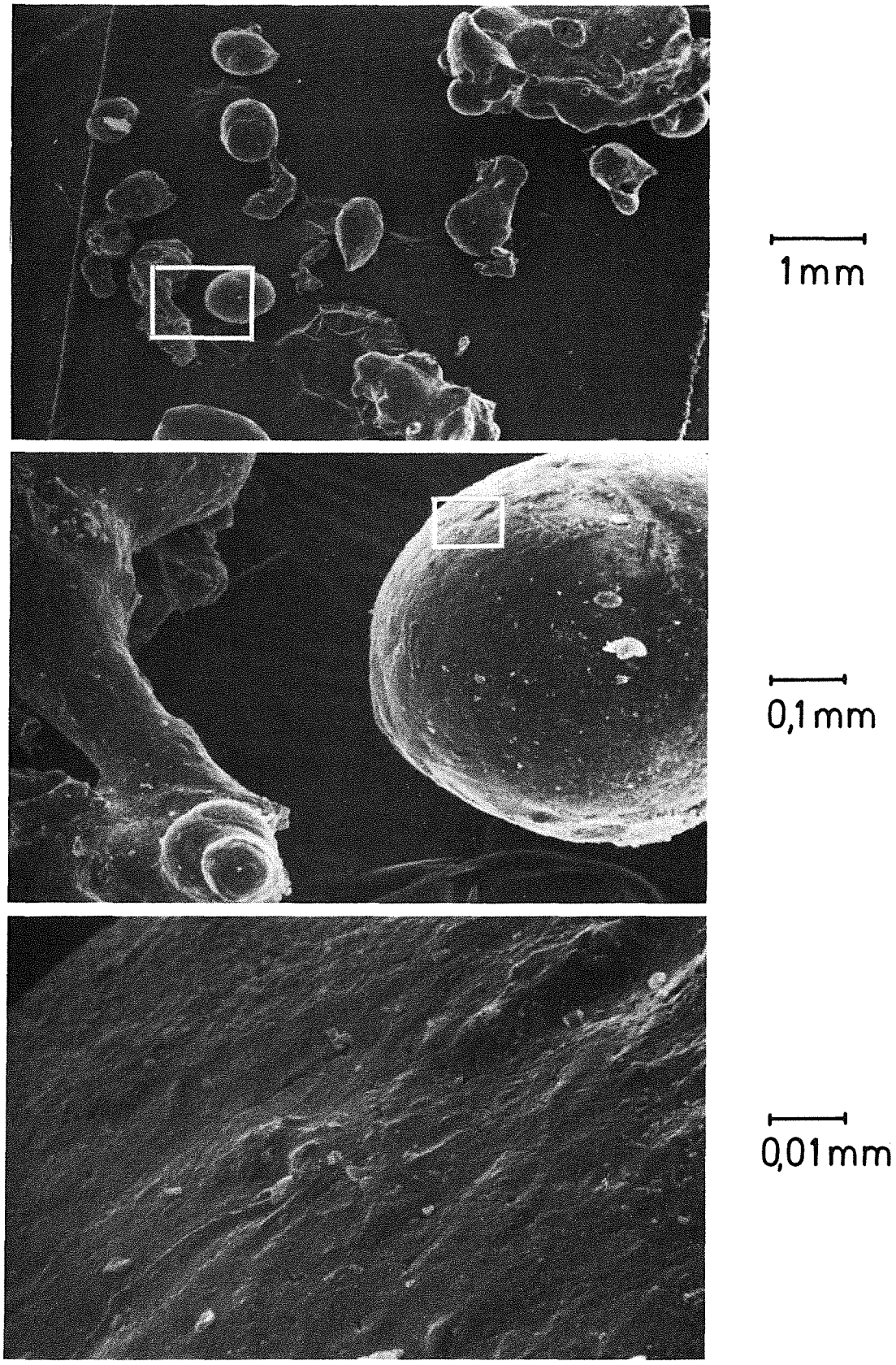

Fig. 15 Test AOW6, Photomicrographs of some Fragments

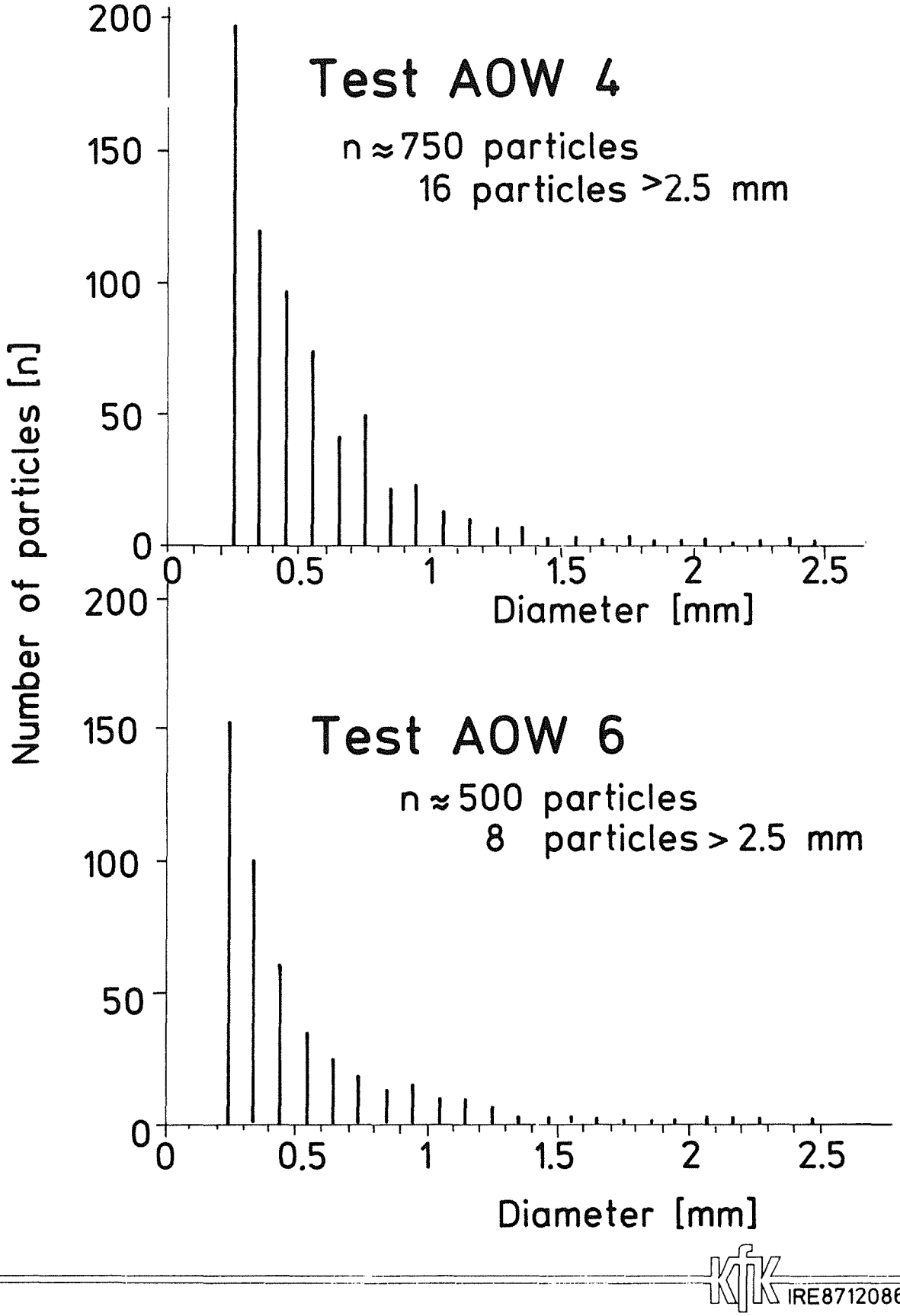

Fig. 16 Test AOW4 and AOW6, Histogrammes of Fragments

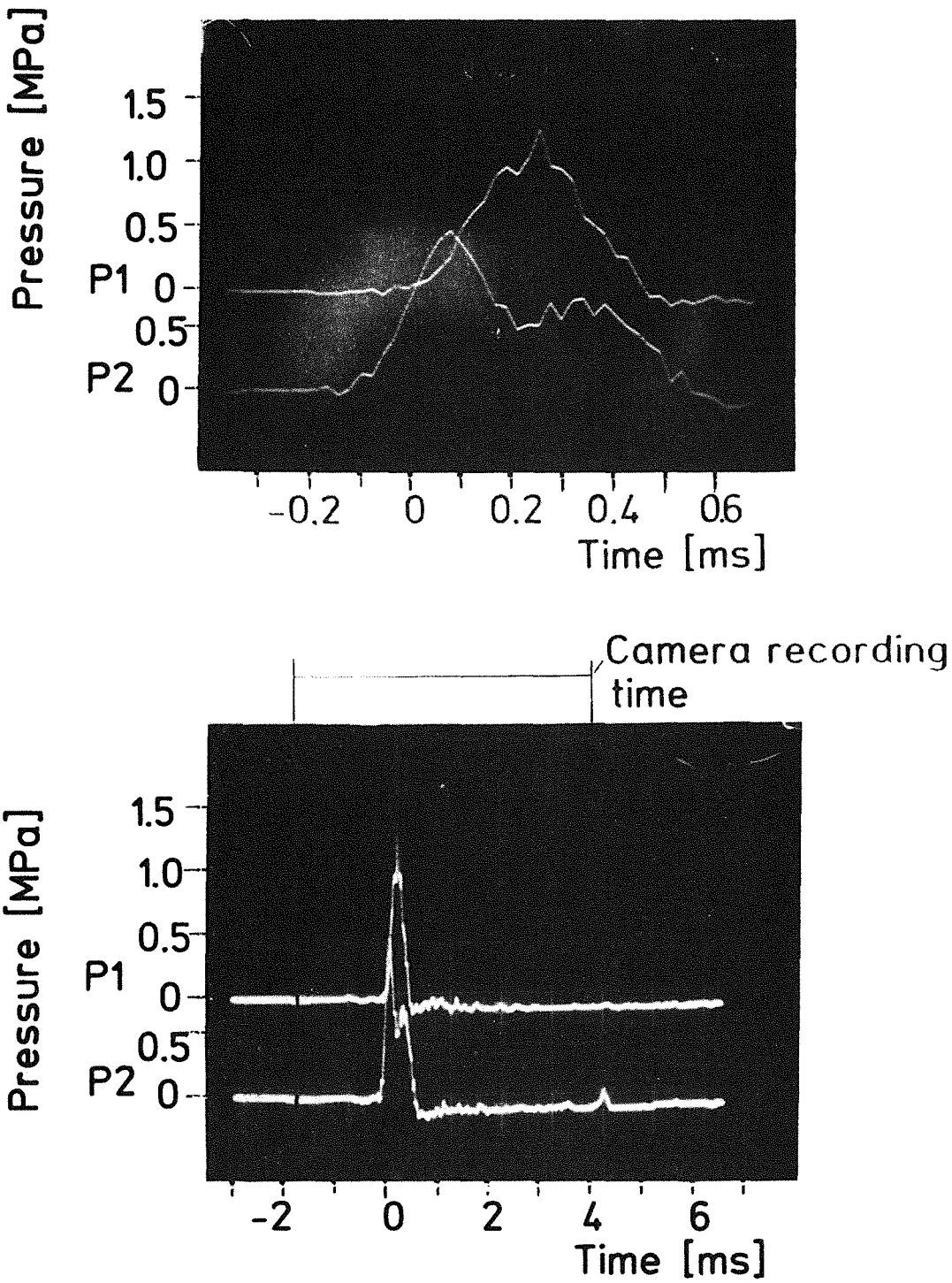

KfK IRE8712087

Fig. 17 Test AOW4, Course of Pressures
($U = 1350\,V$, $f_R = 45\,kHz$)

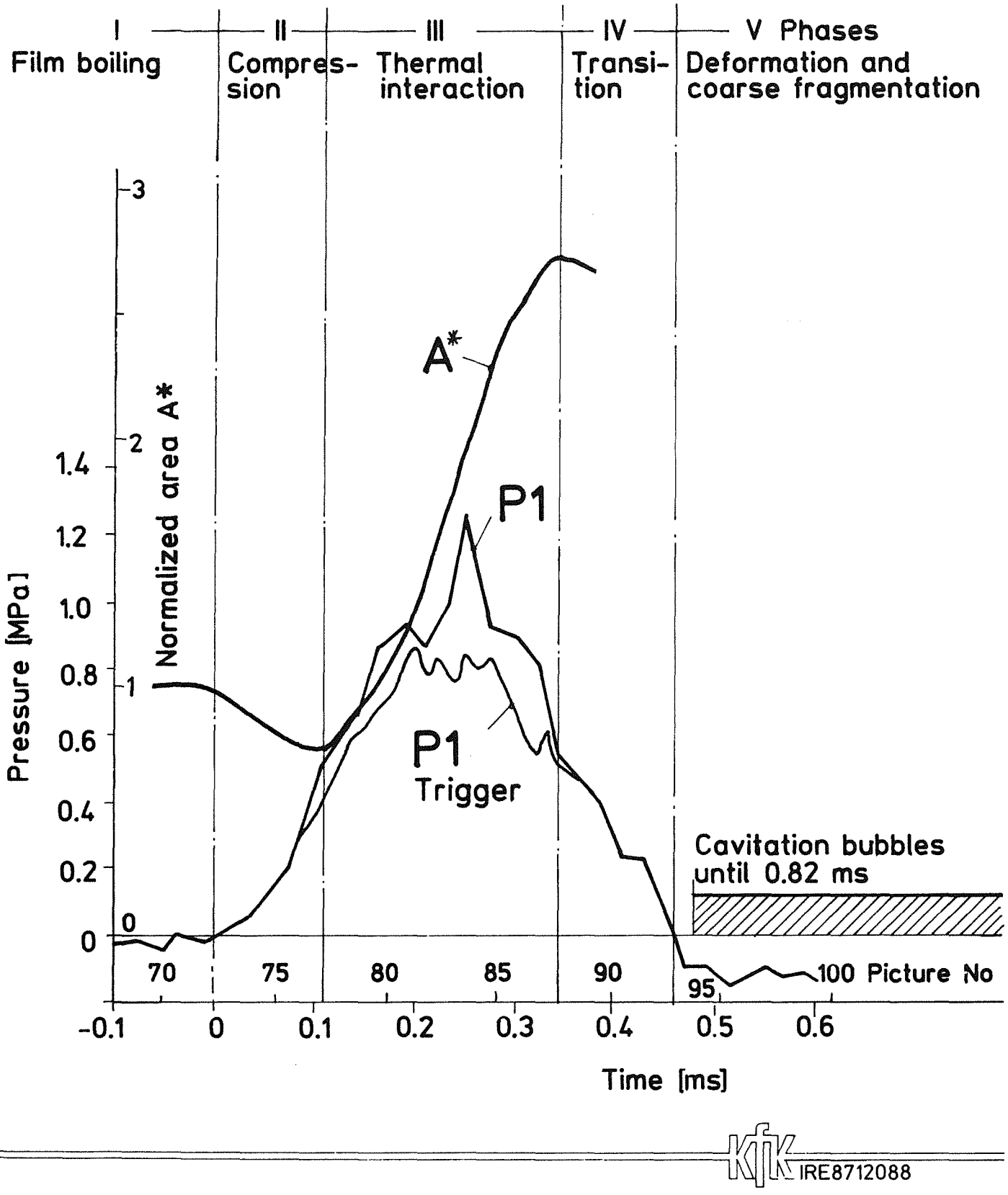

Fig. 18 Test A0W4, Sequence of Events

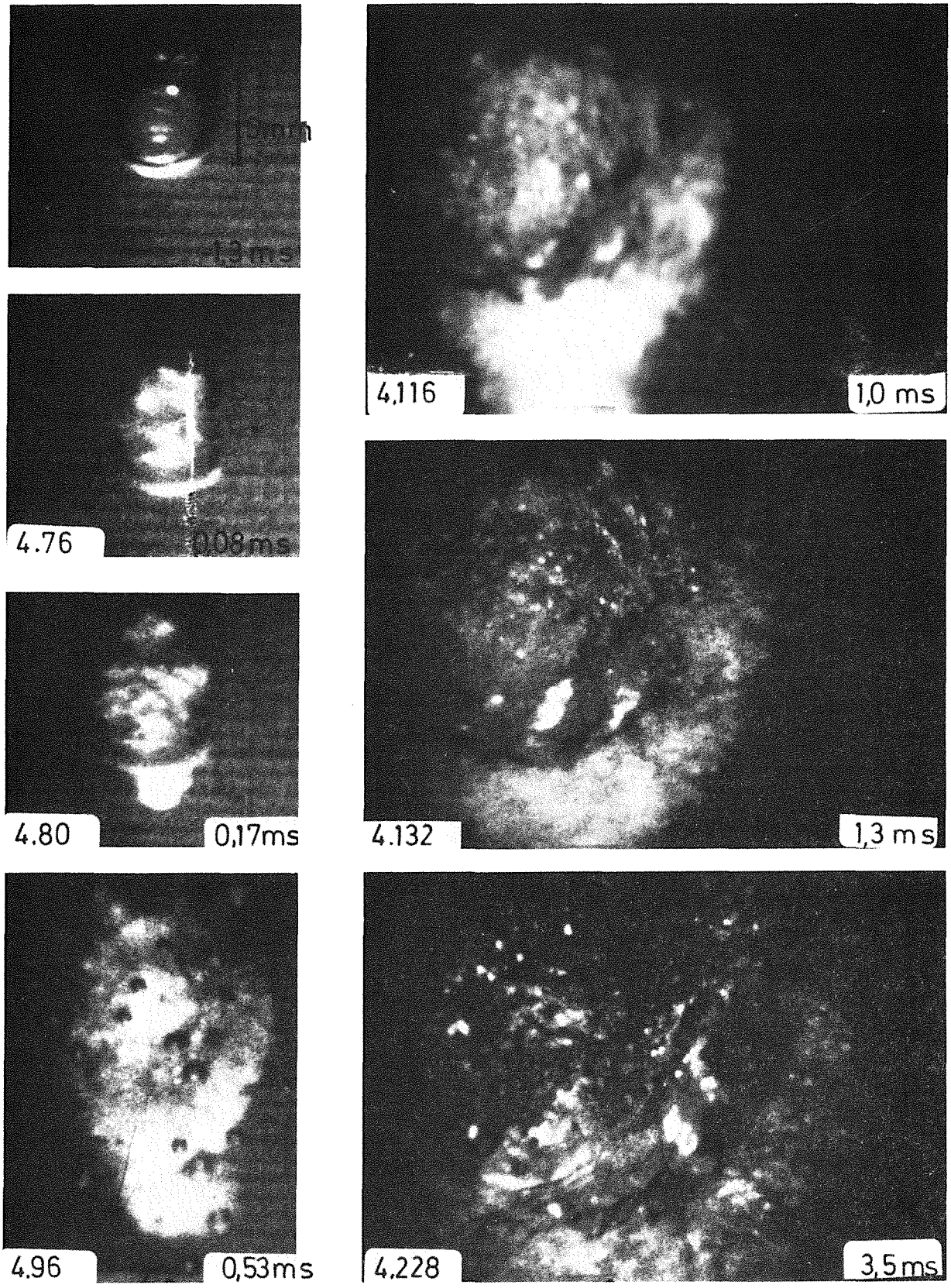

KfK IRE8712089

Fig. 19 Test AOW4, Sequence of Pictures

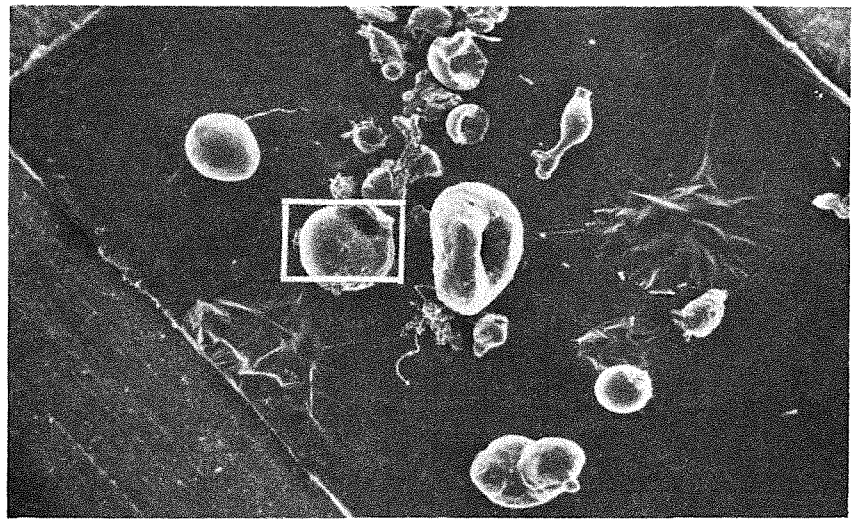

1mm

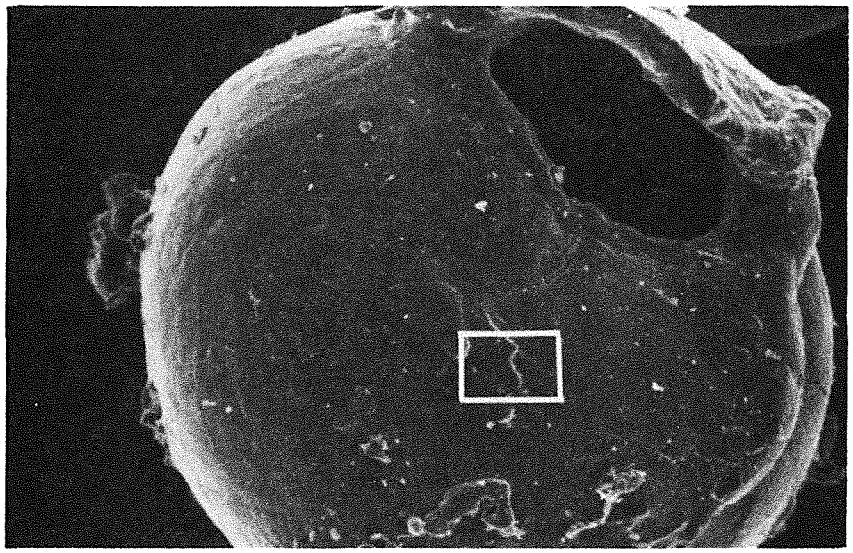

0,1mm

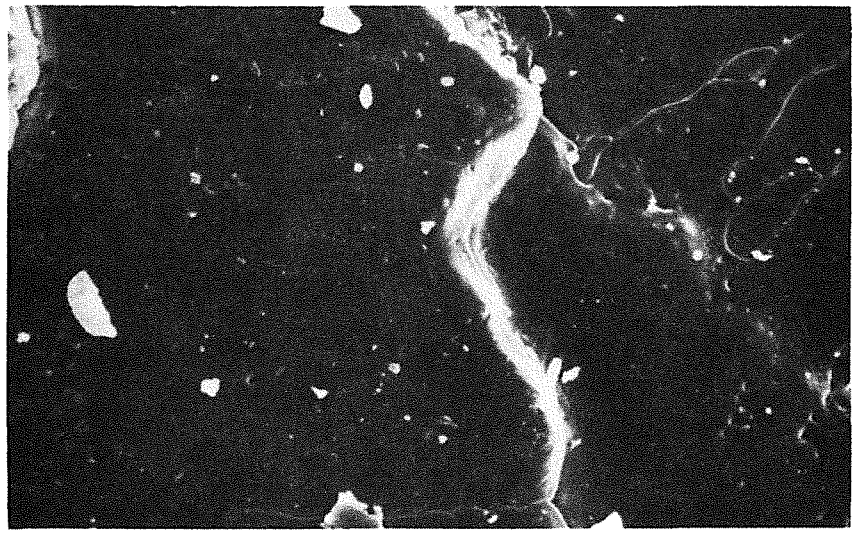

0,01mm

Fig. 20 Test AOW4, Photomicrographs of some Fragments

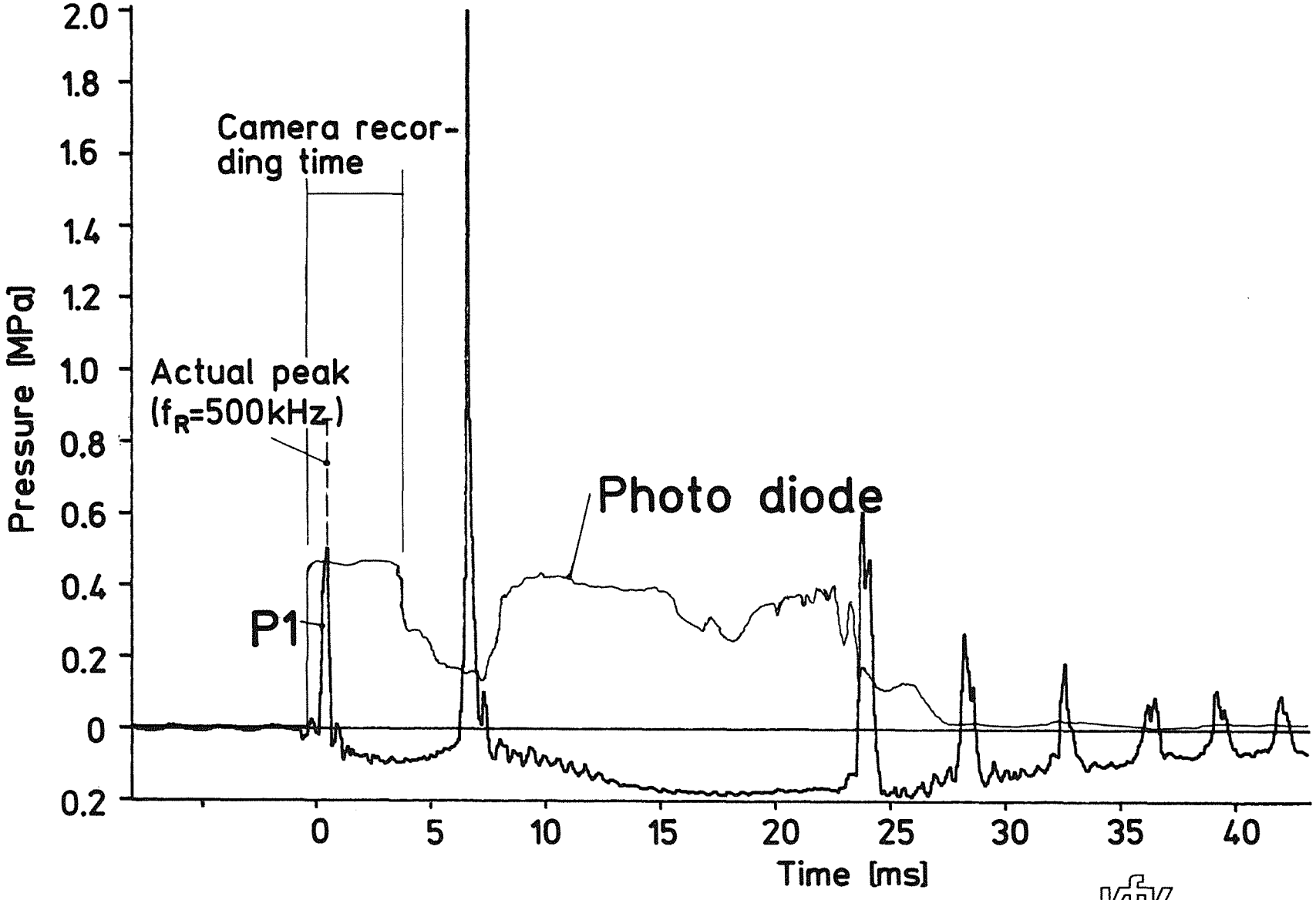

Fig. 21 Survey of Test AOW8, (f_R= 10 kHz)

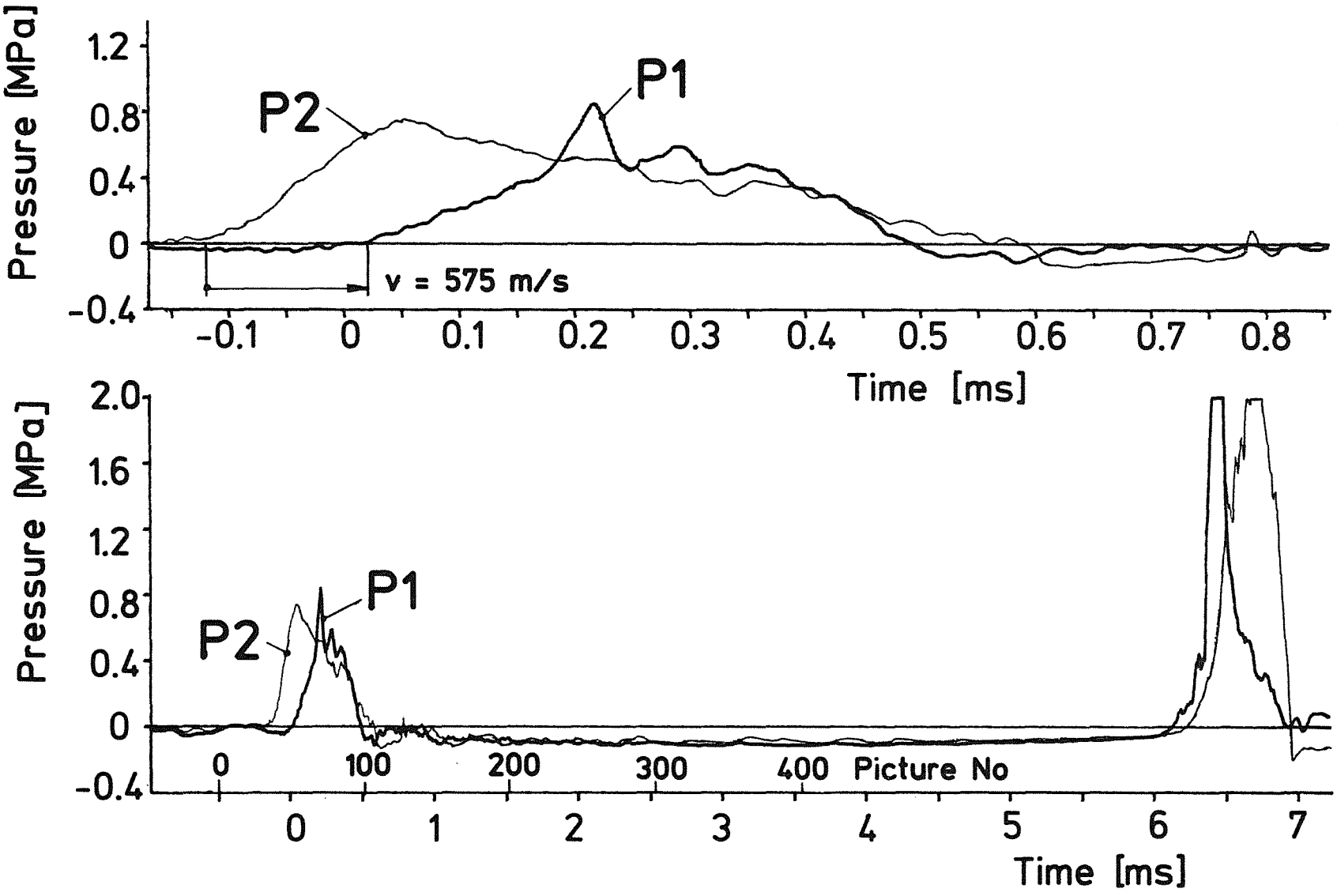

KfK IRE8712092

Fig. 22 Test AOW8, Course of Pressures
(U = 1000 V, f_R = 500 kHz)

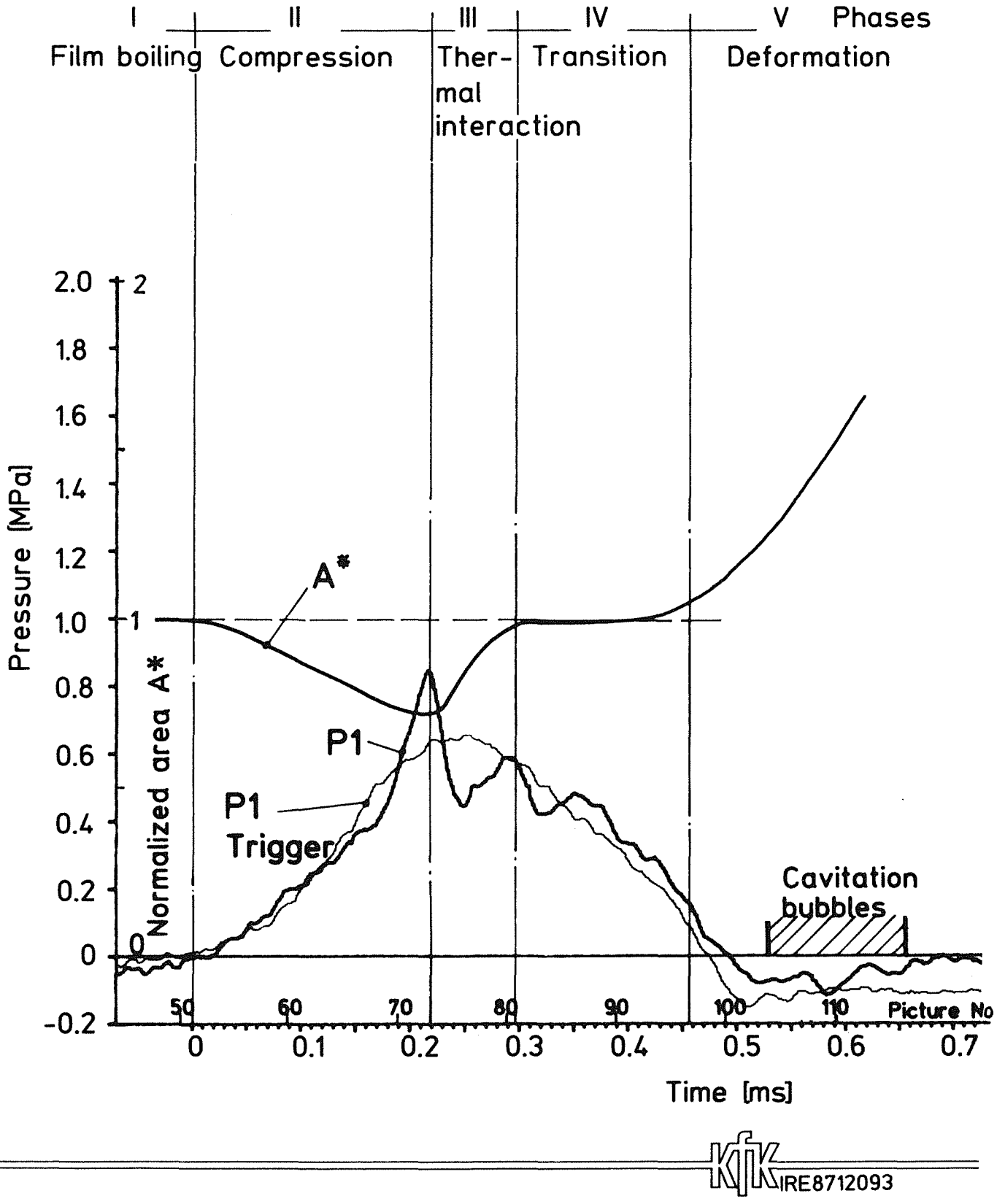

Fig. 23 Test A0W8, Sequence of Events

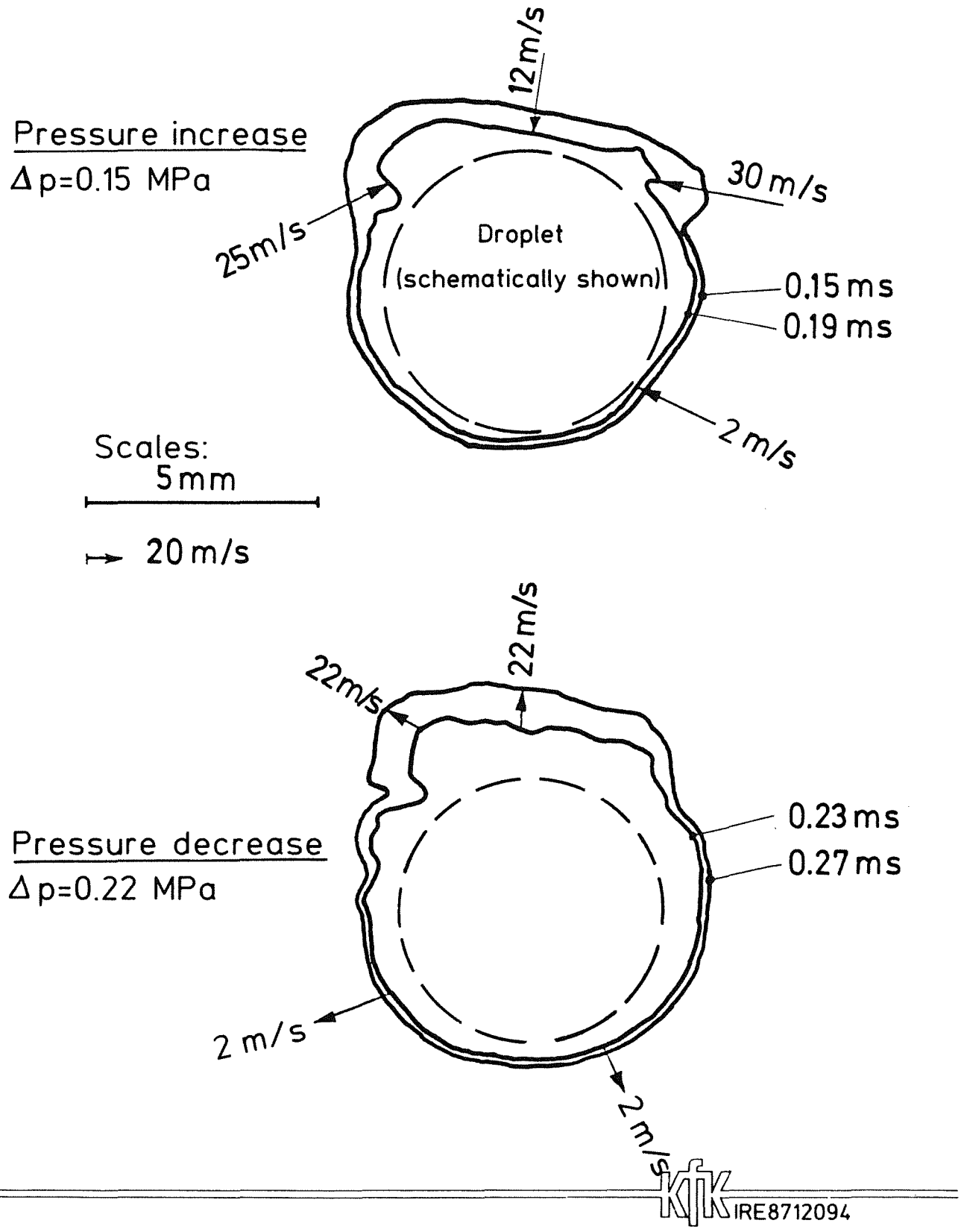

Fig.24 Test AOW8, Velocity of Water-Vapour Interface

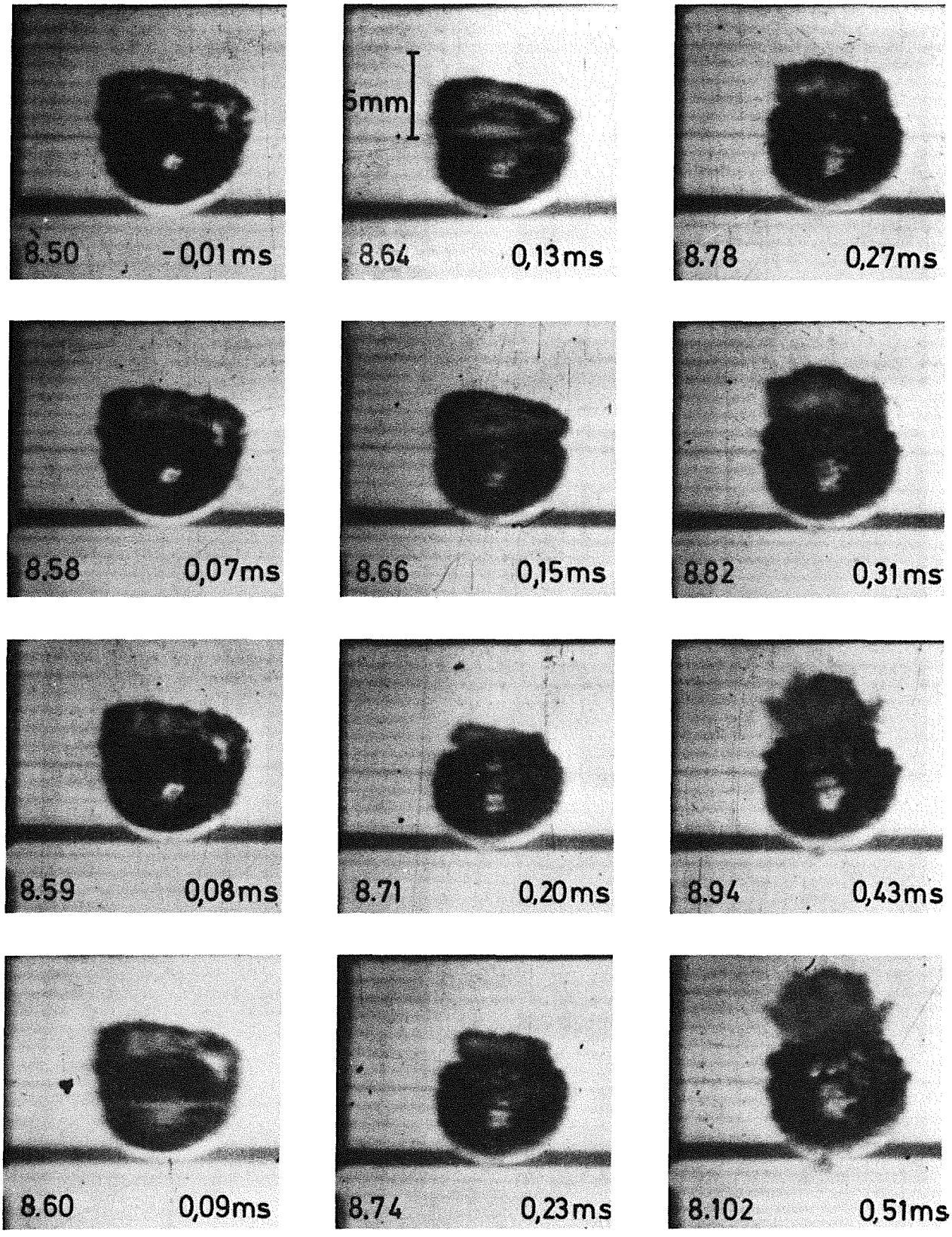

KfK IRE8712095

Fig. 25 Test AOW8, Sequence of Pictures (Phases I ... IV)

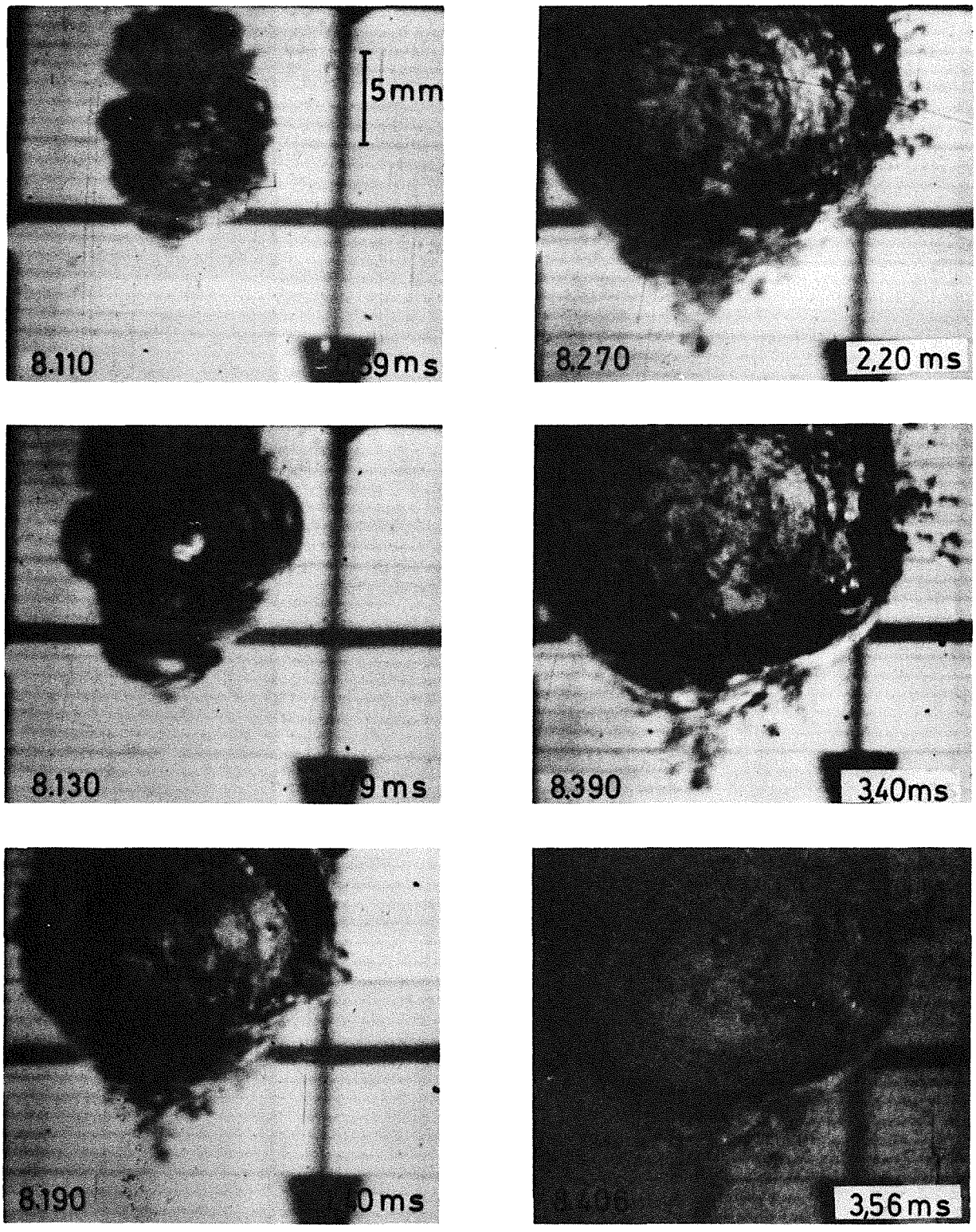

Fig. 26 Test AOW8, Sequence of Pictures (Phase V)

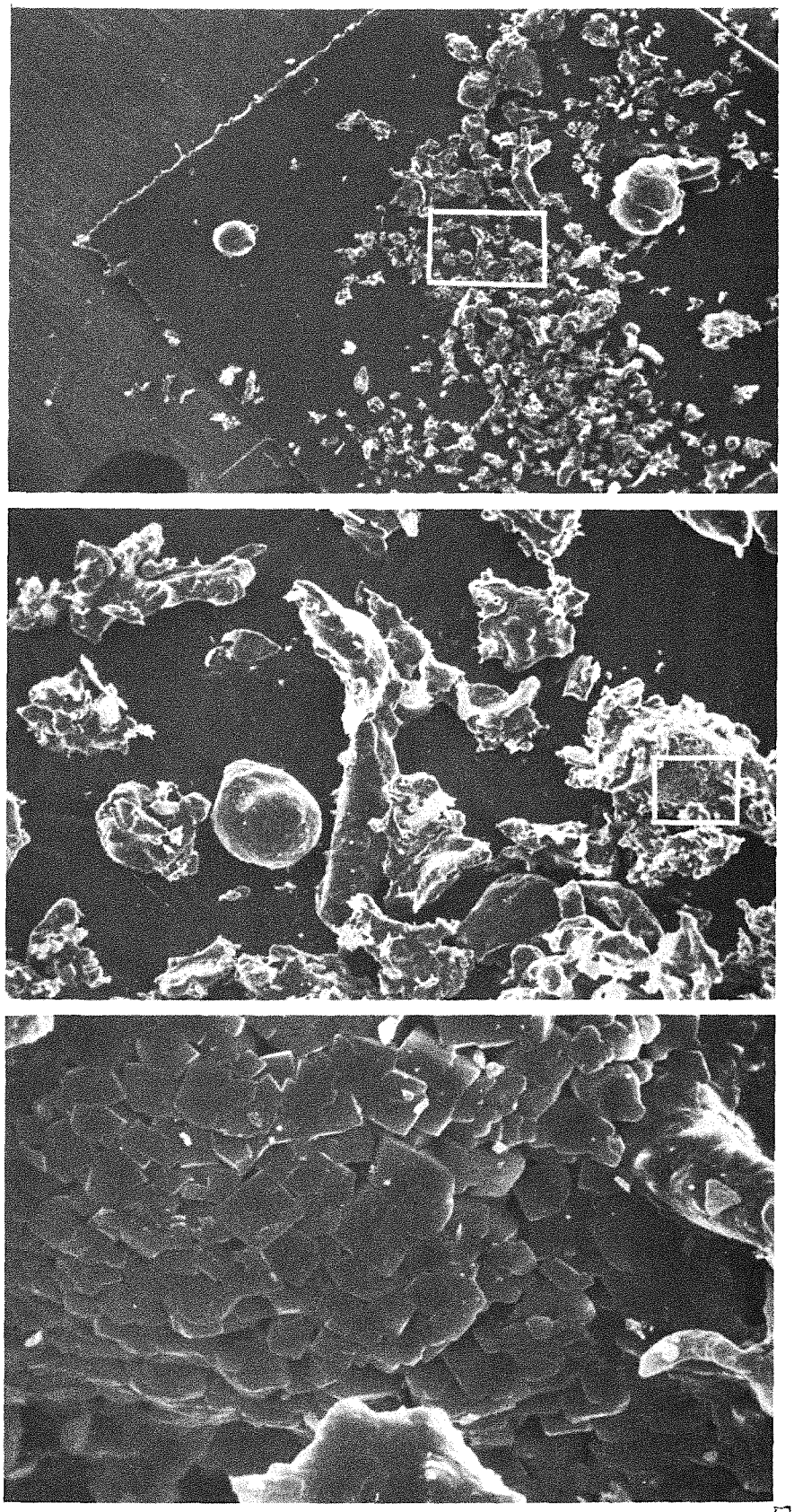

KfK IRE8712097

Fig. 27 Test AOW8, Photomicrographs of some Fragments

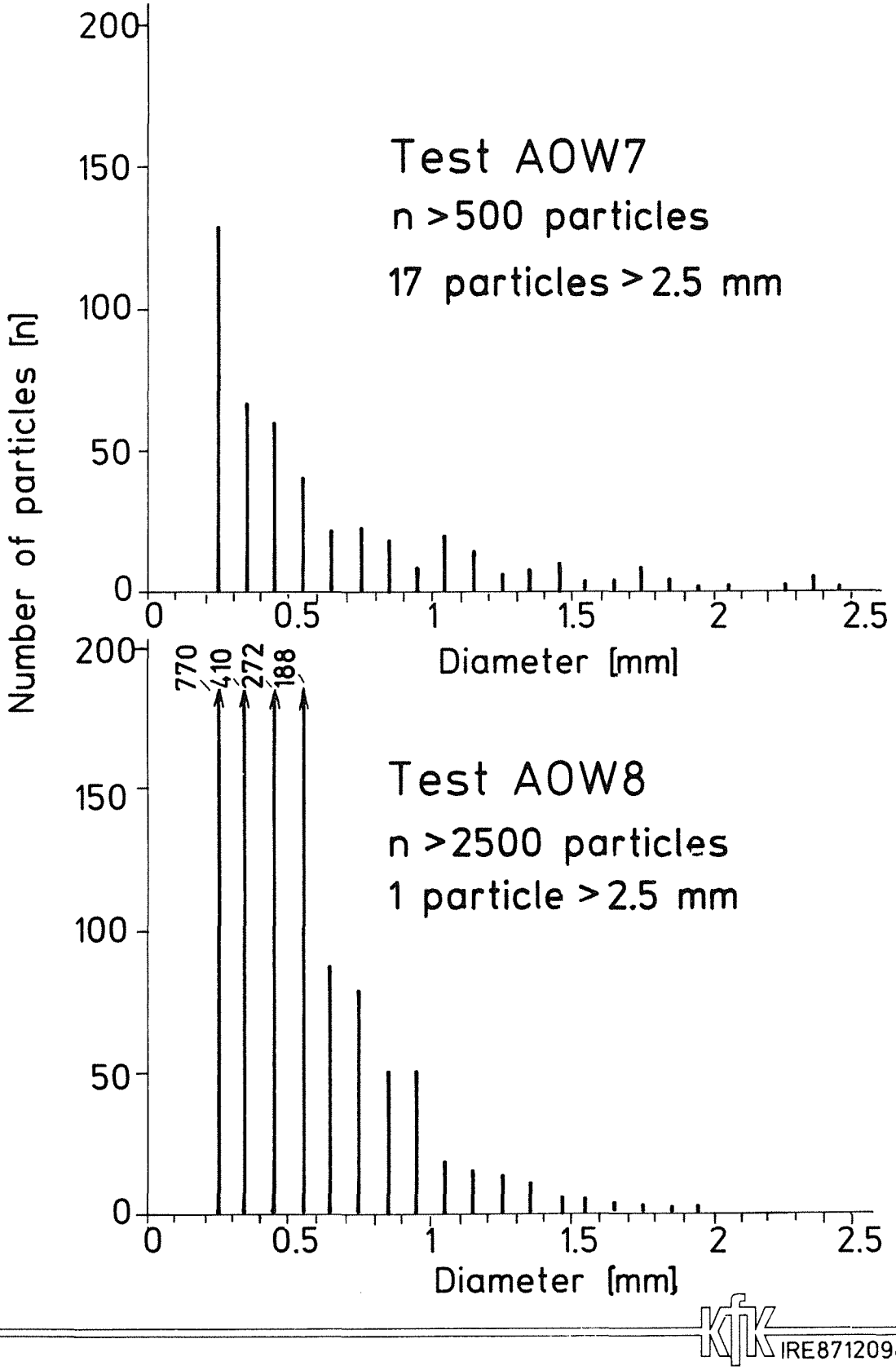

Fig. 28 Test AOW7 and AOW8, Histogrammes of Fragments

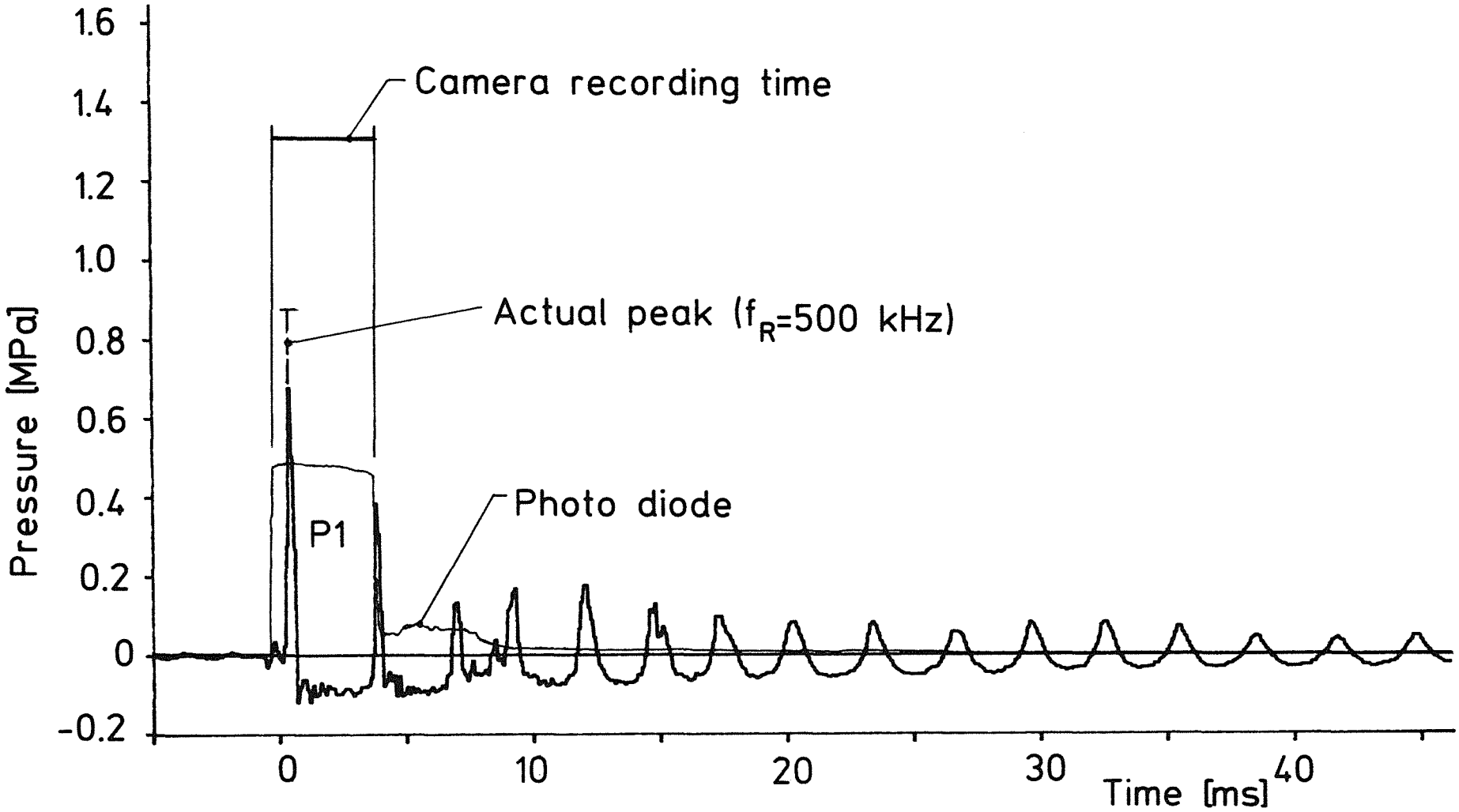

Fig. 29 Survey of Test AOW7 (f_R= 10 kHz)

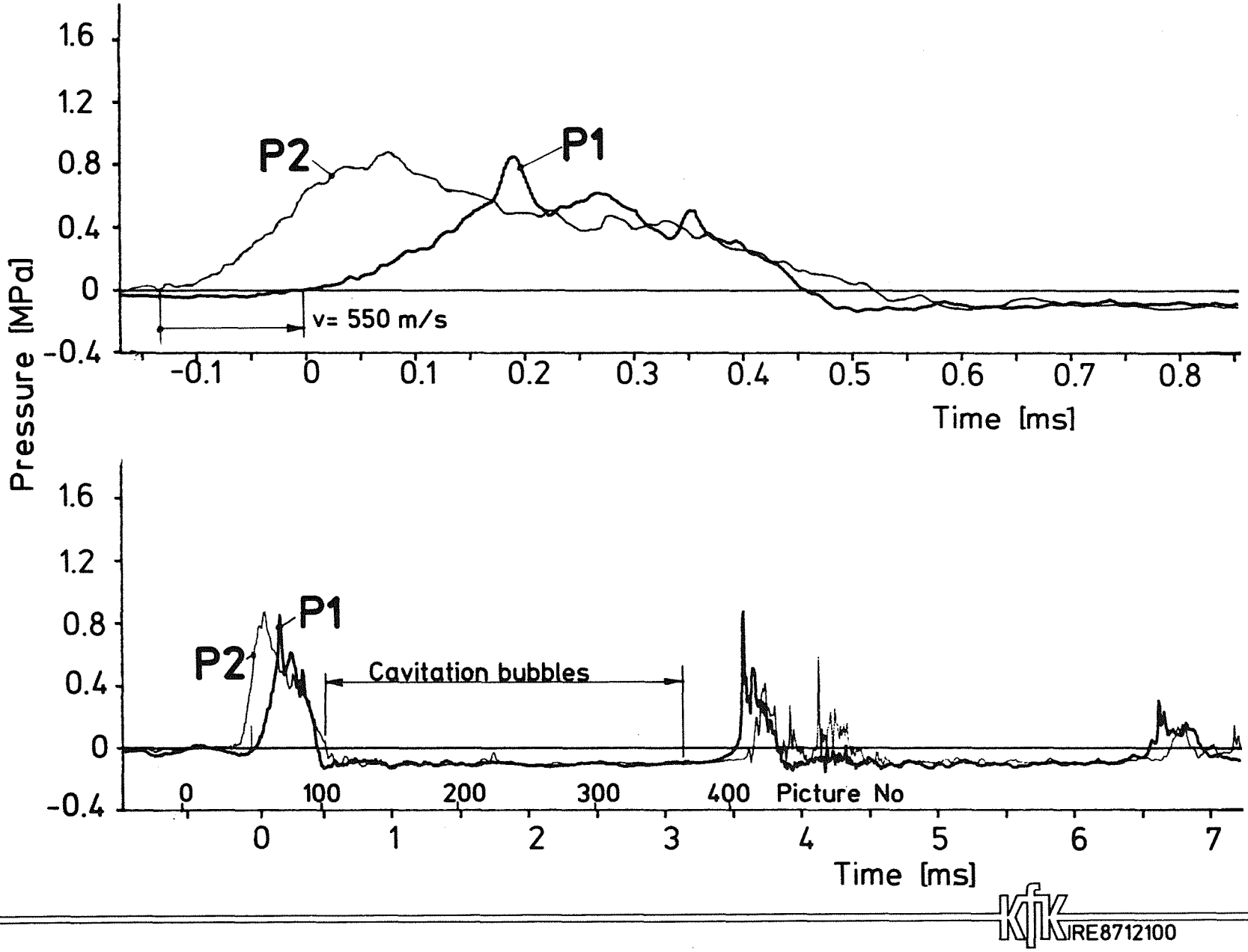

KfK IRE8712100

Fig. 30 Test AOW7, Course of Pressures
(U= 1000 V; f_R = 500 kHz)

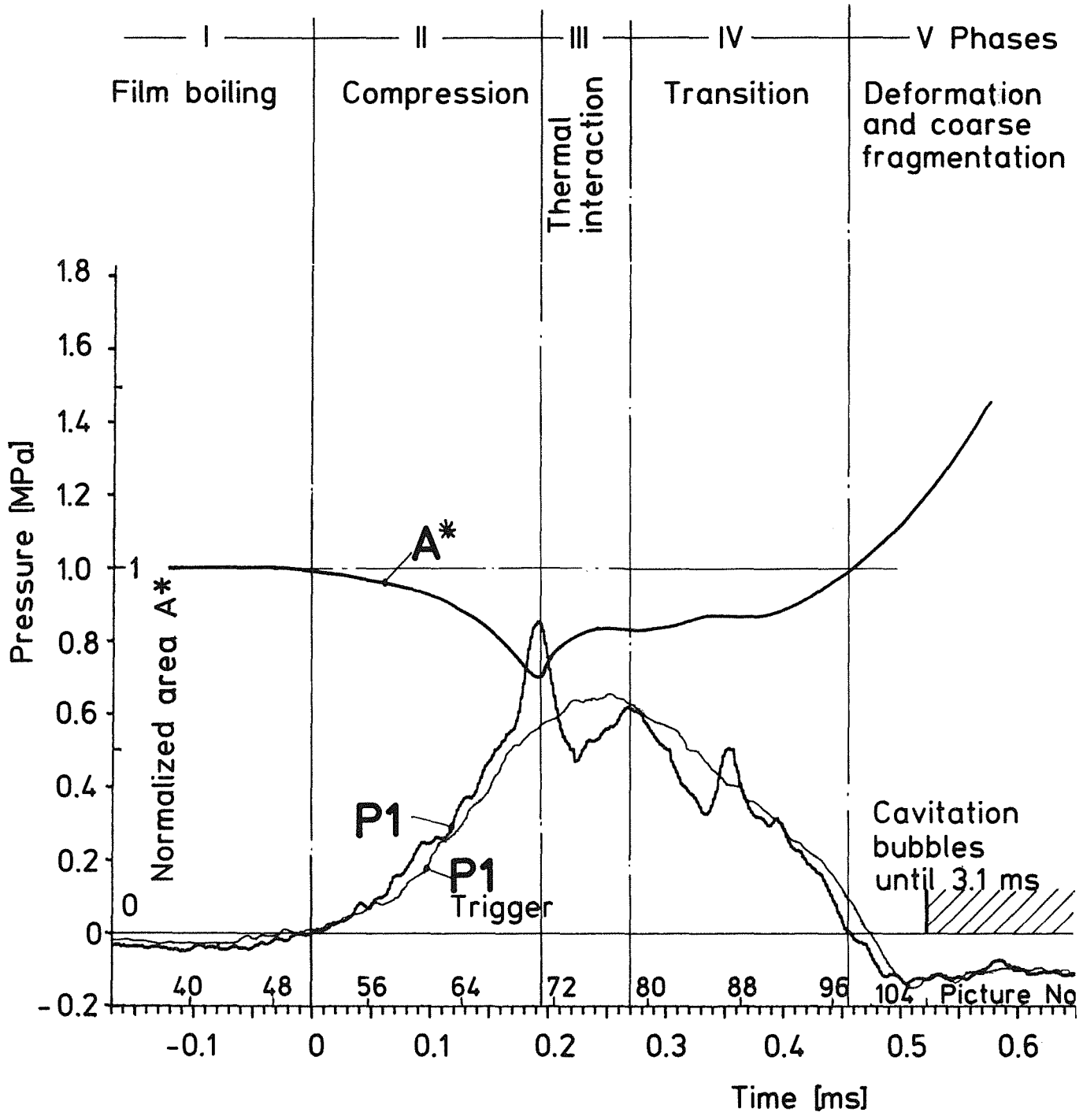

Fig. 31 Test AOW7, Sequence of Events

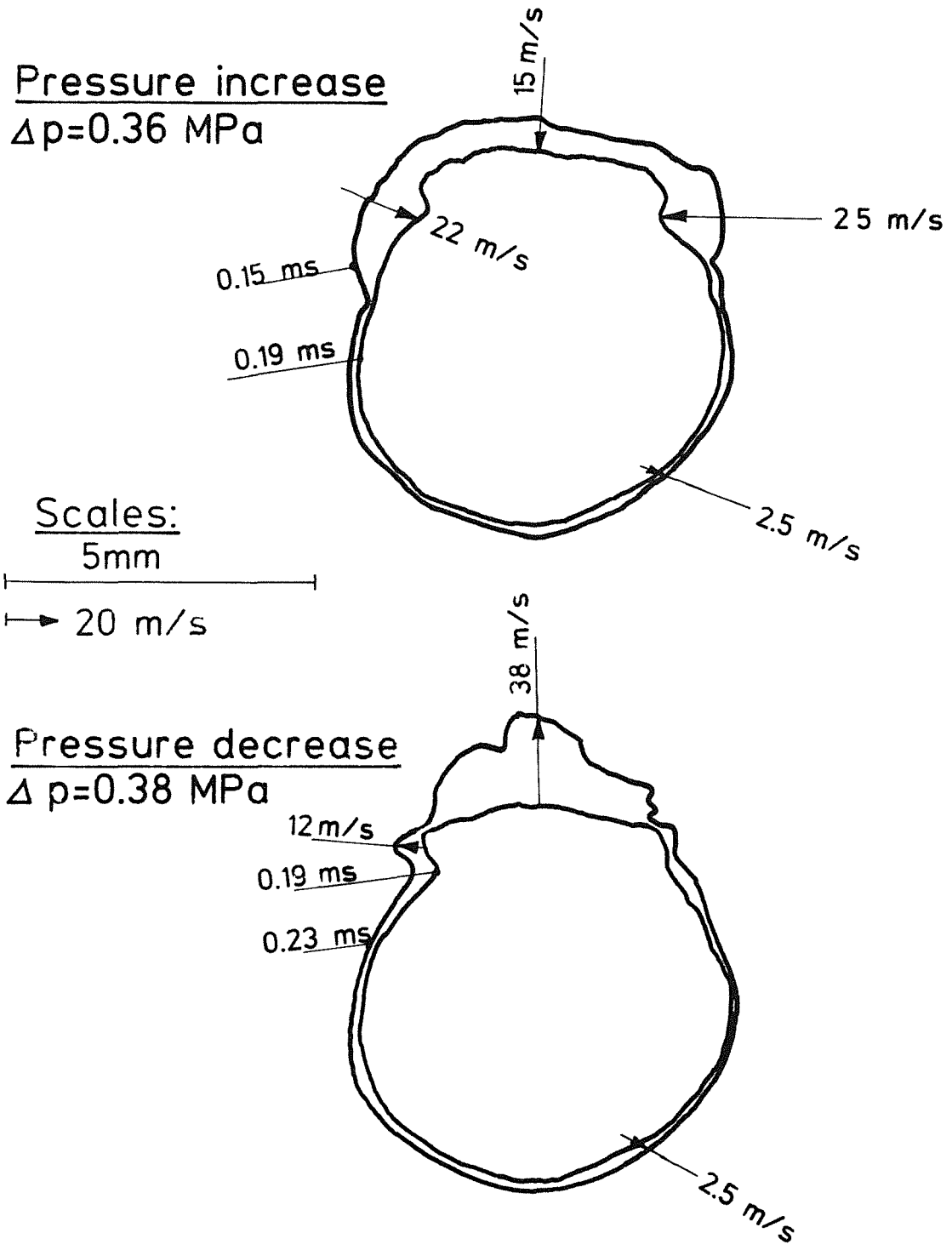

Fig. 32 AOW7, Velocity of Water-Vapour Interface

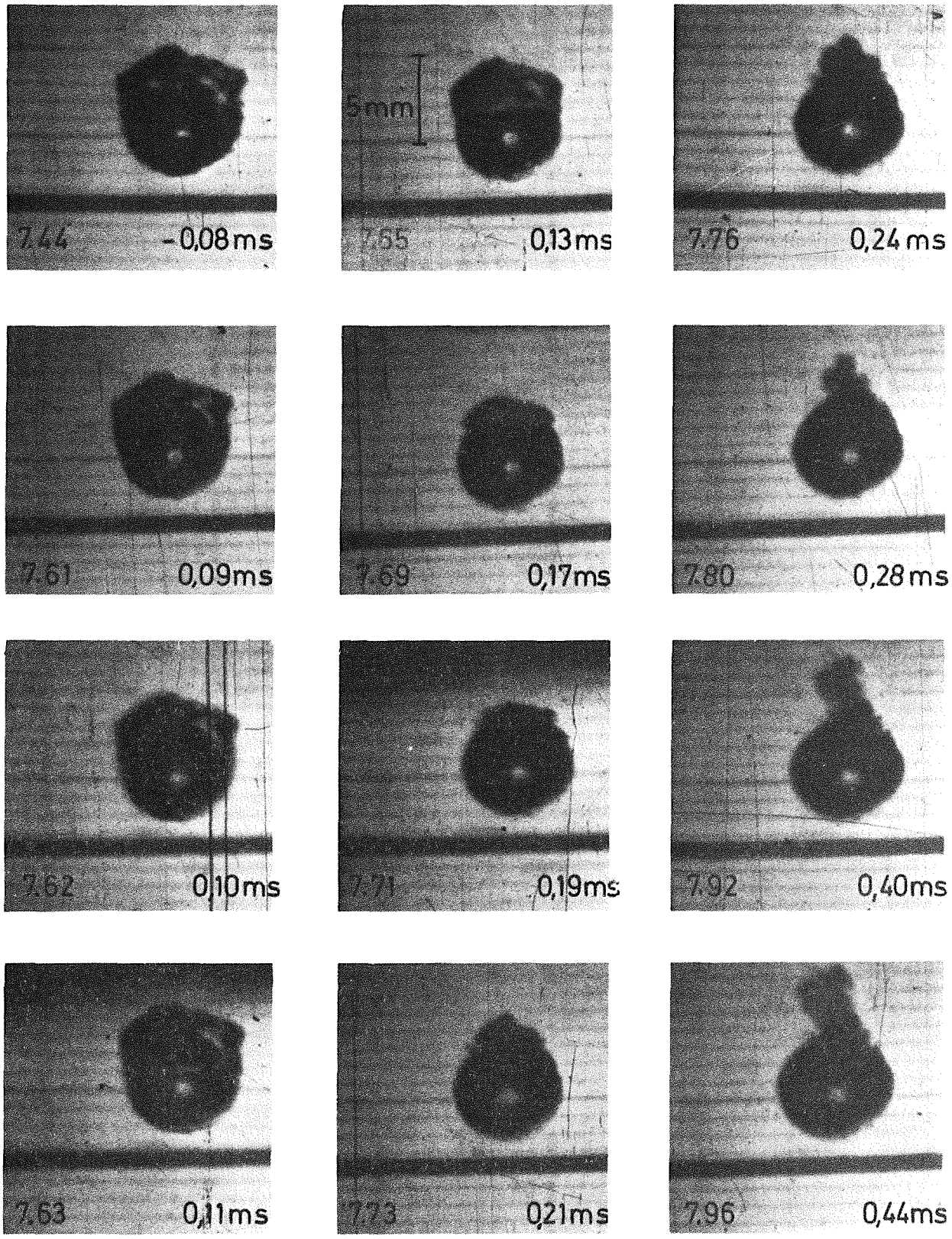

KfK IRE8712103

Fig. 33 Test AOW7, Sequence of Pictures (Phases I ... IV)

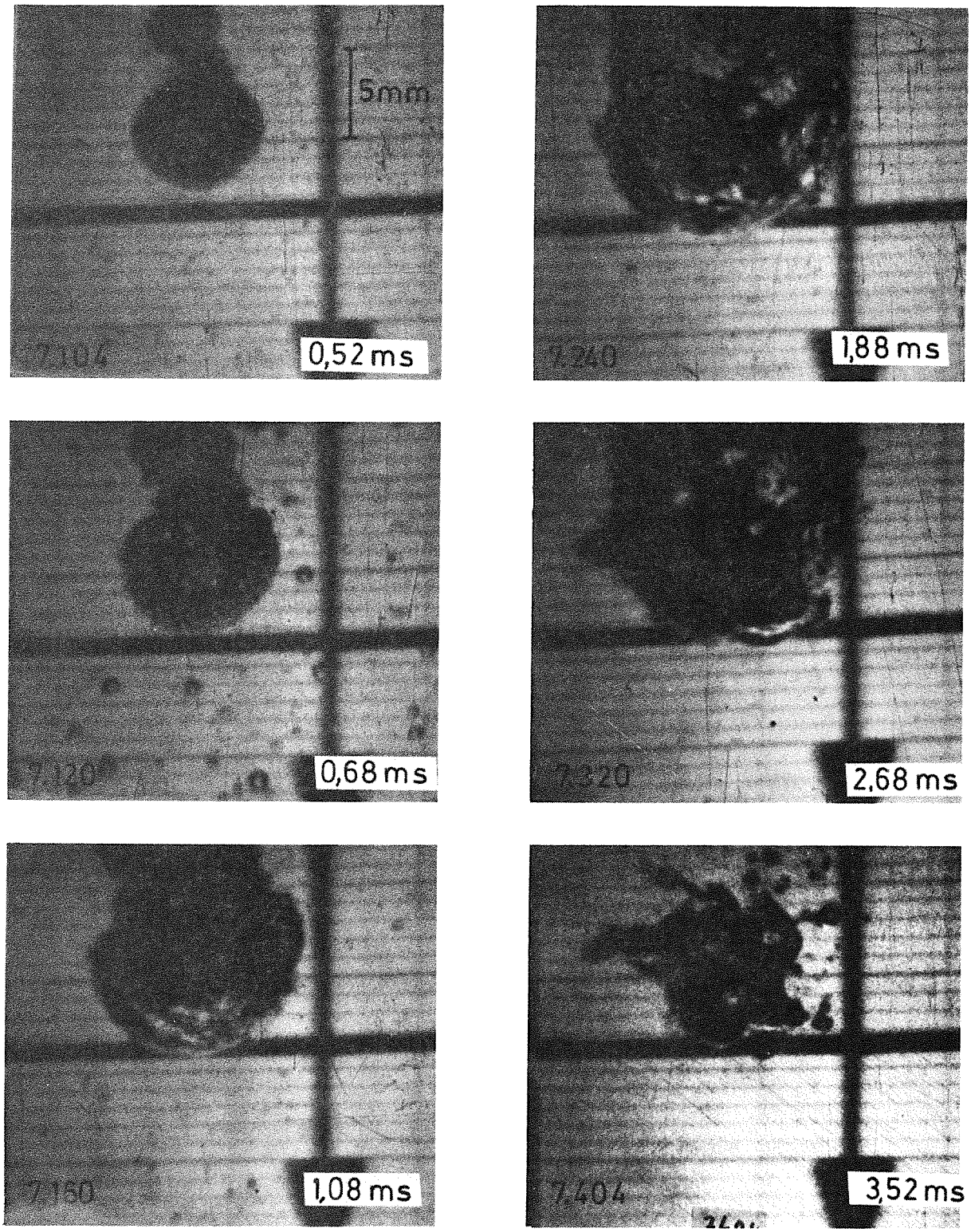

Fig. 34 Test AOW7, Sequence of Pictures (Phase V)

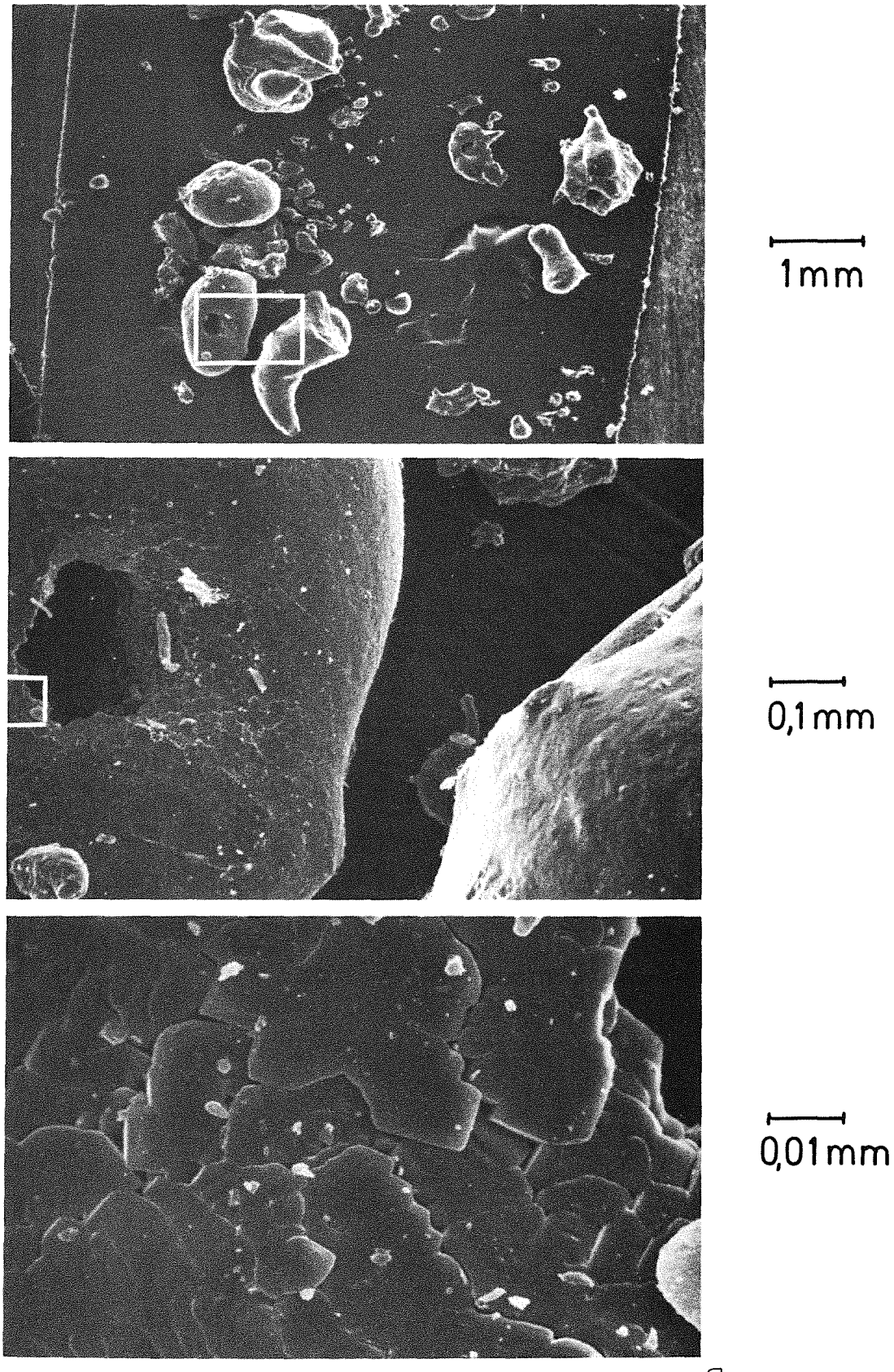

KfK IRE8712105

Fig. 35 Test AOW7, Photomicrographs of some Fragments

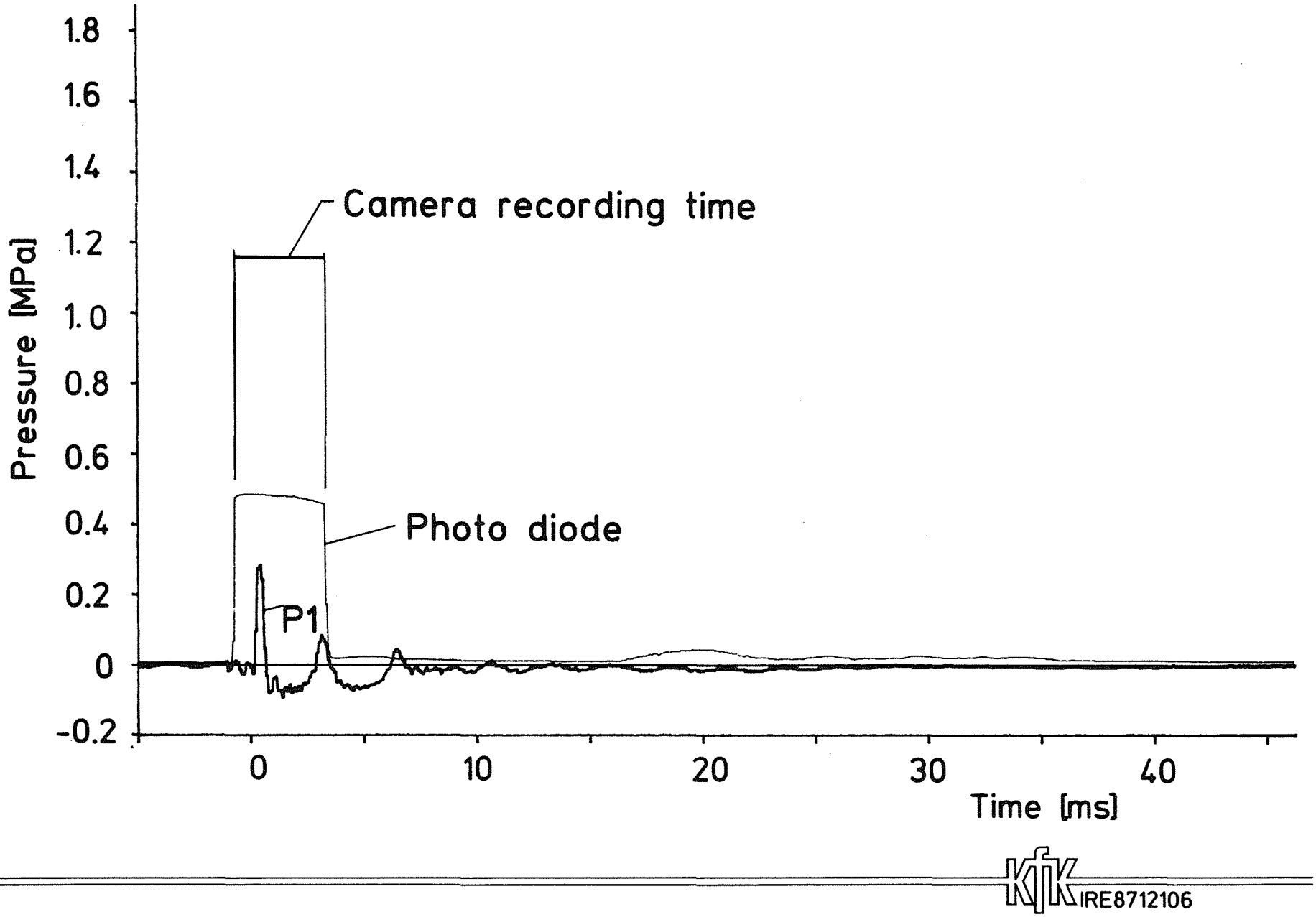

Fig. 36 Survey of Test A0W9, (f_R = 10 kHz)

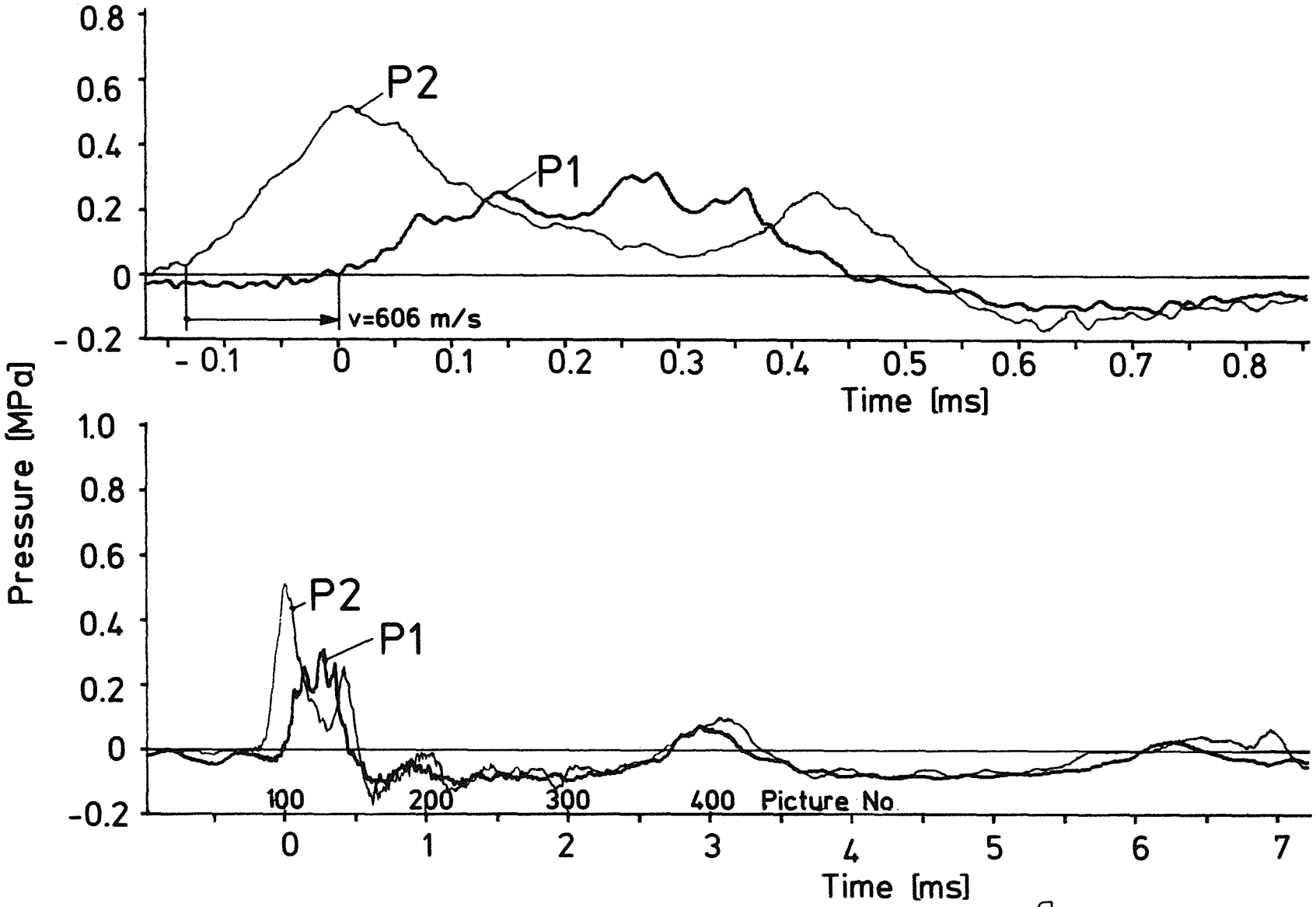

Fig. 37 Test AOW9, Course of Pressures
(U= 700 V; f_R = 500 kHz)

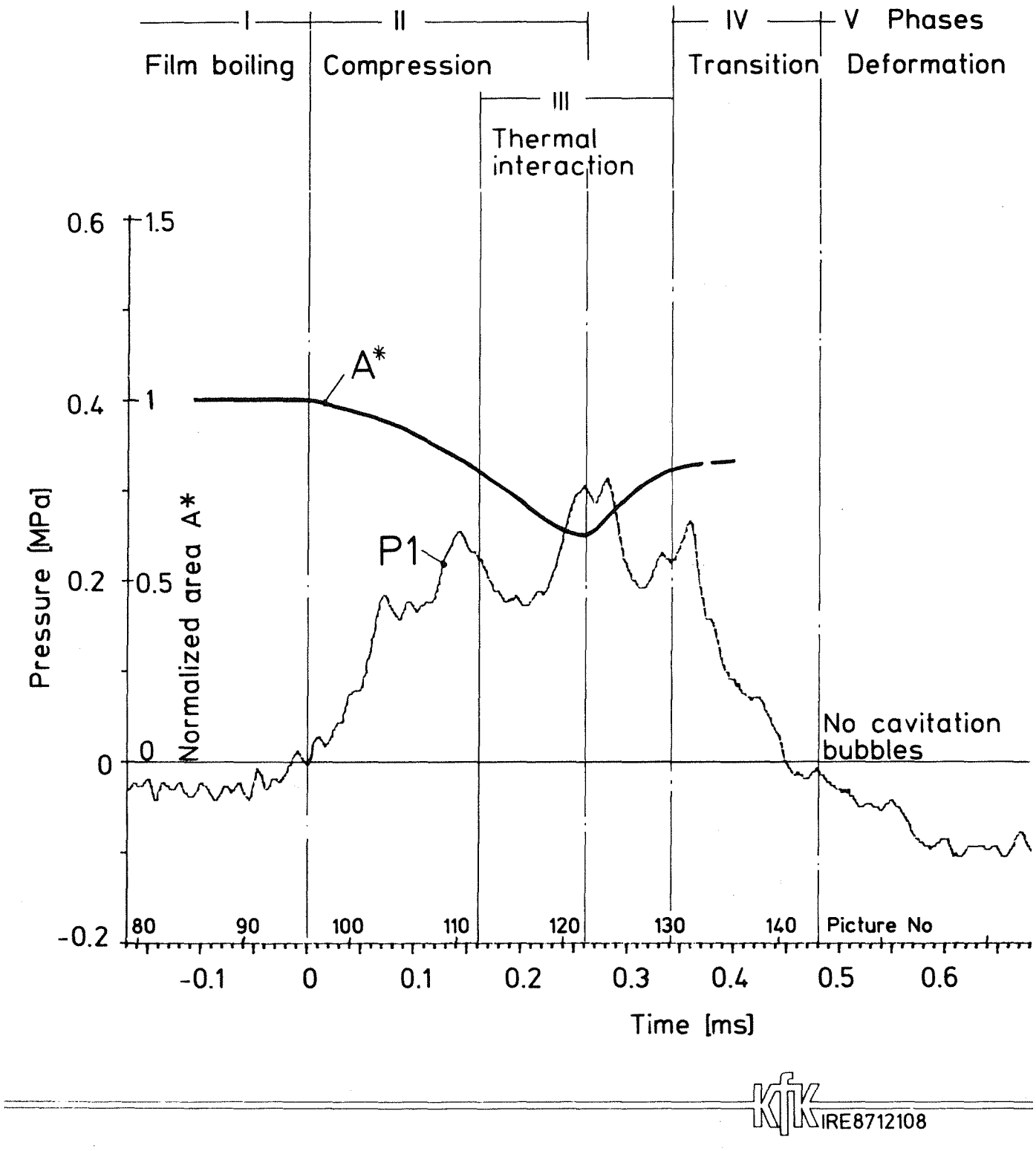

Fig. 38 Test A0W9, Sequence of Events

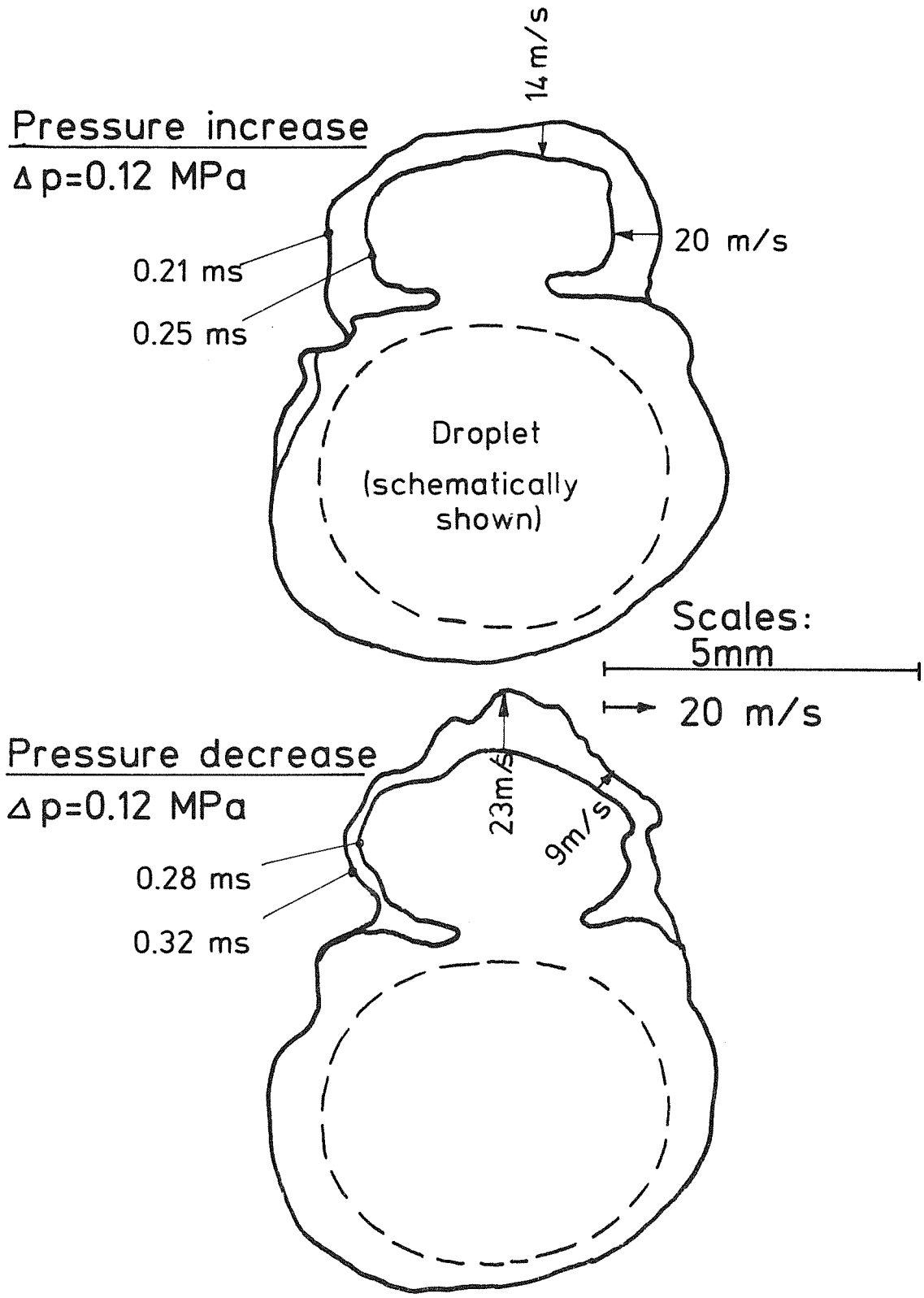

Fig. 39 Test A0W9, Velocity of Water-Vapour Interface

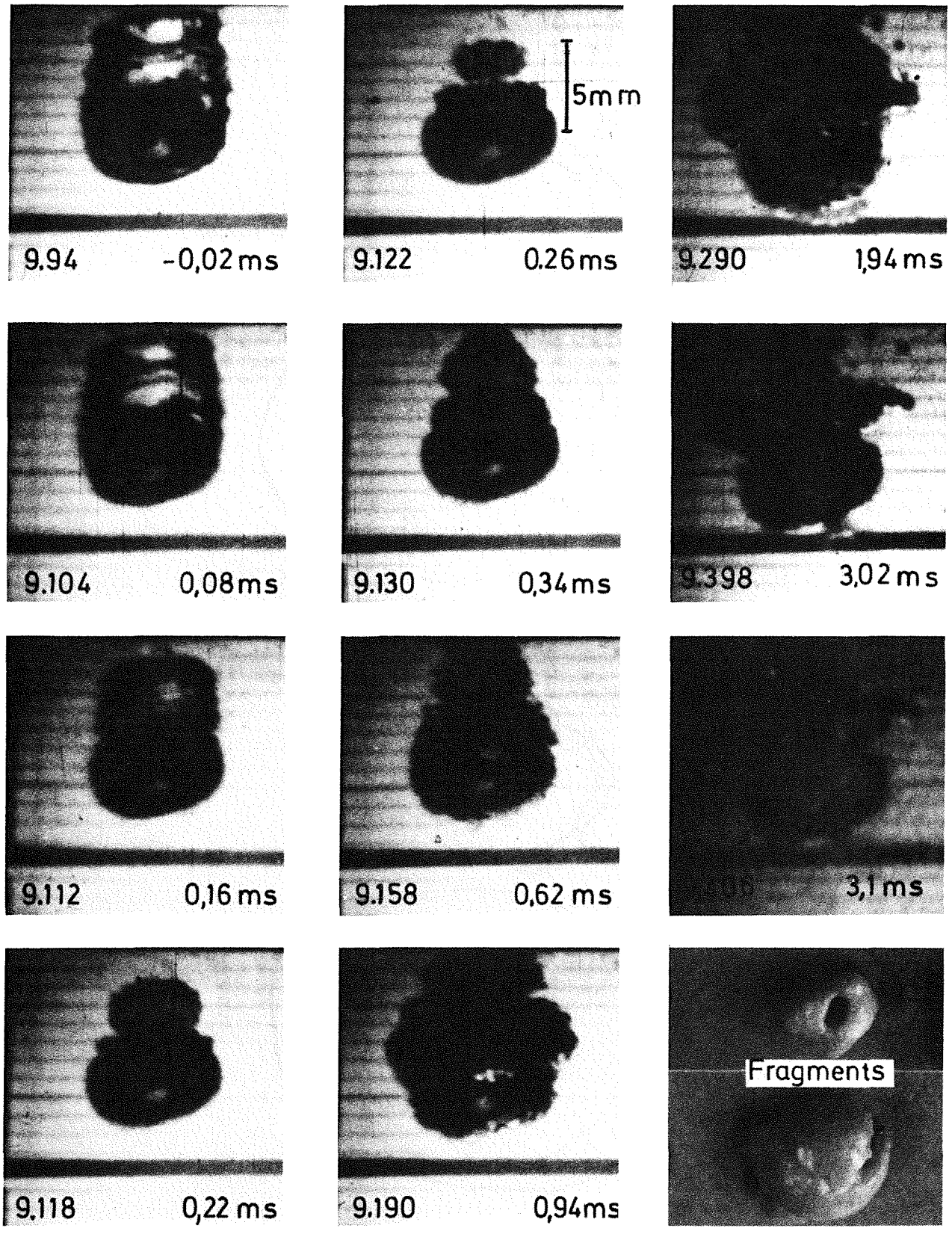

Fig. 40 Test AOW9, Sequence of Pictures and View of Fragments

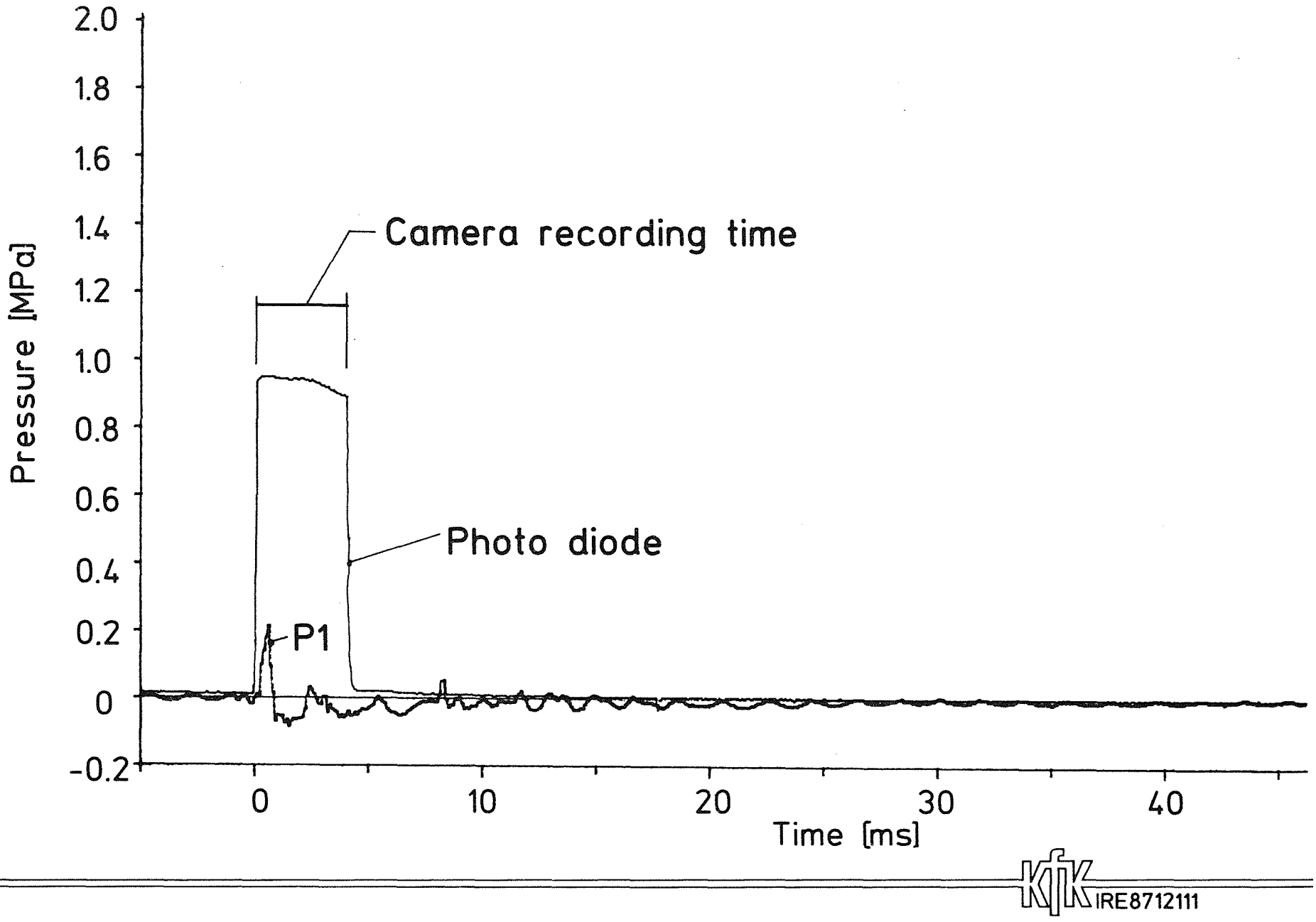

Fig. 41 Survey of Test AOW11, (f_R= 10 kHz)

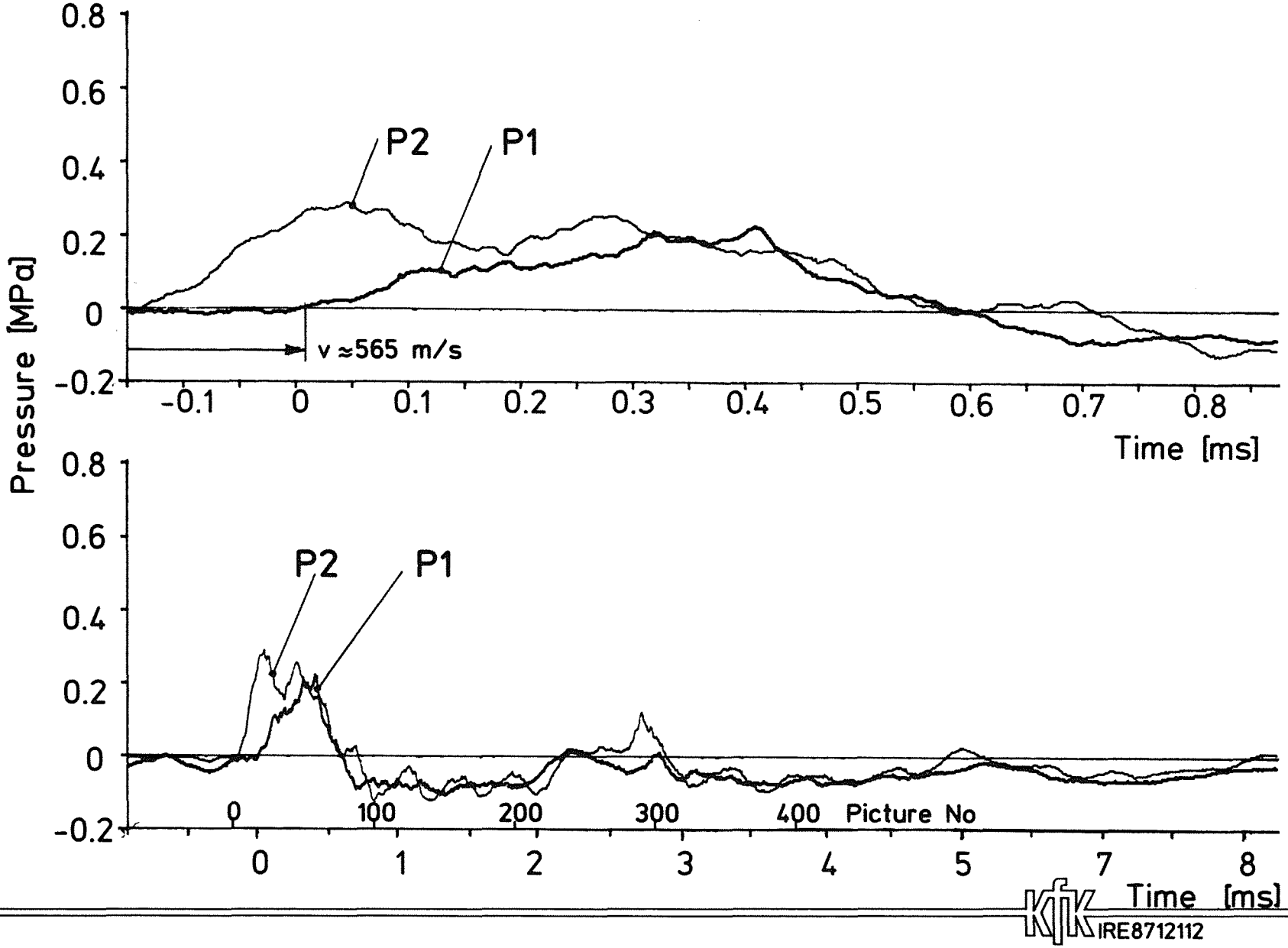

Fig. 42 Test AOW11, Course of Pressures
(U= 700 V; f_R= 500 kHz)

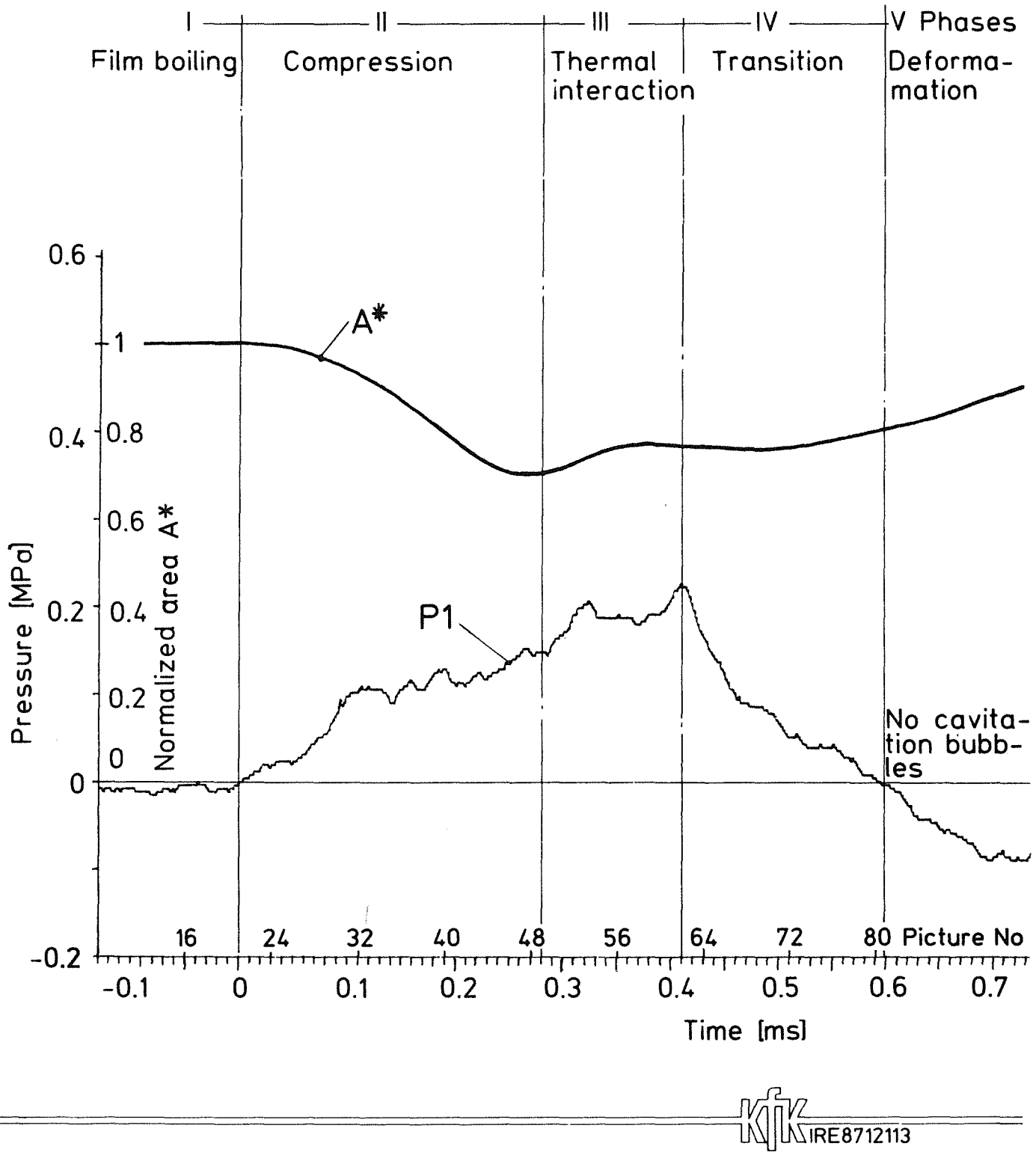

Fig. 43 Test A0W11, Sequence of Events

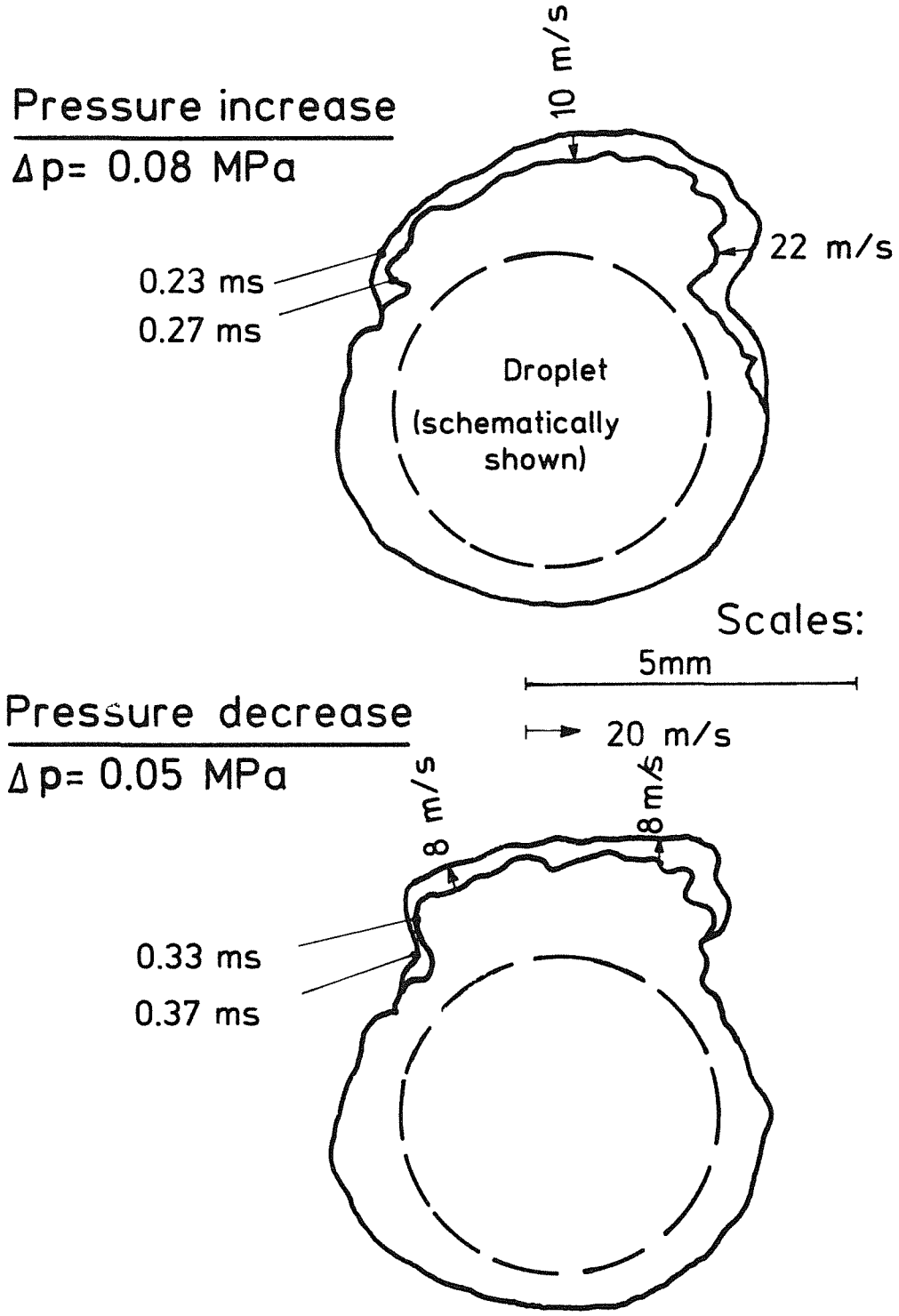

Fig. 44 Test AOW11, Velocity of Water-Vapour Interface

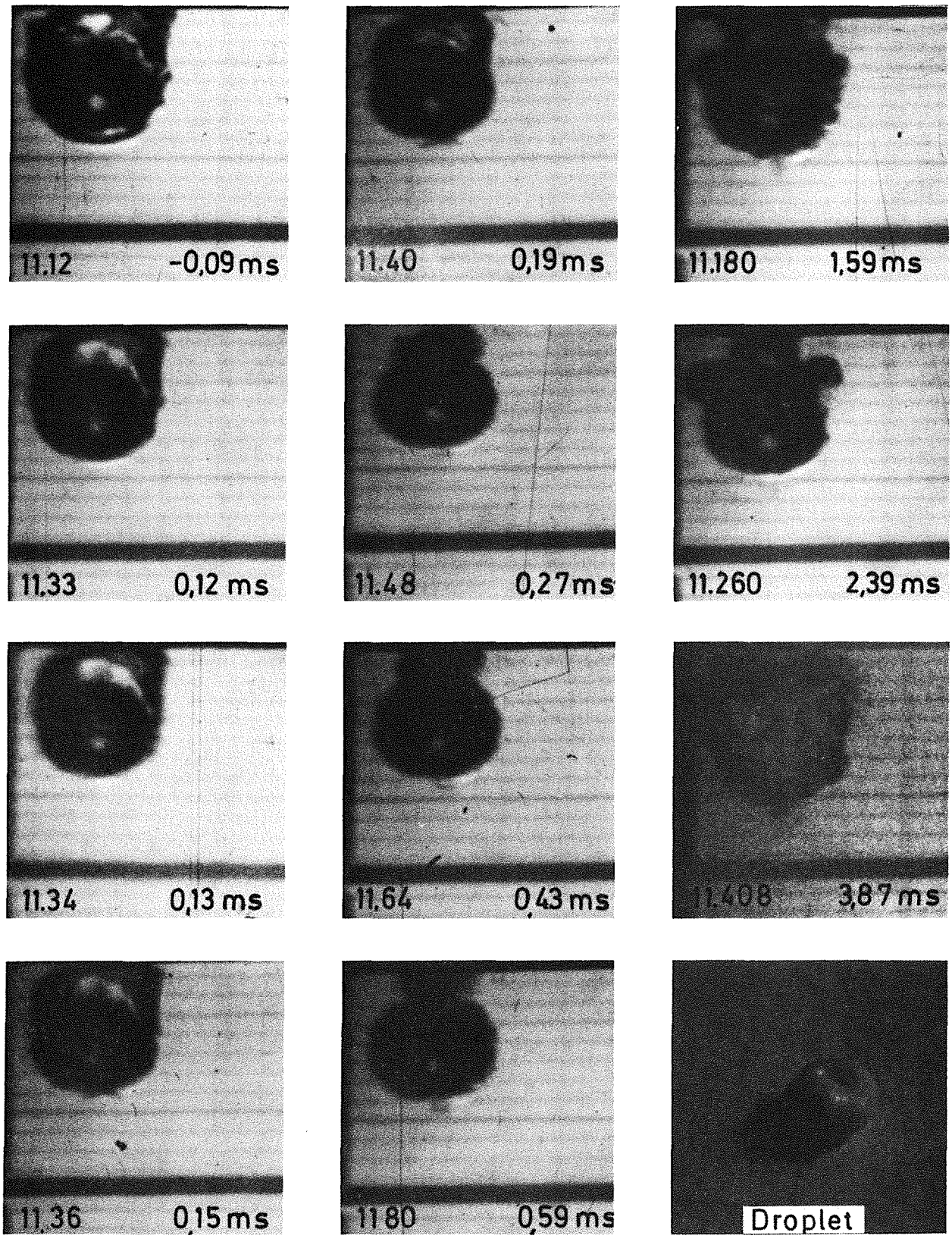

Fig. 45 Test AOW11, Sequence of Pictures and View of deformed Droplet